Downloaded from orbit.dtu.dk on: May 06, 2023

DTU Library

Partical discharges in artificial gas-filled cavities in solid high voltage insulation

Luczynski, Bohdan; Pedersen, Aage; Vørts, S.

Publication date:
1979

Document Version
Publisher's PDF, also known as Version of record

Link back to DTU Orbit

Citation (APA):
Luczynski, B., Pedersen, A., & Vørts, S. (1979). *Partical discharges in artificial gas-filled cavities in solid high voltage insulation*. Publication / Electric Power Engineering Department, Technical University of Denmark No. 7902

General rights
Copyright and moral rights for the publications made accessible in the public portal are retained by the authors and/or other copyright owners and it is a condition of accessing publications that users recognise and abide by the legal requirements associated with these rights.

- Users may download and print one copy of any publication from the public portal for the purpose of private study or research.
- You may not further distribute the material or use it for any profit-making activity or commercial gain
- You may freely distribute the URL identifying the publication in the public portal

If you believe that this document breaches copyright please contact us providing details, and we will remove access to the work immediately and investigate your claim.

PARTIAL DISCHARGES IN ARTIFICIAL GAS-FILLED CAVITIES IN SOLID HIGH VOLTAGE INSULATION

BOHDAN LUCZYŃSKI

PUBLICATION NO. 7902

JUNE 1979

Electric Power Engineering Department
Technical University of Denmark
DK 2800 Lyngby

CONTENTS.

PREFACE.

The solid dielectric insulating the conductive parts of a high voltage apparatus is exposed to strong, local electric stresses due to electrical field concentrations on the sharp points or edges of the conductors, field concentrations occurring at the connections between conductors and solid insulation, and inhomogenities and defects in the insulation material. Various breakdown mechanisms can lead to the loss of insulating properties in an insulating system stressed in this way.

In solid dielectrics, the slow acting deterioration processes initiated by or associated with internal partial discharges in gasfilled voids are those most likely to cause insulation failure in practice. Such internal discharges occur in voids at stresses of some 1/100 - 1/1000th of the intrinsic breakdown strength of the insulant, and degrade the insulation in different ways.

Since the power dissipated in such discharges is limited by the resistivity of the dielectrically sound part of the system, the discharges give rise to slow changes in the properties of the insulant. After varying periods of time, when the electric conductivity in the insulation becomes sufficiently high to maintain a current limited only by the impedance of the high voltage supply, breakdown occurs. The loss of insulation properties in solid dielectrics is normally an irreversible process in strong contrast to the processes in gaseous dielectrics. Failures in such a system are frequently equivalent to damage to the high voltage apparatus and can - if the apparatus is a vital component of the power system - result in a disconnection of the electric energy supply.

The replacement of classical insulation materials by polymeric dielectrics allows a size reduction with maintained ratings. Polymeric materials with attractive electrical and mechanical properties include epoxy and polyurethane resins (easily machined and moulded, possibilities of great variations of properties), polyethylene (high resistivity, low loss), polypropylene (high mechanical and electrical strength), teflon and silicone (elevated working temperature). Although the use of polymeric dielectrics in high voltage equipment has undergone a remarkable expansion during the last few years, the application of these materials to high voltage systems is still rather limited because of their low resistance to internal discharges. The low resistance to the

long term deterioration processes substantially limits the operating stress in the polymeric insulation, for instance in cables, to 1 % of the short term stress.

Of special interest is the prediction of the rate of deterioration and the life time of insulation based on quantities measured during the testing of high voltage equipment. Such a prediction, however, is not possible today since the interaction of the fundamental physical processes occurring in a partial discharge with the exposed insulating material has not been sufficiently clarified.

FOREWORD.

The present thesis deals with the results of a study of distinct types of partial discharges occurring in solid high voltage insulation under alternating voltage conditions, and of the behaviour of the insulation subjected to the investigated discharge types. The study, which constitutes part of the requirements for the degree lic.techn. (Ph.D.), has been undertaken at the High Voltage Laboratory, Electric Power Engineering Department, Technical University of Denmark, under the auspices of professor S. Vørts and associate professor Aage Pedersen.

I am indebted to LK-NES, the LK-NES Foundation, the Thomas B. Thrige Foundation, the Selmer Trane Foundation, and prof. Hyldgaard-Jensen Foundation for making this investigation possible.

It is a pleasure to express my appreciation to associated professor Aa. Pedersen of the High Voltage Laboratory, Technical University of Denmark, for his enthusiastic support and helpful critisism of the investigation. I am greatly indebted to my colleagues and the staff at the High Voltage Laboratory and in LK-NES for their professional help. Especially, I must thank mr. F. Levring and dr. H. Boyd for much valuable discussion.

Finally, I am deeply grateful to professor S. Vørts of the Electric Power Engineering Department, Technical University of Denmark, and to chief engineer, dr. T. Laubst, LK-NES, for the help which they have given me during the investigation.

1. INTRODUCTION.

The autographs of *partial discharges* were discovered in 1777 by Lichtenberg (litt. 1) who observed that the resin dust settling on a resin surface which had been subjected to a discharge, formed starlike patterns. The mechanisms of formation of the Lichtenberg figures have been investigated by P.O. Pedersen (litt. 2). Until the appearance of the results obtained independently by Devins (litt. 3) and Degn (litt. 4), the description of the electrical phenomena related to *internal discharges* in gas-filled cavities was founded on a capacitive model proposed by Burstyn (litt. 5) and Gemant and Philipoff (litt. 6). A considerable number of useful investigations was carried out by Whitehead (litt. 7), Mason (litt. 8), and Kreuger (litt. 9) with this model as a starting point. The model explained the occurrence of current impulses in the external circuit, which were according to the model due to a complete or partial discharge of the capacity of the cavity through a gap connected in parallel with the capacity. An explanation of the different waveforms of the current pulses connected to distinct types of partial discharges, however, was not possible because the model does not give a rigorous representation of the physical mechanisms and conditions in the cavity (litt. 4). The method applied by Devins and Degn differs from the way of looking at internal discharges adopted by cultivators of the Gemant and Philipoff model. Devins and Degn considered the internal discharge as the phenomena of production and movement of the electrons and ions in the cavity along the lines of electrical field stresses. The current impulses in the external circuit were due to an interaction of the charged particles with the electrical field in the cavity.

Devins, Degn and Neudert (litt. 10) found that at least two distinct types of partial discharges the "rapidly developing" and the "slowly developing" partial discharges occurred in cavities in solid dielectrics.

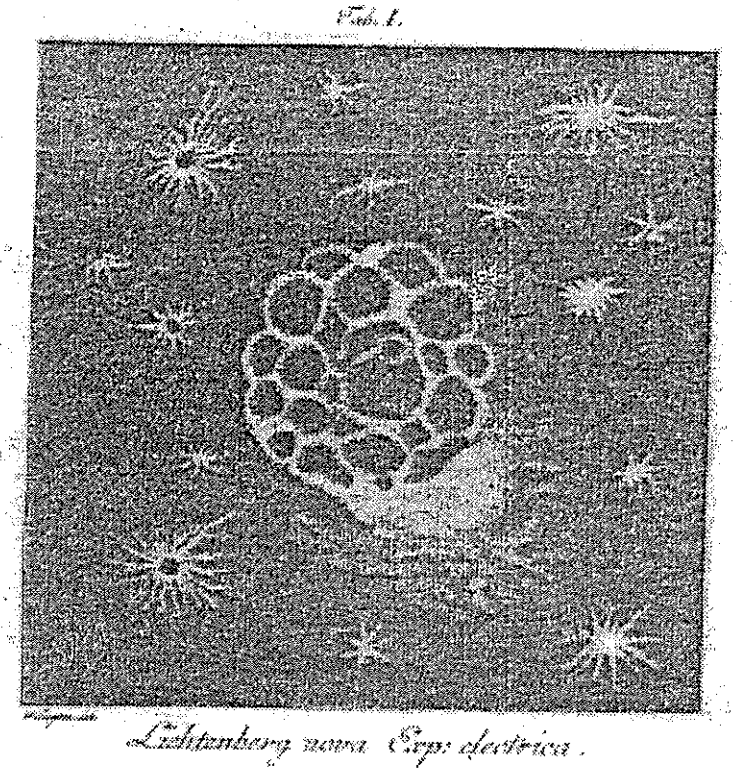

Fig. 1.1.
The positive and negative
Lichtenberg figures. (Litt.-1).

Devins (litt. 3) and his co-workers measured the waveform of current pulses caused by different types of partial discharges occurring in an air gap between a metal electrode and a lime glass plate soldered to the other electrode. A dc voltage was applied with a small voltage pulse superimposed. Lichtenberg figures were detected by means of lycopodium powder. According to Devins, the starlike patterns observed were associated with very rapidly developing partial discharge pulses which were concluded to be streamerlike in nature. These streamerlike partial discharges occurred at high values of overvoltage. When the value of overvoltage was small, however, another type of partial discharge occurred which Devins concluded to be Townsendlike in nature. The same two distinct types of internal discharges have also been observed by Neudert (litt. 10) between two glass surfaces during the application of a slowly rising dc voltage. Both types of discharges also occurred when a slowly alternating voltage was applied to a solid dielectric containing a cavity.

Close quantitative support for the concept of the streamerlike partial discharges was obtained by Mayoux and Goldman (litt. 11) who investigated the temporal growth of light emitted from partial discharges. The velocity of propagation of the discharges through the cavity was

found to agree with the velocity of discharge propagation associated with streamer formation.

The Townsendlike or slowly developing partial discharges have been closely investigated under ac voltage conditions by Degn (litt. 4). Degn also observed that the formation of slowly developing partial discharges required many electron transit times in the cavity, and consequently concluded, similar to Devins (litt. 3) and Neudert (litt. 10), that a Townsend regenerative mechanism was operative.

For the slowly developing partial discharge, both Devins and Degn proposed a generation mechanism which was governed by the changes of the space charge in the cavity. Degn supported this concept by the above mentioned measurements of the rise times and durations of the current pulses and by computations of their fronts and durations based on numerical simulation of physical processes in the partial discharge.

Although there was a general agreement between the measurements and calculations there was a lack of experimental proof of the existence of the generation machanism in this type of partial discharge.

In order to explain the temporal development of slowly developing partial discharges, a rigorous mathematical model based on analytical solutions of the continuity equations should be established and the calculated waveforms should be compared with the observed waveforms within a wide range of the parameter p·d. Such a solution should furthermore fullfil arbitrarily determined initial conditions in the cavity.

According to Degn, the mechanism of the second type of the partial discharges characterized by very fast increasing current pulses was unexplained. Furthermore, it was not possible to measure the waveforms of the rapidly developing discharges by means of the electrode systems used by the mentioned investigators.

Pedersen and J. Fekecz (litt. 12) investigated the internal discharges occurring in closed, cylindrical cavities in polyethylene under ac voltage conditions. The size of the charged areas of these discharges was estimated from the positive and negative Lichtenberg figures observed on the cavity surface. It was not known, however, whether or not the discharged areas were due to a distinct discharge type.

It was not clear, whether or not the deteriorations caused by the two different types are different. Unfortunately the known measuring

methods did not provide any direct information, neither on the lateral extension of the distinct types of partial discharges nor on the occurrence of the possible local discharges over the surface. This would help to identify the discharge types which can result in significant changes in the insulation in terms of insulation structure and properties (dangerous discharge types).

Processes other than partial discharges, for instance conduction, could well contribute to the power dissipation in the cavity during the tests of longer duration. Such processes could precipitate the deterioration processes in regions of local high field concentrations.

The changes in the discharge types and the properties of the insulation during the prolonged tests were not clarified (litt. 13).

At the same time there was a need and a necessity for the further investigations of the relations between the lifetime of the equipment and the discharge intensity (litt. 14).

For the reasons mentioned above, the present work has been undertaken with the particular aim to investigate the different types of individual internal partial discharges occurring in polymeric high voltage insulation under ac voltage conditions, and also to relate this information to observed slow decreases of insulating properties.

2. EXPERIMENTAL METHODS AND APPARATUS.

2.1. Test Samples, Electrode Systems, and Pressure/Vacuum Chamber.

In order to investigate the basic processes in a partial discharge, it is essential to isolate extraneous disturbances and effects and concentrate the investigations on the discharges in the simplest possible systems. Therefore, it was natural that test samples including a single artificial void and plane parallel metallic or dielectric electrodes were frequently used in the past by investigators of the physics of a partial discharge: Devins (litt. 3), Degn (litt. 4), Mason (litt. 8), Pedersen (litt. 12), Neudert (litt. 10), Bailey (litt. 15), the present author (litt. 16), Kärkkainen (litt. 17). The electric current due to the movement of electrons and ions in the cavity was measured in these systems by means of a shunt connected between the low voltage electrode and a coupling capacitor, connected across the electrodes, thereby providing a low impedance return for the measured currents. Bailey (litt. 15) built the test sample, the electrode system, and the coupling capacitor together into one unit. With this integrated system featuring bare electrodes it was possible to measure extremely fast currents with reduced interference from extraneous discharges while operating in the region up to some few kilovolt. The discharge system employed by Degn (litt. 4) was also of the integrated type; embedding the electrodes in epoxy resin further minimized the effect of extraneous discharges even at elevated voltage levels up to 15 kV. The electrodes were built into a vacuum chamber to permit the study of partial discharges in different gasses and at various pressures. The electrical response of this system was somewhat oscillatory. This was due to the inductance in the connection between the coaxial cable and the coupling electrode.

For the present purposes a special integrated test cell system of high sensitivity was designed which allowed non-oscillatory measurements of fast electrical signals with rise times down to few nanoseconds. In addition, facilities were provided for the observance of the low intensity, fast optical signals by means of an externally mounted photomultiplier. Great care was taken to minimize the occurrence of extraneous discharges. The system was assembled in a pressure/vacuum chamber which

was suitable for use over a wide range of the parameters: p, d, and the type of gasses used. The test samples, electrode system, and pressure/ vacuum chamber are described in more detail in this subsection.

Test Samples.

Both open and closed test samples with cylindrical or spherical cavities were used throughout this investigation (fig. 2.1 and 2.2).

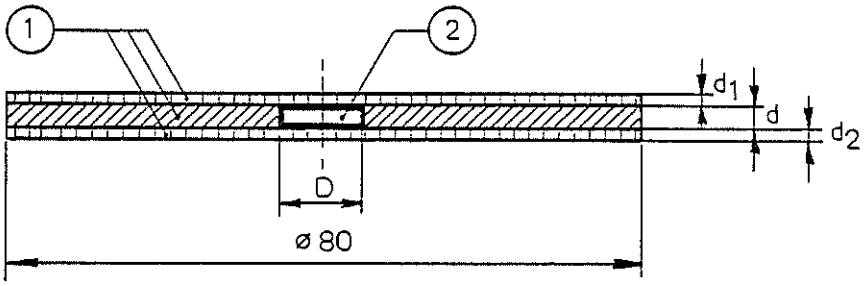

Fig. 2.1.
Closed test sample.

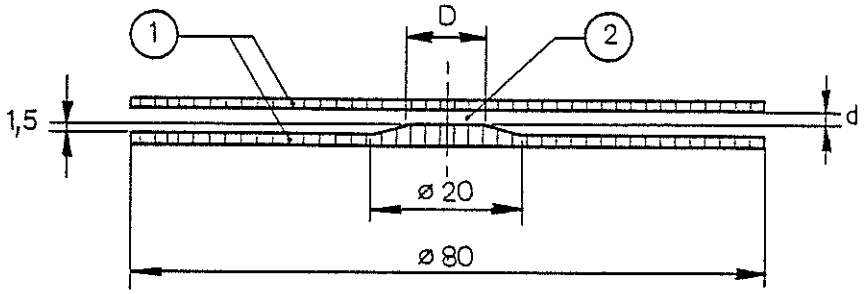

Fig. 2.2.
Open test sample.

Fig. 2.1 and 2.2. Examples of closed and open test samples. 1: discs of insulation material, 2: cavity. D from 5 to 20 mm; d, d_1, d_2 from 0.2 to 2 mm.

The thicknesses d_1, d, d_2 of the discs were determined as a mean value of 5 measurements made with the aid of a micrometer. The micrometer could be read with an accuracy of 0.0005 cm.

The samples were made of a number of typical polymeric materials commonly used as solid insulation of high voltage equipment: polyethylene, polypropylene, and two basic types of epoxy resins: one of the aromatic type, the other one of the cycloalifatic glycidyl ester type. More detailed information about the properties and composition of the polymers used is given below:

	polyethylene	polypropylene
manufacture	BP "Rigidex" 002-55	ICI "Propathene" G PE 102
density g/ml	0.955	0.905
softening point ^{o}C	125	147
tensile strength $MN \cdot m^{-2}$	22	27
power factor at 1 MHz	$< 1 \cdot 10^{-4}$	$< 2 \cdot 10^{-4}$
rel. permittivity at 1 MHz	2.35	2.25
breakdown voltage $kV \cdot cm^{-1}$	> 160	> 130
surface resistivity ohm	10^{17}	$10^{11} - 10^{15}$
volume resistivity ohm · cm	10^{17}	10^{19}
coefficient of thermal conductivity at 20° C $W \cdot m^{-1} \cdot {}^{o}C^{-1}$		0.21
specific heat at 20° C $J \cdot kg^{-1} \cdot {}^{o}C^{-1}$		1930

<u>bisphenol A epoxy resin</u> - Epikote 828:	100 units
methyl anhydrid (MMA) curing agent:	10 units
benzyldimethylamine accelerator:	1 unit
<u>cycloaliphatic glycidyl ester epoxy resin</u> - Araldit CY182:	100 units
hexahydrophtalic anhydrid HT 907 curing agent:	100 units
DY065 accelerator:	6 units

The polyethylene and polypropylene discs were made from foil, whereas the epoxy resin discs were moulded. The resin was degassed and poured into silicon rubber moulds. Finally, the moulded discs were polished. The cylindrical hole in the central disc was turned.

The pressure was measured in the pressure/vacuum chamber, and as the connections between the discs were not tight the pressure in the chamber was a measure for the pressure in the cavity. This was checked by observation of the length of the current pulses which changed immediately after the change of the pressure in the pressure chamber.

Electrode System, Pressure/Vacuum Chamber, and High Voltage Supply.

The partial discharges occurring in the test samples were measured using an electrode system developed in order to minimize the inductance in the measuring circuit. The essential features of the system are illustrated in fig. 2.3. The test samples were assembled between the high voltage electrode 1 and the low voltage electrode 2,3. The low voltage electrode consisted of a coupling electrode 2, which provided the necessary coupling capacitance, and a measuring electrode 3. The measuring electrode was connected to the center terminal of a BNC-type coaxial connector 4. The connector screen was coaxially joined to the coupling electrode. The electrodes were imbedded in epoxy resin, the thickness of which was 0.1 cm in the central region of the electrodes. The low voltage electrode was mounted on a steel base plate.

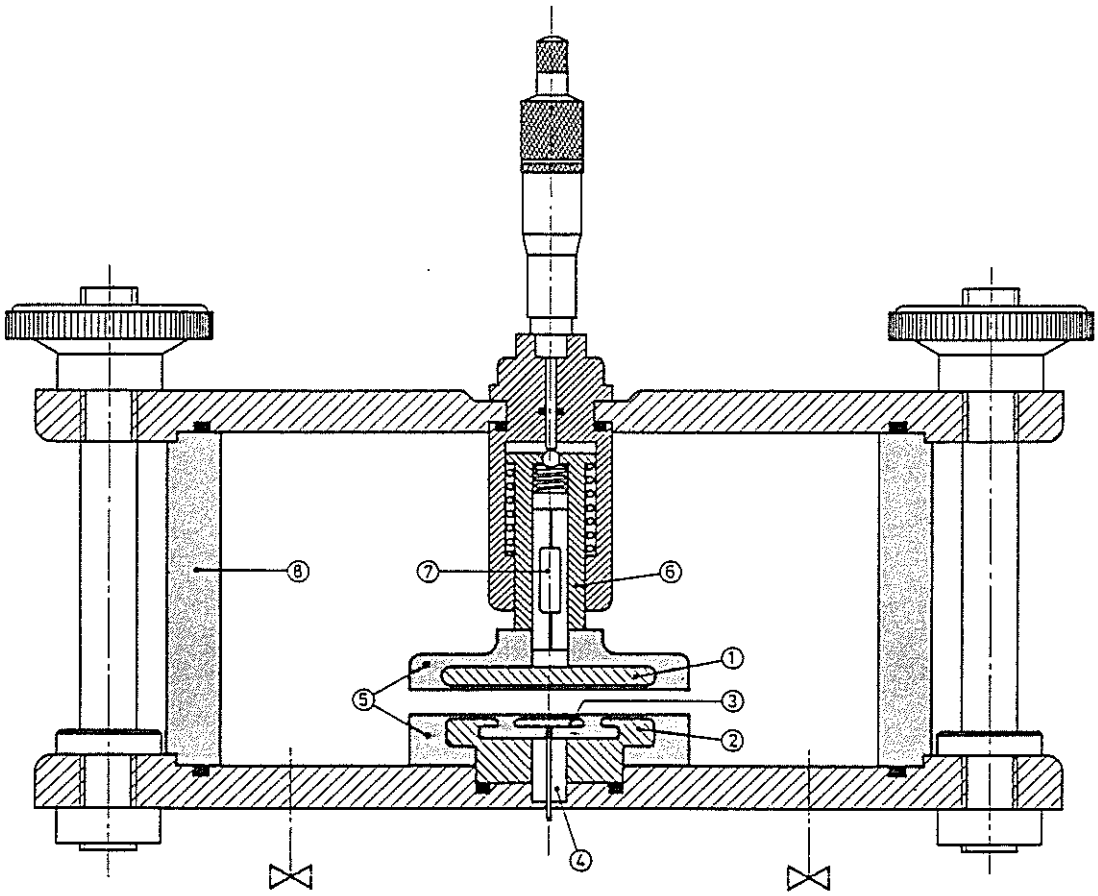

Fig. 2.3.
Cross section of electrode system.
1, 2, 3: High voltage, coupling, and measuring electrodes, respectively. 4: Coaxial connector. 5: Epoxy resin. 6: Guide mechanism. 7: resistor (exchangeable). 8: Plexiglass tube.

Total electrode diameter, including epoxy resin: 80 mm; diameter of measuring electrode: 30 mm. Thickness of epoxy layer covering the central region of electrodes: 1 mm.

The high voltage electrode assembly consisted of an electrode 1, screwed onto an adjustable cylindrical guide mechanism 6, suitably bushed to ensure parallel electrode displacement throughout the vertical range. A precision micrometer was used to adjust the electrode vertical separation. The electrical contact between this electrode and the guide mechanism was maintained by an internal, exchangeable resistor 7. Concerning the fast transients, this resistor isolated the measuring system from the high voltage supply. The outer cylinder of the guide mechanism was screwed onto the upper base plate. The upper and lower base plates were mounted and held in position by six external screws. Rubber gaskets of the "O" ring type were used throughout to provide vacuum tight joints.

To the pressure/vacuum chamber atmospheric air of definite gas was admitted. The impurity of the gases admitted is summarized from manufacturer's data in the following table:

gas	purity	impurities (vpm)			
		H_2O	O_2	H_2	N_2
argon	99.998	3	2	1	10
helium	99.995	10	4	5	5
nitrogen	99.998	3	2	5	-
methane	99.5	-	-	-	-
carbon dioxide	99.7	50	50	10	50
air	atmospheric non-dried	-	-	-	-

Table 2.1.

The gas used was admitted to the chamber directly from the pressure bottle, and pressures were measured by ordinary manometers. The partial discharge investigation was carried out at different gas pressures in the range 0.1 bar to 4 bar. The inaccuracy of the pressure measurements was ± 1 % at 1 bar. An oil diffusion pump was used to evacuate the discharge chamber to pressures down to 50 mb. The temperature of the atmospheric air surrounding the chamber was measured with an accuracy better than ± 1° C.

The ac power supply consisted of a high voltage transformer, 300 V/31 kV, which could be operated at 50 Hz or 500 Hz. The 500 Hz

voltage was supplied from a rotating frequency converter. The voltage applied to the test cell could be measured with an accuracy better than ± 1 % with a precision high voltage transformer or a capacitive divider. The equipment was situated in a test area specially constructed for this purpose together with the high voltage transformer and the necessary control and security circuits (litt. 19).

Before a test sample was used for measurements, the central disc of the sample was temporarily replaced by a disc without the cylindrical hole while it was ascertained that the system was dischargefree up to 15 - 20 kV which is over the operating voltage.

2.2. Methods for the Measurement of the Temporal Development and Lateral Extension of Individual Partial Discharges.

Three independent methods have been developed and employed in order to investigate the development of the partial discharge during its extremely short formation times in the range 10^{-9} - 10^{-8} s, and at very short distances in the range 10^{-2} - 10^{-1} cm. The developed methods are:

- the measurement of the partial discharge current pulses,
- the measurement of the emitted radiation,
- a method permitting a rough estimation of the extension of a partial discharge in directions parallel to the electrode surface and simultaneously permitting the measurement of the discharge current wave form.

The methods are discussed in subsections 2.2.1, 2.2.2, and 2.2.3.

2.2.1. Measurement of the discharge current pulse.

An interpretation of the discharge current as a measure of the velocities and densities of charged particles in the cavity is given in this subsection. The quantity which is directly observed by means of the oscilloscope is the wave form of the voltage u_R across the resistive shunt connected to the measuring electrode. The current flowing through this electrode and through the shunt is a measure for the motion of charged particles in the cavity. This ordered motion of charges constitutes a current which under certain conditions can be represented by a current source $i(t)$ inserted between the measuring electrode and the high voltage electrode. If the time constant of the measuring system is sufficiently small, the current can be calculated from the measured voltage as:

$$i(t) = k_1 \cdot u_R(t)$$

See equation 2.2.14.b on page 24. In this subsection the response and the sensitivity of the measuring system are also considered.

The Current of an Internal Discharge.

When a voltage is applied to the electrodes, the ions and electrons accelerate in the electric field of the gas-filled cavity along the lines of force. The accelerated particles lose their energy by collisions with the gas atoms. The average value of the velocity in the direction of the field between two succeeding collisions, or the drift velocity, depends on the intensity of the applied electrical field. The field-directed motion of charged particles constitute a current. The current density $\vec{j}$ at any point in the cavity is equal to the charge which in a unit time crosses a unit area of a surface orthogonal to the drift velocity $\vec{v}$. Disregarding the corpuscular nature of the charged particles, the charge density ρ is a continuous function of the position, and the current density at any point is given by:

$$\vec{j} = \rho_- \cdot \vec{v}_- + \rho_+ \cdot \vec{v}_+ + \rho_n \cdot \vec{v}_n \qquad (2.2.1)$$

where ρ_-, ρ_+, ρ_n, and $\vec{v}_-$, $\vec{v}_+$, $\vec{v}_n$ are electron, positive ion, and negative ion densities and drift velocities, respectively.

The directed motion of the charges in the cavity produces a change in the density of charges induced on the electrodes. For instance, if a charge approaches an electrode, the charge of opposite polarity induced on the electrode is thereby increased producing a current flow in the external circuit. If the rate of change of the surface charge density on the measuring electrode is $\partial\sigma/\partial t$ the current flowing through the shunt connected to this electrode is:

$$i_R(t) = \int_S \frac{\partial\sigma}{\partial t} \cdot dS \qquad (2.2.2)$$

The integration must be carried out over the surface of the measuring electrode.

The relation between the current flowing in the external circuit and the current densities in the cavity can be established from considerations on the energy transfers between the field and the charges.

A cavity surrounded by insulation with the conductivity $\gamma = 0$ is considered. It is supposed that the electrodes have a mutual capacitance C_{ab}, and that the applied potential difference is a function of time $u(t)$. The energy $i_R(t) \cdot u(t) \cdot \Delta t$ transferred to the electrode system by the high voltage supply in the time Δt is equal to the sum of the energy stored in the capacitance C_{ab} and the work done on all charges moving in the cavity. Since the force exerted on a charge in an infinitesimal volume dV is $\vec{E} \cdot \rho \cdot dV$, and the work done in a displacement of the charge a distance $\Delta\vec{l}$ is $\vec{E} \cdot \Delta\vec{l} \cdot \rho \cdot dV$, then

$$u(t) \cdot i_R(t) \cdot \Delta t = \frac{d}{dt}\left(\frac{C_{ab} \cdot u(t)^2}{2}\right) \cdot \Delta t + \int_V \vec{E} \cdot \Delta\vec{l} \cdot \rho \cdot dV \qquad (2.2.3)$$

where the right-hand integral must be evaluated over the cavity volume V for all the species of the charged particles present. Replacing $\Delta\vec{l}/\Delta t$ by $\vec{v}$, the current i_R becomes:

$$i_R(t) = C_{ab} \frac{d\,u(t)}{dt} + \frac{1}{u(t)} \cdot \int_V \vec{E} \cdot \vec{v} \cdot \rho \cdot dV \qquad (2.2.4)$$

The first term on the right hand side of the equation represents the displacement current flowing between the electrodes:

$$i_c = C_{ab} \frac{d\,u(t)}{dt} \qquad (2.2.5)$$

and the integral term represents the current due to the motion of the charged particles in the cavity, i.e. the internal discharge current:

$$i(t) = \frac{1}{u(t)} \cdot \int_V \vec{E} \cdot \vec{v} \cdot \rho \cdot dV \qquad (2.2.6)$$

In the case of a uniform field an analytical solution of this equation is relatively simple as illustrated in the following examples.

Example 1. A Gap Between Plane Parallel Infinite Electrodes.

A gap with insulating surfaces parallel to the electrodes is considered The depth of the gap is d, the thickness of the insulation layers is d_1 and d_2, and the relative permittivity is ε_1. The x-axis of an orthogonal coordinate system is perpendicular to the electrode surface, and hence ρ depends on x only. In addition, it is assumed that the field intensity due to the charges distributed in the gap is negligible in comparison to the intensity of the applied field.

It can easily be shown that the field intensity in the cavity is:

$$E(x, t) = \frac{u(t)}{d + (d_1 + d_2)/\varepsilon_1} \tag{2.2.7}$$

This equation is inserted in equation 2.2.6 which is integrated over the arbitrary area A(y, z). The density ρ by virtue of the assumptions made does not depend on y and z, and hence the discharge current corresponding to the area A is given by:

$$i(t) = \frac{1}{d + (d_1 + d_2)/\varepsilon_1} \cdot \int_0^d \left[\iint_A \rho \cdot v \cdot dy \cdot dz \right] \cdot dx \tag{2.2.8}$$

$$= \frac{1}{d + (d_1 + d_2)/\varepsilon_1} \cdot \int_0^d A \cdot \rho \cdot v \cdot dx$$

Since E is eliminated from the equation 2.2.8, the equation expresses a simple relation between the discharge current i(t) and the velocities, as well as the densities of the charged particles in the cavity. However, i(t) is still field-dependent since both ρ and v are field-dependent.

The equation 2.2.4 can be written as:

$$i_R(t) = i_c(t) + i(t) \tag{2.2.4 a}$$

where i(t) is the discharge current which for the present case is given by the particular solution (2.2.8) of the equation 2.2.6, and does not depend on the impedances in the external circuit. The equation can thus be interpreted as a current source connected in parallel with C_{ab} as illustrated in fig. 2.4.

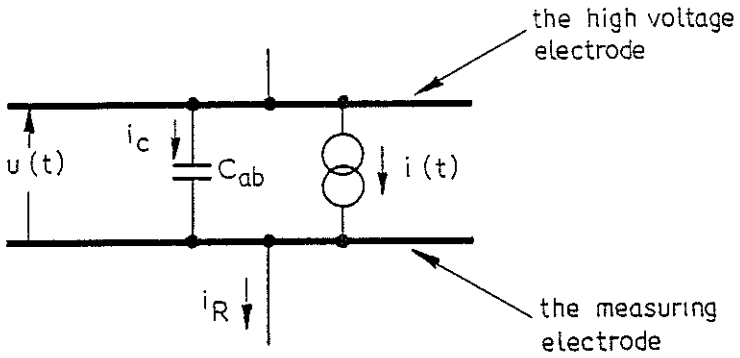

Fig. 2.4.
Equivalent circuit of eq. 2.2.4 a.

In the considered case of a plane parallel gap, the total current flowing through the area A of the gap d is given by (litt. 20):

$$i_d(t) = \frac{1}{d} \cdot \int_0^d A \cdot \rho \cdot v \cdot dx \qquad (2.2.9)$$

Equations 2.2.8 and 2.2.9 lead to:

$$\frac{i_d(t)}{i(t)} = \frac{d + (d_1 + d_2)/\varepsilon_1}{d} \qquad (2.2.10)$$

The function $i_d(t)$ can be interpreted as a current source connected in parallel with the capacitance C_d of the gap d as illustrated in fig. 2.5.

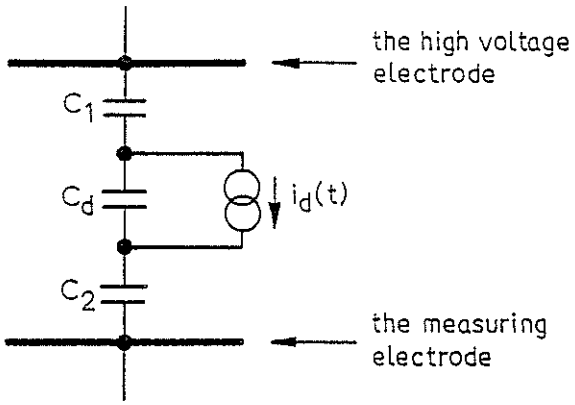

Fig. 2.5.

Equivalent circuit for the current in the gap. C_1 and C_2 are capacitances of the insulation layers having the area A and thicknesses d_1 and d_2, respectively. C_d is the corresponding capacitance of the discharge gap d.

Example 2. Cylindrical Cavity Between Plane Parallel Finite Electrodes.

The axis of the cavity is assumed to be perpendicular to the electrode surface. For cavities the diameter D of which is large in comparison to the cavity depth d, the equation 2.2.8 can be applied with a good accuracy. The errors which arise are partly due to the finite diameter D_1 of the measuring electrode, and partly due to the fringing effects occurring near the cylindrical wall of the cavity. The magnitude of the former error can be estimated on the basis of an error-function computed by Frommhold (litt. 21) under the assumption that the charge transfer takes place along the cavity axis. This error is less than 2.5 % for $D_1/d_r = 0.5$ and $d/d_r = 0.5$, where d_r is the reduced thickness of the insulation given by:

$$d_r = d + (d_1 + d_2)/\varepsilon_1$$

For the range D_1/d_r from 10 to 20 applied in this investigation, the error is considered to be negligible.

The field intensity in the region near the cylindrical wall of the cavity is different from the value given by the equation 2.2.7, as shown in chapter 4. where field distributions are treated in detail. Therefore, the equation 2.2.8 is valid only for the area A in the central part of the cavity where equation 2.2.7 is valid.

Example 3. The Spherical Cavity.

Let us consider a spherical cavity with a diameter of D introduced in the insulation material with the relative permittivity and conductivity $\gamma = 0$ between plane parallel electrodes. If the reduced distance d_r between the electrodes is in the order of twice the cavity diameter, the field is essentially uniform in the cavity (section 4.0). The field intensity is (litt. 22):

$$E(x, t) \simeq \frac{3\varepsilon_1}{1 + 2\varepsilon_1} \cdot \frac{u(t)}{d} \qquad (2.2.11)$$

and the expression for the discharge current becomes:

$$i(t) = \frac{3\varepsilon_1}{(1 + 2\varepsilon_1) \cdot d} \cdot \int_V \rho \cdot \vec{v} \cdot dV \qquad (2.2.12)$$

where V is the cavity volume. The validity of equation 2.2.12 as well as equation 2.2.8 is limited according to the assumptions made concerning the uniformity of the field in the cavity. When the field intensity in the cavity changes during the discharge, the more general equation 2.2.6 must be applied and solved by numerical methods. This approach is treated in chapter 4.

The Relationship Between the Measured Voltage and the Discharge Current i(t) for the Developed Electrode System.

Consider the equivalent circuit for the electrode system shown in fig 2.6. The internal transient discharge current treated above is represented by a current source i(t). Due to the capacitances C_R and C_{ab}, the current

through the measuring shunt R in parallel combination with Z is different from i(t). The relation between the measured voltage $u_R(t)$ and the

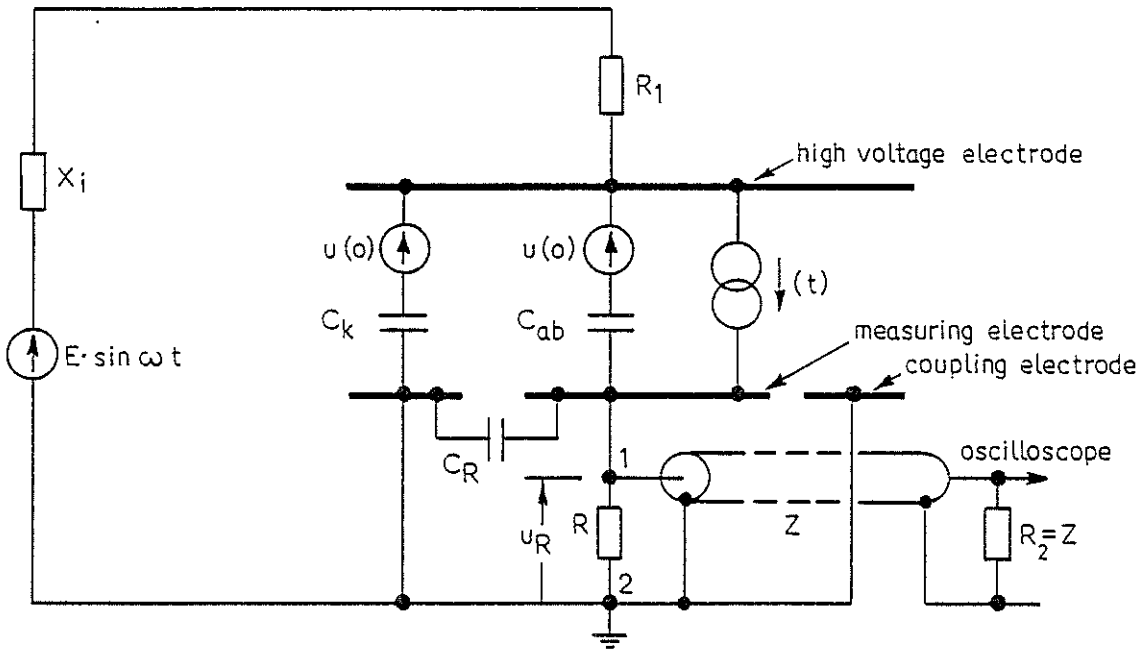

Fig. 2.6.
Equivalent circuit for the electrode system and high voltage supply. $C_k >> C_{ab}$, $C_k >> C_R$, $R_1(C_k + C_{ab}) << \omega$.

i(t) will be determined below. The high voltage is applied to the electrodes through a high resistance R_1 (= 330 kΩ). The charging time constant is in the order of 20 μs. This time constant is large in comparison to the duration of the individual partial discharges. Hence, it is permissible to neglect the exchange of energy between electrodes and the high voltage supply during a discharge. Consequently, the circuit traced from the measuring electrode through C_{ab}, the high voltage electrode, the coupling capacitance, and back to the measuring electrode through the measuring resistance R, may be considered as isolated from the high voltage source during a discharge. The capacitances C_k and C_{ab} are at the time t = 0 charged to the voltage u(o). These initial values of the voltages are represented by two step voltage generators u(o) connected in series with the capacitances C_k and C_{ab}.

The initial value of the voltage u_R is assumed to be $u_R(o) = 0$. By Norton's theorem in Laplace plan the current through the parallel combination of Z and R (Z//R) is given by:

$$i_R(s) = i_{sc}(s) - Y_o(s) \cdot u_R(s)$$

where i_{sc} and $Y_o(s)$ are the short circuit current and the equivalent operational admittance at the terminal-pair 1 - 2, respectively. The sum of the step voltage sources u(o) in the circuit considered above is zero. Hence, the short circuit current at the terminal-pair 1 - 2 is:

$$i_{sc} = i(s) \cdot \frac{C_k}{C_k + C_{ab}}$$

Insertion of i_{sc} together with $u_R(s) = i_R(s) \cdot R//Z$ and

$$Y_o(s) = s\left(\frac{C_k \cdot C_{ab}}{C_k + C_{ab}} + C_R\right) = s \cdot C$$

where $C = C_k \cdot C_{ab}/(C_k + C_{ab}) + C_R$, leads to the expression for the measured voltage in the s domain:

$$u_R(s) = \frac{C_k}{C_k + C_{ab}} \cdot \frac{Z//R}{1 + s\ R//Z \cdot C} \cdot i(s) \qquad (2.2.13)$$

For an arbitrary current i(t), the measured voltage is given in the time domain by the convolution integral:

$$u_R(t) = \frac{C_k}{C_k + C_{ab}} \cdot \frac{1}{C} \cdot \int_o^t e^{-\frac{(t-\tau)}{R//Z \cdot C}} \cdot i(\tau) \cdot d\tau \qquad (2.2.13\ a$$

As an example, the case where i(t) is a step function is considered. Then evaluation of the right hand integral in equation 2.2.13 a gives:

$$u_R(t) = \frac{C_k}{C_k + C_{ab}} \cdot R//Z \cdot \left(1 - e^{-\frac{t}{Z//R \cdot C}}\right) \cdot i(t) \qquad (2.2.13\ b)$$

and

$$u_R(t) \approx \frac{C_k}{C_k + C_{ab}} \cdot R//Z \cdot i(t) \quad \text{for} \quad t > 3 \cdot R//Z \cdot C \qquad (2.2.13\ c)$$

The expression for the discharge current i(t) can be obtained from equation 2.2.13 by inverse Laplace transformation. The result is:

$$i(t) = \frac{C_k + C_{ab}}{C_{ab}} \cdot \frac{1}{R//Z} \left(u_R(t) + R//Z \cdot C \frac{d\,u_R}{dt}\right) \qquad (2.2.14)$$

When the time constant $\tau_2 = R//Z \cdot C$ is small in comparison to the rise time of the voltage u_R, then

$$u_R(t) \gg R//Z \cdot C \cdot \frac{d\,u_R}{dt} \qquad (2.2.14\ a)$$

and the discharge current can be calculated as:

$$i(t) = \frac{C_k + C_{ab}}{C_k} \cdot \frac{1}{R//Z} \cdot u_R(t) = k_1 \cdot u_R(t) \qquad (2.2.14\ b)$$

This equation is of great practical importance since the discharge current can be computed in a simple manner from the measured voltage, if the validity of the presupposition 2.2.14 a has been proved.

The Time Constant and the Sensitivity of the Electrode System.

The time constant is:

$$\tau_2 = R//Z \cdot \left(\frac{C_k \cdot C_{ab}}{C_k + C_{ab}} + C_R\right) \qquad (2.2.15)$$

C_k and C_{ab} are mainly affected by the thickness and permittivity of the test sample, C_R is determined as the resultant capacitance between the measuring electrode and the coupling electrode, measured at the terminals 1-2 (fig. 2.6) with the high voltage electrode removed. In principle, R can be chosen arbitrarily. Under practical conditions, R was omitted in order to obtain maximum sensitivity.

In order to minimize the time constant, a study was made of the influence of the geometry of the low voltage electrode, its termination, and the influence of the material isolating the measuring electrode from the coupling electrode. For different constructions, the time constant τ_2 was calculated from equation 2.2.15 and independently determined from measurements of the reflection at the terminals 1-2 for a unit step applied to a measuring cable. As regards the construction of the low voltage electrode, it was found that the predominant factors affecting C_R, and thereby τ_2, were: the area of the measuring electrode, the thickness and permittivity of the insulation between this electrode and the coupling electrode and the symmetry of its termination. Reduction of the area and the permittivity as well as an increase of the distance between the electrodes decreased the value of τ_2.

Great care was taken to eliminate the inductance in the termination of the low voltage electrode. This was possible only by means of a coaxial connection. In this way, it was possible to achieve a step reflection from the terminals 1-2 which was non-oscillatory.

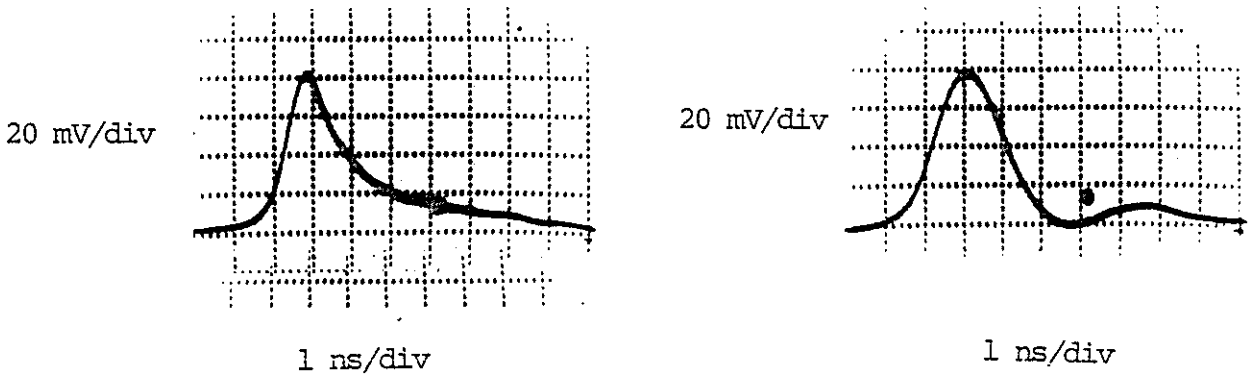

Fig. 2.7.
Comparison of the responses of two different electrode systems to the same types of partial discharges. a: the system shown in fig. 2.3 with a coaxial connection built into the coupling electrode; b: the system using non-coaxial terminals on the measuring and coupling electrodes. The same test sample was used in both cases: $d_1 = d_2 = d = 0.02$ cm, polyethylene.

A comparison of the responses of two differently terminated systems to partial discharges of the same type is shown in fig. 2.7. The rise time of the impulse measured in the present system, fig. 2.7 a, is obviously less than that in fig. 2.7 b. The oscillations in fig. 2.7 b are due to inductance in the second system which arises due to a non-coaxial termination.

In table 2.2 are listed the measured capacitances and time constants determined from equation 2.2.15 for two typical test samples mounted between the electrodes. The capacitances C_k and C_{ab} were measured using a three terminals method by means of the capacitance bridge (litt. 23) at 1 kHz; capacitance C_R was measured by a two terminals method as the capacitance in excess of the capacitance of a short coaxial cable by means of which the electrode was connected to the bridge. The accuracy of the bridge was better than 0.1 %. The uncertainty in the values of C_k and C_{ab} were of the order of 0.5 % because of the change of the force with which the high voltage electrode and low voltage electrode were compressed when the test cell system was fully assembled.

TEST SAMPLE $d_1=d_2=d$ $\varepsilon_1=2.3$	$\frac{d_3}{\varepsilon_3}$	C_k	C_{ab}	C_R	C	τ_2	k_2
cm	cm	pF	pF	pF	pF	ns	mA/mV
0.20	0.05	12.2	1.1	7.9	9.0	0.45	$43 \cdot 10^{-3}$
0.02	0.05	30.4	4.0	7.9	11.4	0.57	$87 \cdot 10^{-3}$

Table 2.2.

The time constants τ_2 and the factors k_2 for two typical test samples assembled between the electrodes.

The Sensitivity of the System.

For the present purposes, the sensitivity is defined as the smallest current flowing along the axis of a cylindrical cavity, detectable by the measuring system within its bandwidth. Insertion of equation 2.2.10 into equation 2.2.14 b gives for $i_d(t)$:

$$i_d(t) = k_2 \cdot u_R(t) \qquad (2.2.16\ a)$$

$$\text{in which } k_2 = \frac{C_k + C_{ab}}{C_k} \cdot \frac{1}{R//Z} \cdot \frac{d + (d_1 + d_2)/\varepsilon_1}{d}$$

When the electrodes are embedded in epoxy resin with the permittivity ε_3, the total thickness d_3 of both resin layers covering the electrodes must be taken into account; k_2 thus becomes:

$$k_2 = \frac{C_k + C_{ab}}{C_k} \cdot \frac{1}{R//Z} \cdot \frac{d + (d_1 + d_2)/\varepsilon_1 + d_3/\varepsilon_3}{d} \qquad (2.2.16\ b$$

where d, d_1, d_2, ε_1 are the cavity depth, the thicknesses of the insulation discs, and their relative permittivity, repectively. Since pulses of a magnitude of 1 mV were observable on the display, the existence of internal discharges of the magnitude order $i_d = k_2 \cdot 1$ mV could be detected. Values of the factor k_2 calculated for two typical test samples are listed in table 2.2. The values of k_2 were determined with an accuracy better than 2 %.

The current pulses were observed and recorded by means of a digital transient recorder (Tektronix, type R 7912 Transient Digitizer, rise time 0.8 ns), or alternatively by means of an oscilloscope. The oscilloscope used, Tektronix type 485, had a bandwidth of 350 MHz corresponding to a rise time of 1.0 ns. The advantage of the use of the digital transient recorder was that it became possible to observe and simultaneously record even the fastest impulses within the bandwidth of the electrode system. The longest resulting rise time for the coaxial measuring system including the electrode system, cables, and the oscilloscope was calculated to 1.6 ns.

2.2.2. Measurement of the light emission from a partial discharge.

The radiation is emitted from the partial discharge when atoms or molecules excited by inelastic collisions with the drifting electrons return to the ground state. Hence, the measurement of the photon flux emitted from a partial discharge provides information about the electronic component of the total discharge current given by equation 2.2.1. A suitable application of both methods allows the measurement of the total discharge current together with its electronic component. The

waveform of both components could be computed for a slowly developing discharge (section 4.1). The use of both methods made it possible to prove whether there was any correlation between the theoretically computed and the measured values. These were the main reasons for the development of the technique which allowed the measurement of very fast photon flux pulses emitted from a partial discharge in an open test sample.

In a photomultiplier tube, a part of the radiant energy emitted from a partial discharge is converted into electrical energy. In this subsection, the relation between the photomultiplier anode current and the number of photons emitted per unit time from a partial discharge within the range of the spectral sensitivity of the photomultiplier is evaluated, and the uncertainty of the measuring method is discussed.

The Number of Photons Emitted From a Partial Discharge.

The total number of atoms and molecules excited by one electron drifting a unit of length in the field direction is defined as the excitation coefficient δ. The number of excited states per ionizating collission Q is thus the ratio between the excitation and the ionization coefficients:

$$Q = \frac{\delta}{\alpha} \tag{2.2.17}$$

Due to the fact that the mean life time of excited states is short in comparison to the mean time between inelastic collissions, and that each excited atom (or molecule) emits one photon when it returns to the ground state, the mean number of photons emitted from the discharge in the cavity in the unit time is:

$$\frac{dp'}{dt} = \int_V Q \cdot \alpha \cdot \frac{\rho_-}{e} \cdot \vec{v} \cdot \vec{d} \cdot dV \tag{2.2.18}$$

where ρ_- and $\vec{v}$ are the electron density and the drift velocity, respectively; $\vec{d}$ is a unit vector in the field direction and e is the charge of the electron; the integration is extended throughout the

cavity volume V. The photon flux dp'/dt is related to the electron current i(t). By combination of equation 2.2.9 with equation 2.2.18 the relation for a plane parallel gap with uniform field conditions can be expressed as:

$$\frac{dp'}{dt} = \frac{\alpha \cdot d \cdot Q \cdot i_{-}(t)}{e} \qquad (2.2.18\ a$$

Spectral Emission Characteristics of a Partial Discharge.

The radiation emitted during the formation of a partial discharge in an air-filled cavity has been measured by Bashara (litt. 24) in a test range of 220 - 700 nm in open and closed gaps. The measured wave lengths λ were found in the range between 300 nm and 450 nm, centered around 350 nm. These values agree with those measured by Legler (litt. 25) for discharges in air between plane parallel electrodes: $330 < \lambda < 360$ nm with maximum light at 345.0 ± 15 nm, in the range of the parameter p · d (pressure x gap distance) of 20 - 120 torr · cm.

The spectra of the radiation emitted from the corona discharges from both 30 mm hemisphere and 1 mm cone tip to a plane in atmospheric air have been measured by Galimberti, Hepworth and Klewe (litt. 26) in the test range of 330 - 560 nm. The corona spectra were composed of the radiation of neutral and ionized oxygen molecules. In the region 330 - 450 nm, which is approximately the same as the sensitivity range of the photomultiplier used in the present measurements, the emission of the neutral nitrogen molecules was predominant. The most intense band within this system was centered at 358 nm.

Since there is a quantitatively close agreement between Bashara's (litt. 24), Legler's (litt. 25), and Galimberti, Hepworth and Klewe's (litt. 26) determinations of wave lengths of the light from partial discharges, discharges between parallel electrodes, and corona discharges, respectively, it can be assumed that the spectrum emitted from partial discharges in the wave length range 330 - 560 nm is mainly determined by emission of the neutral nitrogen molecules. The intensities of the different bands normalized to the intensity of the 381 nm band are listed in table 2.3.

WAVELENGTH λ_i	RELATIVE INTENSITY	q_i
354	0.55	0.29
358	2.01	0.30
371	0.18	0.31
375	0.60	0.31
381	1.0	0.32
395	0.12	0.31
400	0.33	0.31
406	0.31	0.30
420	0.1	0.28
427	0.13	0.26
435	0.10	0.25
458	0.07	0.23

Table 2.3.

The intensities of the bands of neutral nitrogen molecules (litt. 26) normalized to the intensity of the 381 nm band. The typical bandwidth is less than 2 nm, and the intensity between the bands is equal to zero.

Photomultiplier Anode Current.

A photomultiplier converts an incident flow of light quanta into an electric current by means of the photoemission process. The electrons are liberated from a cathode by the interaction of incident photons with the cathode material. The efficiency of the emission from the photocathode depends on the photocathode material and the wavelength of the incident radiation. Accordingly, the number of photoelectrons liberated from the photocathode per incident light quant with the wavelength λ_i is defined as the quantum efficiency $q(\lambda_i)$. The spectral response of a function of the wavelength - $q(\lambda)$. The spectral response for the photomultiplier used in the present measurements is shown in fig. 2.8.

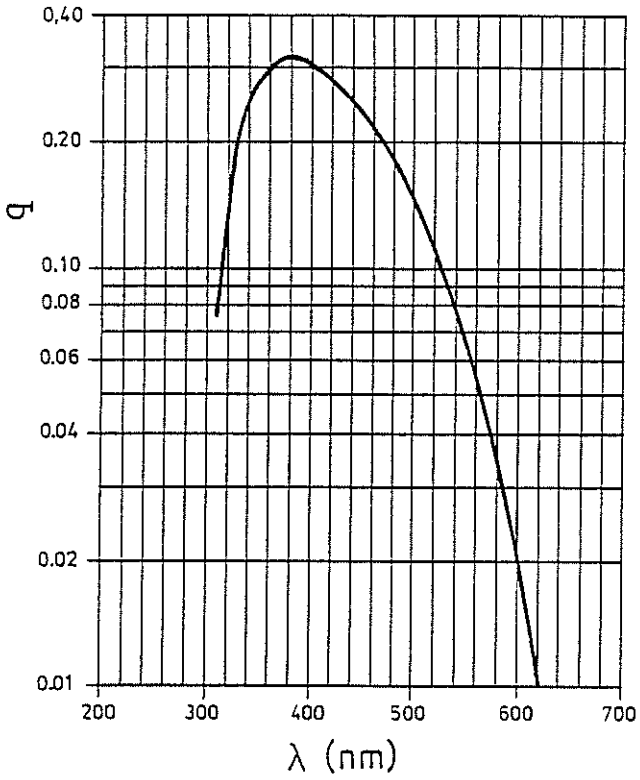

Fig. 2.8.
The quantum efficiency q as a function of wavelength for the RCA type C 31024 photomultiplier.
Potassium - Cesium - Antimony cathode.

The photoelectrons emitted from the photocathode are accelerated towards the first dynode where they release secondary electrons by inelastic collisions. The secondary emission, which is repeated in the succeeding dynodes, causes a multiplication of the electrons. The photomultiplier gain V due to the electron multiplication is equal to the mean number of electrons collected at the anode per photoelectron liberated from the photocathode.

In order to measure the photon flux emitted from a partial discharge, the probability that one emitted photon will liberate a photoelectron must be determined. Assume that photons originating from a partial discharge are emitted in random directions from the discharge cen-

tre. Since the photons striking the photocathode are emitted into a solid angle Ω, the probability that a photon will strike the photocathode is given by a geometry factor:

$$g = \frac{\Omega}{4\pi} = \frac{A_c \cdot \cos\Theta}{4\pi r_c^2} \qquad (2.2.19)$$

where A_c is the effective area of the photocathode, r_c is the distance between the discharge centre and the photocathode, and $\cos\Theta$ is the angle between the line of radiation and the normal to photocathode.

If a diaphragm with a diameter d_d is placed directly in contact with the photomultiplier face at a distance r_d from the discharge centre, the geometry factor becomes:

$$g = \frac{1}{16}\left(\frac{d_d}{r_d}\right)^2 \qquad (2.2.19\ a)$$

Under the assumption that the incident photons are continuously distributed in the wavelength interval (o, λ), the distribution is given by:

$$N(\lambda) = \int_o^\lambda n(\lambda) \cdot d\lambda \qquad (2.2.20)$$

where $N(\lambda)$ is the number of photons in the wavelength interval (o, λ), $n(\lambda)$ is the spectral density of photons per unit wavelength, and $n(\lambda) \cdot d\lambda$ is the number of photons in the wavelength increment $d\lambda$. Hence, the number of photoelectrons emitted from the photocathode becomes:

$$\int_o^\infty n(\lambda) \cdot q(\lambda) \cdot d\lambda \qquad (2.2.21)$$

With equations 2.2.20 and 2.2.21 the probability of emitting one photoelectron per incident photon is given by:

$$m_d' = \frac{\int_0^\infty n(\lambda) \cdot q(\lambda) \cdot d\lambda}{\int_0^\infty n(\lambda) \cdot d\lambda} \qquad (2.2.23)$$

where the integral in the denominator gives the total number of incident photons. The factor m_d', which quantitatively describes the degree of matching of the photomultiplier spectral response to the total spectrum emitted from the partial discharge, will henceforth be called the discharge matching factor in agreement with the terminology applied in electro-optics.

Equation 2.2.23 which expresses the matching factor m_d' was derived under the assumption that the incident photons were continuously distributed. However, from the values given in table 2.3 it is evident that for a gas discharge the distribution is discrete, since the radiation intensity in intervals between the bands is equal to zero. The matching factor for such a distribution becomes:

$$m_d = \frac{\sum_{i=1}^{\ell} n(\lambda_i) \cdot q(\lambda_i)}{\sum_{i=1}^{\ell} n(\lambda_i)} \qquad (2.2.23\ a)$$

where ℓ is the number of bands emitted from the partial discharge within the spectral range of the sensitivity of the photomultiplier. Consequently, the factor m_d describes the degree of matching of the photomultiplier spectral response to the spectrum emitted from the partial discharge. If the spectral densities are normalized to the density of the band λ_k, then:

$$m_d = \frac{\sum_{i=1}^{\ell} \frac{n(\lambda_i)}{n(\lambda_k)} \cdot q(\lambda_i)}{\sum_{i=1}^{i=\ell} \frac{n(\lambda_i)}{n(\lambda_k)}} \qquad (2.2.23\ b)$$

For the photomultiplier used in the present measurements, the matching factor was determined by inserting the relative intensities from table 2.3 as the relative spectral densities in equation 2.2.23 b. The matching factor was calculated as $m_d = 0.30$. The region of the maximum sensitivity of the used photomultiplier corresponded closely to the wavelength of the most intense radiation. Hence, the factor m_d can also, as a first approximation, be computed equal to the quantum efficiency $q(\lambda)$ at the wavelength equal to 358 nm (≈ 0.30).

By means of equations 2.2.19 and 2.2.23 it is now possible to relate the photon flux radiated from the partial discharge in the range of the spectral sensitivity of the photomultiplier to the anode current. If it can be assumed that the photons are emitted at random intervals, the anode current i_a is given by:

$$i_a = V \cdot g \cdot m_d \cdot e \cdot \frac{dp}{dt} \qquad (2.2.24)$$

where V is the photomultiplier gain, g is the probability that the emitted photon will strike the cathode, m_d is the probability of the emission of a secondary electron per incident photon, i.e. the matching factor, e is the charge of electron, dp/dt is the average number of photons emitted from a partial discharge in unit time within the spectral range of the photomultiplier sensitivity.

During the measurements the photomultiplier was mounted in a tube built into the cylindrical wall of the discharge chamber, fig. 2.3, 8. The multiplier tube was held in position by adjustable screws so that the photocathode surface was orthogonally oriented towards the path of the light emitted from the partial discharge. The measuring circuit is shown in fig. 2.9. When the time constant of the multiplier output is small in comparison to the rise time of the voltage u_{R1} the photon flux can be determined as:

$$\frac{dp}{dt} = k_3 \cdot u_{R1}(t) \qquad (2.2.25)$$

where

$$k_3 = \frac{1}{R_1 \cdot V \cdot g \cdot m_d \cdot e} \qquad (2.2.26)$$

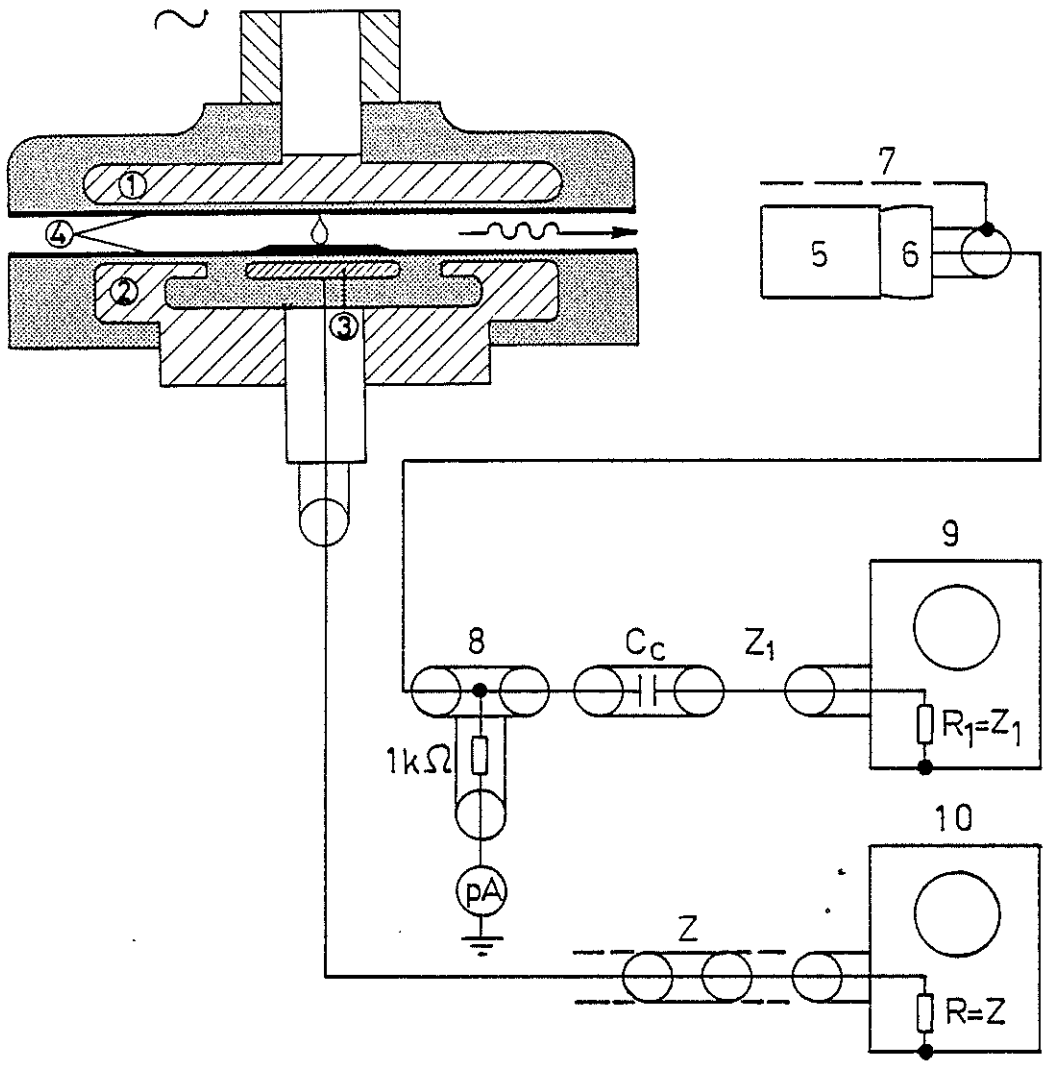

Fig. 2.9.

The fast photomultiplier light detection circuit. 1, 2, 3: high voltage, coupling, and measuring electrodes, respectively; 4: open test sample (fig. 2.2.); 5: photomultiplier, RCA C 31024; 6: photomultiplier assembly including a voltage divider network; 7: external shield; 8: coaxial GR-"tee" unit; pA: picoammeter Keithley 601; 9, 10: oscilloscopes Tektronix 485, t_r = 1 ns, and Tektronix 454, t_r = 1.5 ns, respectively; Z_1; low distortion RG 13 U cable (Z_1 = 50 Ω); Z: RG 58 cable (Z = 50 Ω). The "tee" unit was ordinarily used only for initial measurements of the dark current. The electrodes are shown in true size.

The Accuracy of the Measurements.

The RCA type C 31024 photomultiplier used, operating with AJ 2219 auxilliary assembly at negative cathode voltage, was specially tested by the manufacturer. The test data supplied are given below:

- photocathode sensitivity: 10 μA/lm ± 5 %.
- current gain: $V = 1.5 \cdot 10^5$ at 2000 volts
  $= 1 \cdot 10^6$ at 2970 volts.
- dark current: 1.3 nA at 2000 volts
  and 3 nA at 3000 volts.

The photomultiplier gain characteristic can be approximated by a simple empirical function:

$$V = k_4 \cdot \{U\}^{k_5} \qquad (2.2.27)$$

where V is the gain, {U} is the numerical value of the operating voltage, and the coefficients $k_4 = 2.18 \cdot 10^{-11}$ and $k_5 = 4.798$. From the equation above, the relative gain variation $\Delta V/V$ due to a small variation of the operating voltage $\Delta U/U$ is given by:

$$\frac{\Delta V}{V} = k_5 \cdot \frac{\Delta U}{U} \qquad (2.2.27\ a)$$

The stability of the operating voltage was better than 10 p.p.m., and the voltage was known within ± 1 %. Hence, by virtue of equation 2.2.27 a, the gain was determined with an accuracy better than ± 5 %.

The specified anode-pulse rise time as supplied by the manufacturer is 1.2 ns with the photomultiplier operating at 3000 V. According to the manufacturer, this specified rise time was not corrected for the rise time of 0.5 - 0.8 ns of the light source used. In the case of measurements of partial discharges with high specific radiation and short rise time a reduction of the rise time was obtained by illuminating only a small central area of the photocathode through a 0.5 cm diaphragm. The advantage in time performance using the diaphragm was that a time

broadening of the electrons produced due to a longer transit time for electrons liberated at the photocathode and dynode edges was avoided. In order to obtain a fast overall rise time RG-13/u cable and GR high frequency connectors were used. The overall rise time of the photomultiplier in connection with the 350 MHz oscilloscope used was calculated to be better than 1.5 ns.

Below are listed those values of the factors and quantities attributed to equations 2.2.19 - 2.2.26 which were essential for the present measurements:

R_1 : $50\ \Omega \pm 0.1\ \%$

V : $1.48 \cdot 10^5 \pm 5\ \%$ (a)

g : $1.0 \cdot 10^{-3} \pm 5\ \%$ for $d = 0.05$ cm
$1.1 \cdot 10^{-3} \pm 5\ \%$ for $d = 0.07$ cm
$1.3 \cdot 10^{-3} \pm 5\ \%$ for $d = 0.1$ cm } (b)

g : $4.8 \cdot 10^{-5} \pm 2\ \%$ (c)

m_d : $0.30 \frac{\text{electron}}{\text{photon}} \pm 5\ \%$

$r_c \approx r_d$: 18.7 cm ± 0.1 cm (b)
18.0 cm ± 0.1 cm (c)

d_d : 0.5 cm ± 0.01

k_3 : $5.3 \cdot 10^{16} \pm 15\ \% \frac{\text{photon}}{\text{s}}/\text{V}$ (c)

k_3 : $2.5 \cdot 10^{15} \pm 12\ \%$ for $d = 0.05$ cm
$2.3 \cdot 10^{15} \pm 12\ \%$ for $d = 0.07$ cm
$1.9 \cdot 10^{15} \pm 12\ \%$ for $d = 0.1$ cm } (b)

(a) - at cathode voltage 1995 ± 1 %.

(b) - without a diaphragm; the solid angle was limited by the electrodes.

(c) - with a diaphragm.

The changes in operating stability of a photomultiplier due to the tube fatigue or loss of sensitivity was not taken into account in the above analysis. These changes were believed to be less than 15 %.

2.2.3. Estimation of the lateral extension of partial discharges.

The methods described in the previous subsections have particularly made it possible to study the wave forms of definite types of partial

discharges. It was expected that the extension of partial discharges in directions orthogonal to the field direction, i.e. the lateral extension, varied with the discharge type. As a matter of fact, a study of the topography of a surface deteriorated by discharges clearly showed that craters appeared along the cylindrical wall of the cavity. The craters could very well be remains of the action of a specific discharge type which occurred only along this wall. The methods employed at that time, however, did not provide any direct information, neither on the lateral extension of the distinct types, nor on the occurrence of the possible local discharges over the surface. For these reasons, a method was developed permitting a rough estimation of the lateral extension of a discharge and the place of occurrence of a discharge, and additionally, the measurement of the waveform of the current induced by a discharge.

A cross-sectional view of the low voltage electrode used for this method is shown in fig. 2.10. On the measuring part of the electrode there are three small, conductive islands 1, 2, and 3, separated from each other and from the electrode 4 by a narrow non-conductive area. The islands together with the electrode 4 constitute a system of current probes connected with their respective coaxial cables 5, the screens of which are joined to the coupling electrode 6. Thus, a partial discharge produces a change in the density of charges induced in the probes. It was experimentally established that a current induced by a local partial discharge crossing the gap directly in the space over a given probe was 100 - 1000 times greater than the currents induced by the same discharge in the remaining probes. This was valid when the cavity debth was small in relation to the probe diameter $d/D < 5$. The currents induced in the probes are compared on the screen of the dual-beam oscilloscope thus providing information about the lateral extension of a discharge.

The oscillograms obtained by the methods described in the three previous subsections were frequently additionally elaborated by means of a digitizer developed at the laboratory in connection with the computer which plotted the obtained oscillograms in suitable coordinate systems.

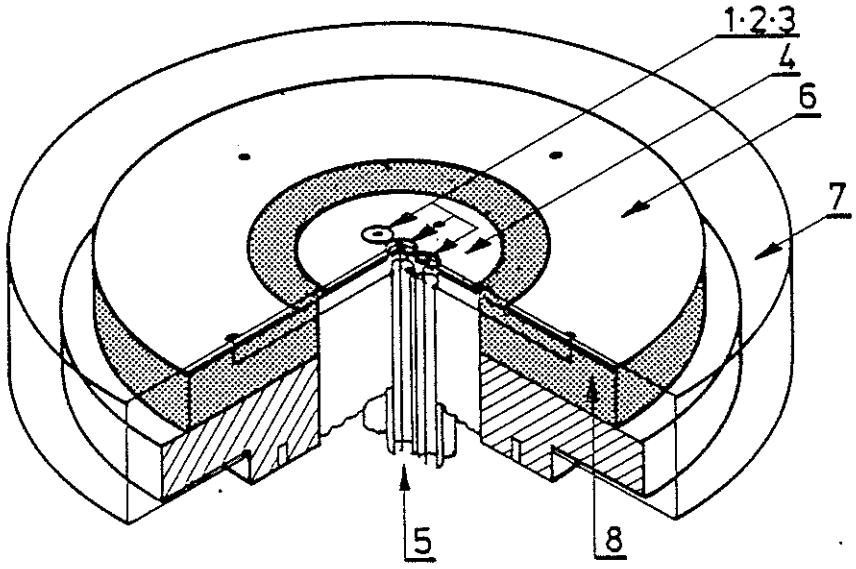

Fig. 2.10.
Low voltage electrode used for the measurement of the lateral extension of a partial discharge.

1, 2, 3: current probes insulated from the electrode; 4: electrode; 5: coaxial cables; 6: coupling electrode; 7, 8: insulation.

2.3. Methods for the Measurement and Automatic Recording of Magnitude Distributions and Repetition Rates.

According to equations 2.2.7 and 2.2.11, the field intensity in the cavity is a function of the voltage applied to the electrodes, and consequently under alternating voltage conditions it becomes a periodic function of time. When the amplitude of the field intensity reaches a certain value, called the ignition fiels stress E_i, a current will flow through the cavity in the form of consecutive current pulses the waveforms of which can be measured by means of the methods described in subsection 2.2. The total number of current pulses occurring in unit time is defined as the discharge repetition rate $\dot{N}$. Within a given pulse sequence the pulses with a particular peak value u_i appear at the corresponding repetition rate $\dot{n}(u_i)$. The cumulative discharge repetition rate is thus the sum of repetition rates of all pulses with peak

values smaller than or equal to u:

$$\dot{N}(u) = \sum_{u_i \leq u} \dot{n}(u_i) \qquad (2.3.1)$$

where $\dot{n}(u_i)$ is the repetition rate at peak value u_i.

$$\dot{n}(u) = \begin{cases} \dot{n}(u_i) & \text{when } u = u_i \quad (i = 1, 2, \ldots) \\ 0 & \text{otherwise} \end{cases}$$

2.3.1. Measurements of repetition rates and magnitude distribution.

In practice, it is difficult to obtain the cumulative distribution given by equation 2.3.1 due to the finite sensitivity of the measuring equipment, because it is impossible to measure the number of discharges having magnitudes below the sensitivity level of the detecting oscilloscope. Therefore, the repetition rate of current pulses with amplitudes greater than or equal to u have been measured instead. The distribution is thus given by:

$$\dot{N}'(u) = \sum_{u_i > u} \dot{n}(u_i) \qquad (2.3.1\ a)$$

The distributions have been obtained by means of a frequency counter connected to the gate output of the oscilloscope by counting the pulses with a magnitude higher than a preset triggering threshold. The counting was performed for different triggering levels, and the mean curve between the measured points (u, N'(u)) was interpolated graphically. Some points of the distribution were recorded several times in order to examine the time dependence of the distribution.

2.3.2. Automatic recording of repetition rates.

In order automatically to analyse the current pulses and record the repetition rates during long term tests, a technique employing an extremely fast analyzer was developed at the laboratory. The elements of the measuring system are shown in fig. 2.11.

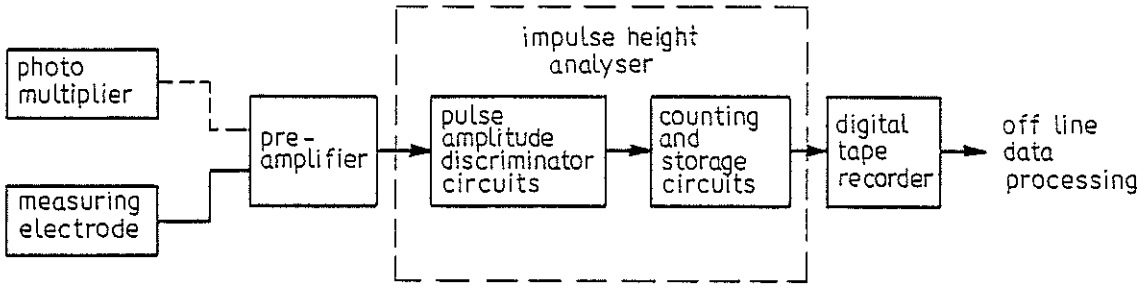

Fig. 2.11.

Elements of a fast pulse counting system.

The pulses are amplified in the preamplifier before they enter the adjustable pulse amplitude discriminator. The pulse discriminator contains the voltage controlled attenuator, amplifier circuits, pulse shaping circuits and a comparator circuit. The attenuator changes cyclically at five preselected values of attenuation. During each measuring period, only the pulses of the amplitude greater than the triggering level are able to trigger the counters, the number of pulses being stored in a memory. From the storage circuits the number of pulses with amplitudes above a particular level is transferred to the digital tape recorder at the end of each measuring period. The analyser is capable of providing the measuring and sorting of very fast current pulses. The transfer properties of the analyser and its limitations have been discussed in detail by Levring (litt. 27). The general specifications for the analyser together with a Hewlett-Packard, type 462, preamplifier are listed below:

bandwidth: 5 - 100 MHz.
sensitivity: 0.5 mV for slowly developing discharges and 60 μV for step impulses.
5 adjustable triggering levels; counting period at each level: 1 minute.
maximum counting rate: 200 kHz
digital cassette tape recorder output.

The results of the measurements recorded by the analyser were evaluated employing numerical techniques for the interpolation of the results and the plotting of the distributions.

2.4. Methods for the Measurement of the Conductivity and Topography of the Test Sample Surface.

During partial discharge action the surface of the cavity notably changes its microscopic parameters in terms of mobilities and densities of charged particles within the insulant, and its structure and composition. During prolonged partial discharge action, these changes lead to changes in the experimentally accessible parameters: chemical composition, topography of the cavity surface and its conductivity. The conductivity study seems to be of great importance for the clarification of the microscopic processes leading to an extensive deterioration or to breakdown (litt. 28). An experimental technique, employing a three-terminal probe by means of which the changes in surface conductivity of small areas exposed to discharge action can be detected, is described in the following subsection.

Features of the test sample surface are usually too small to be studied by the naked eye. A scanning electron microscope was therefore employed, its extraordinary combination of high resolution and great depth of focus permitting a stereoscopic examination of the surface topography. In subsection 2.4.2, some information is given on the theory of operation of the electron microscope which is sufficient as a guidance for the preparation of the test specimens and the microscopic methods.

2.4.1. Measurement of the surface conductivity.

The electrical conductivity is generally described by the equation:

$$\sigma = \sum_k \rho_k \cdot \mu_k \qquad (2.4.1)$$

where ρ_k is the volume densities, and μ_k the mobilities (the drift velocities per unit field) of charge carriers within the material. For the homogeneous material the bulk conductivity measured between two plane parallel electrodes may be calculated from Ohm's law:

$$\sigma = \frac{j}{E} = \frac{d}{R \cdot A} \qquad (2.4.2)$$

where j is the current density, E is the field intensity, d is the di-

stance between the electrodes, A is the electrode area, and R is the resistance measured between the electrodes.

In the case of low conductivity materials, the surface is often the path of the largest conductance in which case the surface conductivity σ_s is a conductance measured between two opposite sides of a surface square. It is desired to express the surface conductivity in terms of the resistance measured between a circular electrode and a concentric, ring-shaped electrode, both placed on the surface. The inner and outer radii of the ring-shaped surface between the electrodes are r_1 and r_2, respectively. Hence, the resistance dR of a ring with radius r and width dr becomes:

$$dR = \frac{1}{\sigma_s} \cdot \frac{dr}{2\pi r}$$

Upon integration of the above equation from r_1 to r_2, the surface conductivity can be calculated as (litt. 29, 30):

$$\sigma_s = \frac{1}{2\pi R} \cdot \log_e \frac{r_2}{r_1} \qquad (2.4.2)$$

As a rule, the conductivity was measured on the test samples shown in fig. 2.1. The surface conductivity of each specimen tested was measured using a three-terminal probe developed for this purpose (fig. 2.12). The probe contained two coaxial brass electrodes 1 and 2. The guard 3, located between them, collected the internal leakage current flowing through the insulation between the electrodes. This current flowed directly through the voltage supply u bypassing the picoammeter pA. Therefore, only the surface current was measured by the picoammeter.

The test voltage to the electrodes was supplied by a regulated, highly stabilized ($\sim 5 \cdot 10^{-6}$) dc voltage supply, and the current was measured with a Keithley, model 601, picoammeter. The pressure exerted by the electrodes on the sample was typically 250 N/cm^2. During the measurements, the test sample was removed from the discharge chamber (fig. 2.2), the probe was pressed onto the sample surface, and 20 seconds thereafter the picoammeter was read. The test sample was then replaced in the discharge chamber and again exposed to partial discharges. In this way, the surface conductivity of the test sample was recorded as a function of time during tests of a duration of up to 100 hours.

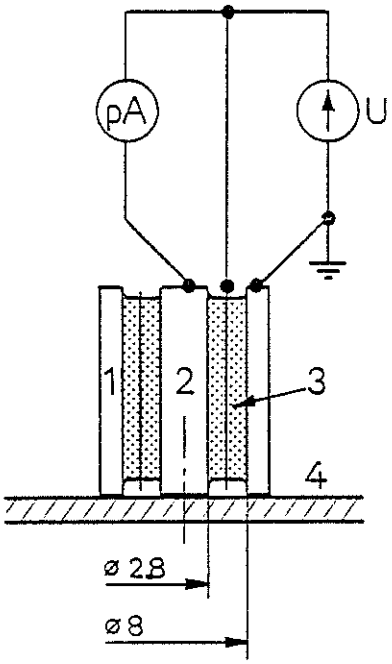

Fig. 2.12.
Circuit for measuring surface conductivity.
1, 2: electrodes; 3: guard; pA: picoammeter;
u: dc voltage supply; 4: test specimen surface.

Great care was taken in establishing known and reproductable conditions. A study was made of the variation of the measured conductivity with the applied voltage, and an ohmic region of conduction was found for the voltage range 50 - 1000 V. In order to obtain maximum sensitivity, almost all the measurements were made with 1000 V applied, and the resistance R entering equation 2.4.2 was calculated from:

$$R = \frac{u}{i_e} \qquad (2.4.3)$$

where u is the applied voltage, and i_e is the picoammeter current. At pressures lower than about 100 N/cm^2 exerted on the test sample by the electrodes, the measured resistance R was greatly dependent on the pressure. Consequently, a pressure of 250 N/cm^2 was applied at which the resistance was independent of the pressure. The electrodes were polished and thoroughly cleaned before each measurement. A drift of room tempera-

ture of ± 2^{o} C was unavoidable. The influence of this drift on the results is considered negligible.

The variations in the measured surface conductivity can be due to changes both in the chemical composition and in the charge densities and mobilities of charge carriers during the tests. In real test samples, the condition of the surface is inherently inhomogeneous in terms of conductivity and topography. In this connection it should be noted that equation 2.4.2 is an expression of the conductivity of a homogeneous equivalent surface.

2.4.2. Imaging with the scanning electron microscope.

In a scanning electron microscope an extremely narrow beam of electrons, i.e. an electron probe, scans the specimen surface. The image is formed on a cathode ray tube screen by an electron beam moving synchronously with the primary electron beam.

The electrons emitted from a heated tungsten cathode are accelerated to high velocity by a high voltage applied to the acceleration plates in the electron gun. Electromagnetic lenses focus the beam of high energy electrons to a very small diameter at a point of incidence on the sample surface. These primary electrons striking the surface liberate secondary electrons in an amount which varies strongly with the slope of the surface at the point of incidence. The secondary electrons are then attracted by an electron detector where they produce an electric signal amplified by a video-amplifier.

The primary beam scans the specimen surface point-by-point. The movement of this beam is synchronized with the movement of a second electron beam in a cathode ray tube on the screen of which the image is displayed. The beam in the cathode ray tube is modulated in brightness by the signal from the video-amplifier, thereby reproducing the surface image. In a similar manner, the scanning micrographs can be obtained using backscattered, absorbed, or transmitted primary electrons or X-rays instead of secondary electrons.

Preparation of Specimens and Microscopic Methods.

From the discs originally constituting the test samples, squares containing the surface exposed to the partial discharges were carefully

cut out. The squares were then coated with a very thin layer of gold to make the insulation surface electrically conductive and thereby prevent the accumulation of electrons from the scanning beam. Gold was evaporated onto the insulation surface from a heated filament in a vacuum chamber. Thereafter, the specimens were affixed to the sample holder with conductive glue, and after a short period to allow evaporation of the solvent in the glue placed on a stage in a specimen chamber. In most cases, the micrographs were obtained, using the secondary electron technique, within a magnification range of 22 - 10000, and the acceleration voltage in the range of 15 - 20 kV. In order to distinguish whether the features protrude from the surface, or whether they constitute cavities, stereo image pairs were taken. The stereo photomicrographs were produced by taking two micrographs with sample tilted 4° in one direction, and thereafter 4° in the opposite direction about an axis perpendicular to the beam. The JSM-U3 electron scanning microscope situated at the Department of Structural Properties of Materials, Technical University of Denmark, was used in the investigation, (litt. 31).

3. ANALYSIS OF EXPERIMENTAL RESULTS.

3.1. Partial Discharge Types.

From the analysis of the oscillograms obtained throughout the investigation in air, nitrogen, and carbon dioxide, two characteristic current waveforms were distinguished. These were attributed to two basic and quite distinct partial discharge types. The properties and behaviour of these discharges during short term tests which extended over some hours are treated in subsections 3.1.1. and 3.1.2.

Terminology Regarding Voltages and Stresses.

U_{inc} - inception voltage. The ac test voltage at which discharges first appear when the test voltage is being raised.

U_{ext} - extinction voltage. The test voltage at which the discharges cease when the voltage is being lowered.

E_{ig} - the ignition field stress for the cavity.

U_{ig} - the corresponding ignition voltage appearing across the cavity.

E_r, U_r - remanent field stress in, resp. voltage appearing across the cavity.

3.1.1. The slowly developing partial discharge.

Three typical current pulses of this discharge type are shown in fig. 3.1. The duration of discharges of this type was in the range 10 ns to $3 \cdot 10^3$ ns and the measured pulse amplitudes were in the range u_R = 0.5 mV to 40 mV, the smaller amplitude being most frequent for all cavity depths and pressures investigated ($\sim 3 < p \cdot d < \sim 300$ cm·mb). Their shape did not alter as the applied voltage increased. Their waveform remained markedly regular for different values of the parameter p·d and the corresponding different inception voltages appearing across the cavity, whereas the shape altered with the pulse amplitude. This variation is shown in osc. 1 of fig. 3.1.

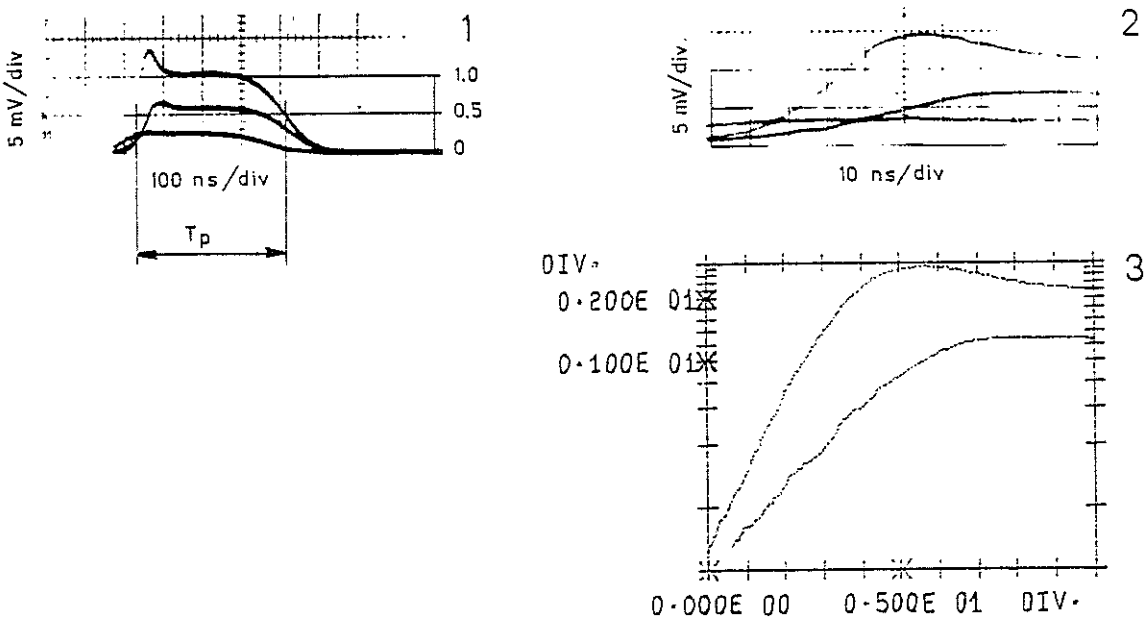

Fig. 3.1.

Typical waveforms of the current of the slowly developing partial discharge. d = 0.058, p = 990 mb, k_2 = 0.050 mA/mV. 2 and 3 show the front of the discharges shown in oscillogram 1. Negative partial discharges have similar waveforms as the positive discharges shown above due to the symmetry of the test cell.

Initially, the discharge current rises approximately exponentially, as shown in fig. 3.1-3. by means of semilogarithmic plots of the current against time. The period T_p of the pulse width at half maximum points (fig. 3.1-1.), determined by the duration of the plateau, corresponds to the transit time of the positive ions across the cavity. According to Degn (litt. 3), T_p can be approximately expressed as:

$$T_p = \frac{d}{\mu_+ \cdot (E_{ig} - \Delta E)} \left(1 - \frac{\ln 2}{\alpha\, d}\right) \qquad (3.1.1.)$$

where d is the cavity depth, μ_+ is the mobility of positive ions in air, E_{ig} is the ignition field stress in the cavity, ΔE is the field correction, and α is the ionization coefficient. The mobility μ_+ is defined as the velocity of positive ions in the field direction per unit applied field and is given by:

$$\mu_+ = \mu_{r+} \cdot \left(\frac{1013\ \text{mb}}{p}\right) \cdot \left(\frac{T}{273^{\circ}K}\right) \qquad (3.1.2.)$$

μ_{r+} being the reduced mobility which varies slightly with the reduced field stress: E/p. With equations 3.1.1. and 3.1.2. and under the assumption of T = 293 ^{o}K the product $T_p \cdot p$ is given by:

$$T_p \cdot p = \frac{p \cdot d}{(\mu_{r+} \cdot 1013) \cdot (E_{ig} - \Delta E)/p} \cdot \left(1 - \frac{\ln 2}{\alpha \cdot d}\right) \qquad (3.1.3.)$$

According to results of measurements obtained independently by Pedersen (litt. 11) and Bertein (litt. 32) the ignition voltage U_{ig} for partial discharges in a cavity is approximately given by the Paschen curve, i.e. as a function of pd. Consequently, the right hand side of the relation 3.1.3. is expected to be a unique function of the product of pressure and cavity depth: p·d. This functional dependence has been verified experimentally. The results of the measurements are plotted in fig. 3.2. together with a curve calculated using equation 3.1.3. The parameters entering equation 3.1.3. were established in the following manner.

According to Bertein (litt. 32), the ignition voltage for partial discharges in atmospheric air can be represented by an empirical function originally given by Ritz (litt. 33) and almost simultaneously by Toepler (litt. 34).

$$U_{ig} = 24.5 \cdot \{d\} + 6.7 \cdot \{d\}^{0.5} \qquad (3.1.4.)$$

where d is the cavity depth in cm, {d} is the numerical value of the cavity depth, and U_{ig} is the voltage in kV at T = 293 ^{o}K and p = 1013 mb. The ignition field stress obtained from equation 3.1.4. is given by:

$$E_{ig}/p = 24.2 + 207.3 \cdot \{p \cdot d\}^{-0.5} \qquad (3.1.4.a.)$$

where E_{ig}/p is the reduced ignition field stress for the cavity in $V \cdot cm^{-1} \cdot mb^{-1}$, p is the pressure in mb referred to T = 293 ^{o}K, d is the cavity depth in cm and {p·d} is the numerical value of the parameter p·d. The values of the product $T_p \cdot p$ were calculated with E_{ig}/p given by equation 3.1.4.a. and $\Delta E \approx 0.02 \cdot E_i$. It was found that the values of the E_{ig}/p calculated from the above equation agreed with the known values of the breakdown field strength for air in uniform field within 0.5 % in the p·d range 40 < p·d < 1000 cm·mb and within -6 % in the range 10 < p·d < 40.

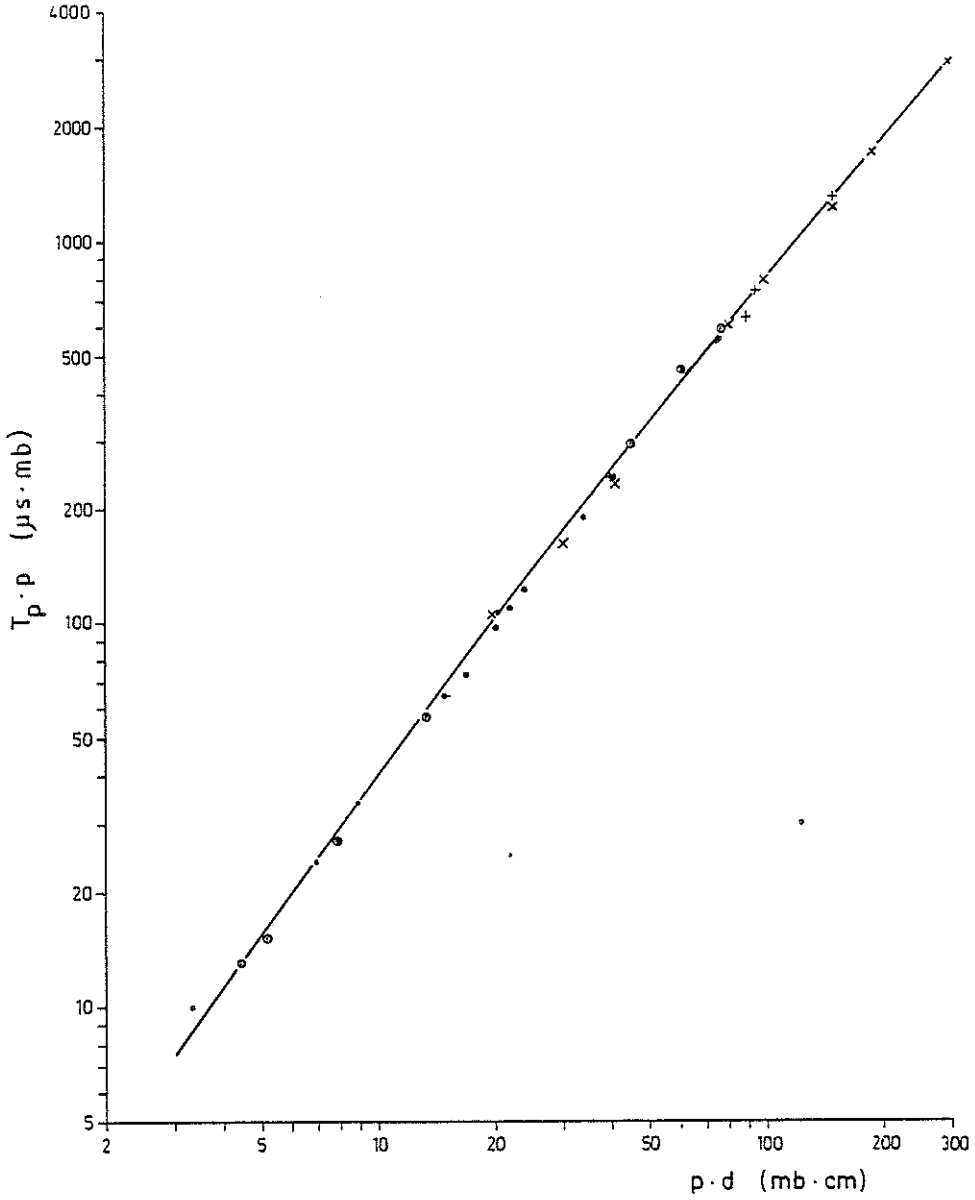

Fig. 3.2.

The product $T_p \cdot p$ versus the parameter pd.

+ - cavity depth d = 0.15 cm.

⊙ - cavity depth d = 0.075 cm.

∘ - cavity depth d = 0.038 cm.

× - pressure p = 1013 mb.

The narrow solid line represents equation 3.1.3.

The value for the mobility $\mu_{r+} = 2.6 \pm 0.3$ cm^2 V^{-1}·s^{-1} was taken from data given in (litt. 35). The value is subject to an uncertainty of ~ 10 %. According to (litt. 35), the μ_{r+} is constant up to E/p = 35 V/cm·mb and for E/p > 40 decreases with increasing E/p. The error due to the assumption of the constant μ_{r+} for E/p > 40 was partly compensated by the mentioned negative error in the calculation of E/p from equation 3.1.4.a. in this range.

The average value of $\alpha \cdot d = 9.1$ was used in all calculations. The error in calculations of $T_p \cdot p$ due to the assumption of the constant $\alpha \cdot d$ was less than ~ 1 %.

The overall error of the calculation of $T_p \cdot p$ was less than ~ 10 %. Within this limit, the calculated values agreed with the measured values (fig. 3.6.). The agreement shown support Degn's (litt. 4) conclusion that the T_p corresponds to the transit time of the positive ions, and also the conclusion that the empirical equations 3.1.3. and primarily 3.1.4.a. can be successfully applied to give approximative values for ignition field stress in the cavities.

From the measurements with the subdivided electrode system it was concluded that a slowly developing discharge extended over the whole cavity surface, as these discharges always induced temporally coincident currents in both current probes connected to the oscilloscope. This is shown in fig. 3.3. Since the induced currents possess unequal amplitudes the intensity of these partial discharges varies in directions orthogonal to the applied fields.

Typical waveforms of the photon flux emitted from a slowly developing partial discharge are presented in the osc. of fig. 3.4. with respective oscillograms of the current obtained for the same partial discharge. For this discharge type the photon flux and discharge current possess dissimilar waveforms. According to equation 2.2.18.a. the photon flux is proportional to the electron current. Its rise time measured from the magnified osc. 2 is $t_r = 40$ ns. It is desired to compare this rise time with the transit time for electrons across the cavity. The transit time is given by:

$$T_{-c} = \frac{d}{v-} \qquad (3.1.6.)$$

where v- is the drift velocity of the electrons.

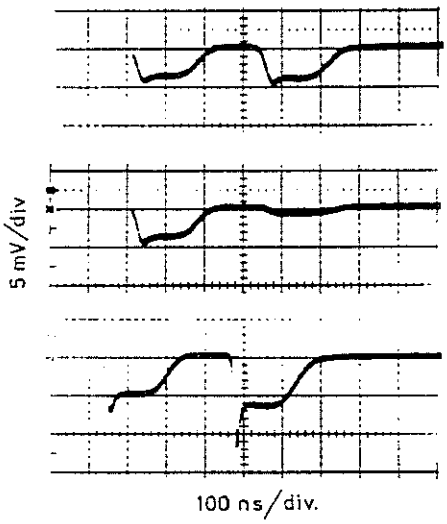

Fig. 3.3.

Three succeeding oscillograms of the partial discharge currents induced in the subdivided electrode-current probes. The signals from two current probes were fed to a two-channel oscilloscope. While the signal on the left of the oscillogram was fed directly, the signal on the right was delayed by means of a 340 ns transmission line and then added to the undelayed signal. Closed test sample; air 1020 mb, polyethylene. The oscillograms show the negative partial discharges.

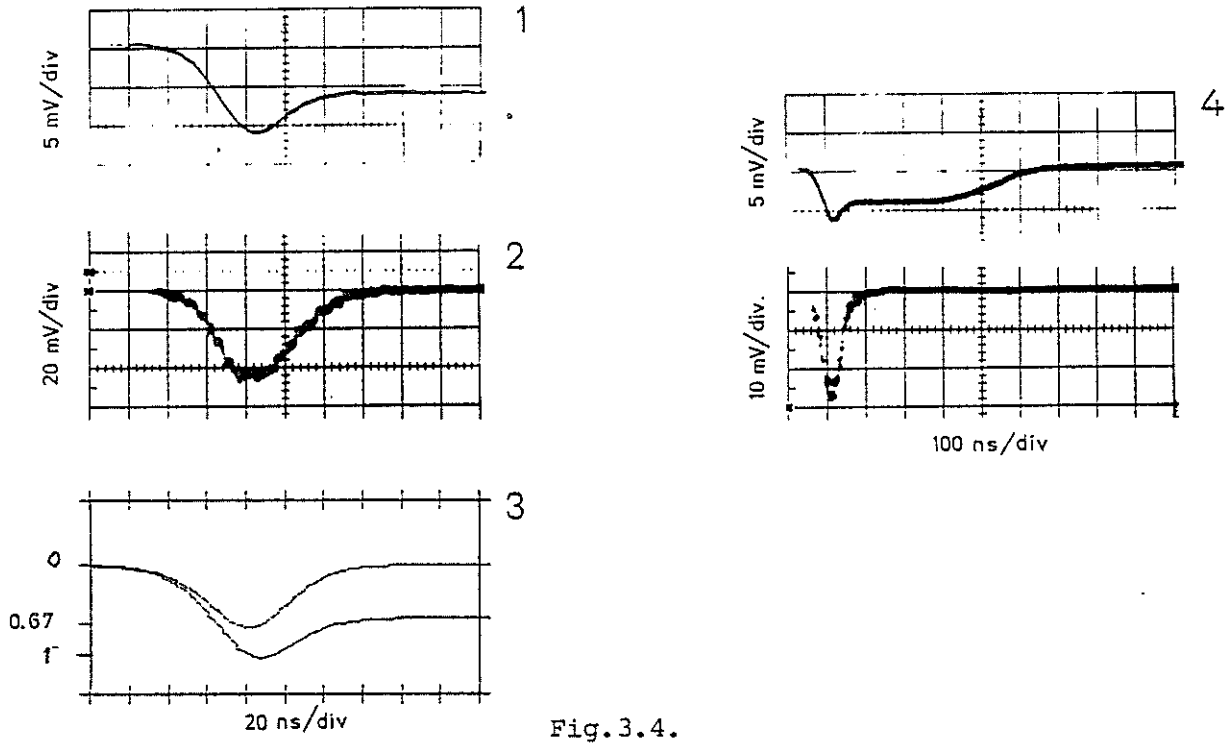

Fig.3.4.

The waveforms of current and photon flux in a slowly developing partial discharge. 1,4: Oscillograms of current, negative discharges, 2,5: Oscillograms of photon flux emitted from the same partial discharge, 3: Plot of computed total and electron currents in relative units for overvoltage 6.1 per mille. Open test sample, polyethylene, d = 0.07 cm, p = 1013 mb, k_2 = 0.070 mA·mV^{-1}, k_3 = 2.3·10^{15} photon s^{-1}V^{-1}.

According to (litt 35), the dependence of the electron drift on the reduced field intensity is given by the empirical function:

$$v_- = 1.23 \cdot 10^6 \cdot \{E/p\}^{0.715} (cm \cdot s^{-1}) \quad \text{for } \frac{E}{p} \leq 75 (V \cdot cm^{-1} \cdot mb^{-1}) \qquad (3.1.7.)$$

where {E/p} is the numerical value of the reduced field stress. The transit time versus cavity depth computed by means of equation 3.1.6. with v_- obtained from equation 3.1.7. and E/p obtained from equation 3.1.4. is given in fig. 3.5. Comparison of the computed electron transit time and the measured electron current rise time shows that the latter is one order of magnitude greater.

Consequently, it can be concluded that the electron current is not due to an individual avalanche or a single generation of individual avalanches. This is consistent with the results obtained throughout the range of cavity depths investigated: 0.01 - 0.2 cm.

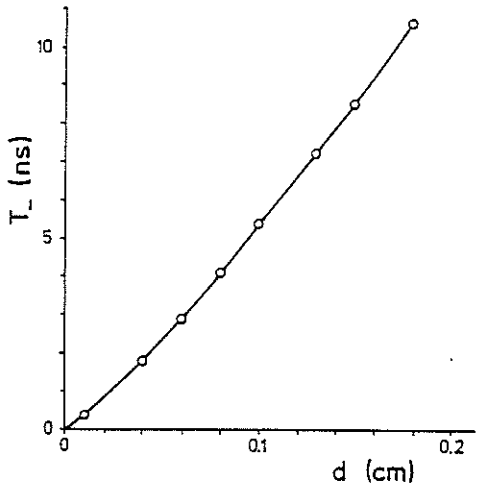

Fig. 3.5.

Computed transit time for electrons versus cavity depth. Air, p = 1013 mb.

Both the rise of the electron current preceding the region of maximum and the following decay of the electron current are approximately exponential. It can be seen that the pulse duration measured as the period of the pulse width at half maximum points in the osc. 2, fig. 3.4. is 45 ns. Initially, the total current is equal to the electron current. This situation is radically altered after the electron current ceases and only ions are present in the cavity. The slowly drifting ions produce a nearly constant current which is seen as the plateau of the right hand side in osc. 1, fig. 3.4. It will be noted that the number of ions in

the cavity initially decreases very slowly.

There is clear experimental evidence (litt. 36, 37), that in air negative ions are produced by virtue of the attachment of free electrons produced by ionization processes. The number of attaching collisions an electron is subject to per unit of its path in the field direction, is defined as the attachment coefficient η. For values of the reduced stresses $E/p > 45\ V \cdot cm^{-1} \cdot mb^{-1}$, η is at least one order of magnitude smaller than the ionization coefficient α. Furthermore, since the carriers are largely created immediately in front of the positive cavity surface, the average distance the negative ions travel before collection, is much shorter than the average distance covered by the positive ions. Therefore, the current seen as the plateau is mainly due to the movement of positive ions. With equation 2.2.9. and 2.2.16.a. the number of positive ions can be determined as:

$$n_+ = \frac{i_+ \cdot d}{e \cdot v_+} = \frac{k_2 \cdot u_{R+} \cdot d}{e \cdot \mu_+ (E_{ig} - \Delta E)} \qquad (3.1.8.)$$

where u_{R+} is the magnitude of the plateau and e the charge of the electron. The number of ions calculated for osc. 1, fig. 3.4. with: $\mu_{r+}' = 2.6\ cm^2\ V^{-1} \cdot s^{-1}$ and $E_i = 48.8\ V \cdot cm^{-1} \cdot mb^{-1}$ is $n_+ \simeq 1.7 \cdot 10^9$ ions. This high number of ions cannot be explained by a single avalanche since in this case the amplitude of the electron current would be much greater. This is in close agreement with the former conclusion regarding the rise time t_{r-}.

For the reasons given, it can be assumed, in agreement with Degn (litt. 3), that the high number of ions is produced by successive generation. The initial build up of the partial discharge current by individual generations is not visible on the oscillograms, as their magnitude in air is too small to be measured due to the limited sensitivity of the measuring equipment. For instance, one avalanche started by one electron in a cavity of d = 0.07 cm would produce a current of 0.38 µA which is below the maximum sensitivity level of the measuring system. Even a generation of ten avalanches will give a current below the sensitivity level.

Since it was not clear if, or how such individual generations developed in the front of a partial discharge current pulse, a study was undertaken in carbon dioxide. On the basis of data for ionization coefficient and breakdown potentials given in (litt. 38, 39), it was expected that partial discharges will develop at greater values of the parameter $\alpha \cdot d$ in carbon dioxide filled cavities than in air for the $p \cdot d$ range $10 < p \cdot d < 200$ cm·mb. Hence, the number of electrons produced on d in each avalanche approximately given by $\exp((\alpha-\eta) \cdot d)$ should be much higher in carbon dioxide than in air, and for this reason it was expected that single generations could be measured in carbon dioxide.

The typical waveforms of the partial discharge current are shown in fig. 3.6. - for which the discharge parameters are computed under the assumption that the ignition field stress is determined by the Paschen curve. The values for the reduced ignition field stress: E_{ig}/p, ionization and attachment coefficients: α/p and η/p are calculated using data given in (litt. 38, 39), while the electron and ion drift velocities are calculated using data given in (litt. 40, 41, 42). The duration of the ionic current is computed using equation 3.1.1. Since the attachment coefficient η is in the considered case very small in comparison to the ionization coefficient α, the measured ionic current is due to the movement of the positive ions. The number of these ions is computed using equation 3.1.8.

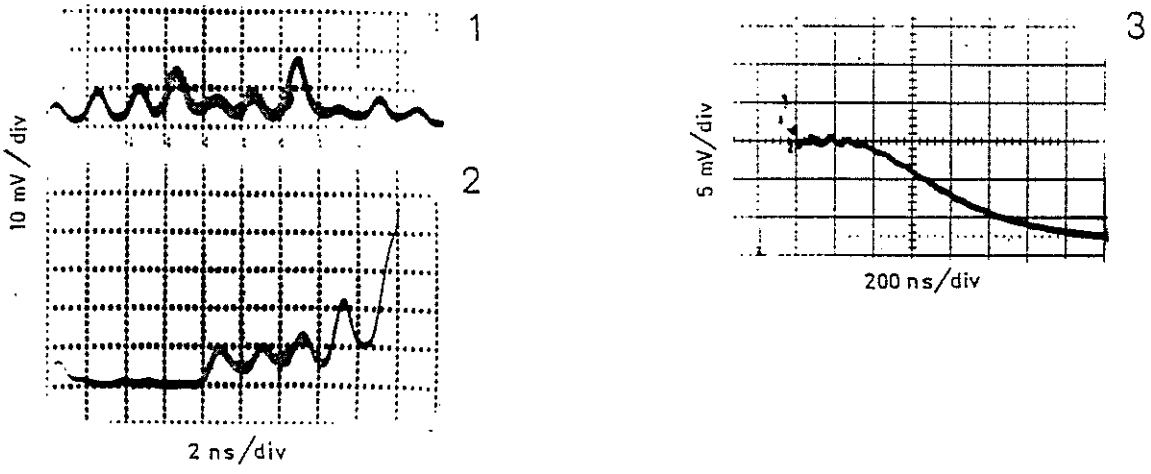

Fig. 3.6.

Development of the partial discharge current in carbon dioxide. Osc. 1: a series of generations, which decrease to zero, osc. 2: transition of four generations into a fast rising current front, osc. 3: the tail of the discharge corresponding to the drift of ions in the cavity. Cavity depth 0.06 cm, pressure 990 mb, polyethylene, closed test sample. $k_2 = 0.047$ mA/mV.

The number of electrons in generations of the magnitude of 10 - 20 mV shown in osc. 1 and 2 is computed in a similar manner as the number of positive ions. The calculated parameters are listed below:

$p = 990$ mb
$p \cdot d = 59.4$ cm·mb
$E_i/p = 49.5$ V·cm^{-1}·mb^{-1}
$\alpha/p = 0.22$ cm^{-1}·mb^{-1}
$\eta/p << 0.01$ cm^{-1}·mb^{-1}
$\alpha d = 13$
$v_+ = 5.6 \cdot 10^4$ cm·s^{-1}
$v_- = 1.9 \cdot 10^7$ cm·s^{-1}
$n_+ \approx 5 \cdot 10^9$ ions
$n_- \approx (0.9\text{-}1.8) \cdot 10^7$ electrons
$T_p = 1.0 \cdot 10^{-6}$s

The computed value of T_p agrees very well with the value measured on the magnification of osc. 3. Since the number of electrons created per avalanche is $\exp((\alpha-\eta) \cdot d) = 4.5 \cdot 10^6$, the oscillations visible in osc. 1 and 2 consist of some 20 - 40 individual electron avalanches.

The results substantiate that the regenerative mechanism is operative during the initial stages of the development of the partial discharge in carbon dioxide and support the concept of a similar mechanism in other gasses.

In air, the slowly developing discharges were observed in test samples of polyethylene, polypropylene and both types of epoxy resins. The current waveform did not depend on the chemical composition of the test sample material. The pulse duration of partial discharges obtained in a nitrogen filled cavity was shorter than the duration of the discharges in air in the same cavity due to higher field stress and associated higher drift velocity of ions in the case of nitrogen.

In air, a transition of an individual slowly developing discharge into a fast developing was also frequently observed. The transition was visible as a rapidly rising current pulse, temporally coinciding with a photon flux pulse, which occurred in an overlapping fashion on the front of the slowly developing discharge or alternatively, on its tail. An immediate transformation of the slowly developing type into a rapidly developing type was observed after addition of very small amounts of methane. According to (litt. 43) methane absorbs the ra-

diation with wavelengths $\lambda < 250$ nm, which are supposed to be responsible for the photoionization processes. Therefore, this radiation is likely to be of importance for the formation of the slowly developing partial discharge. This fact is consistent with the important conclusion that the regenerative mechanism is responsible for the current growth in this partial discharge type.

3.1.2. Rapidly developing partial discharges.

Typical waveform of the rapidly developing partial discharge currents are shown in fig. 3.7. osc. 1 and 2. It is seen, however, that initially the steepness of the current pulse increases slowly with time after which it reaches a well defined maximum. The steepness of the decaying section is decreasing with time. An evaluation of oscillograms 1 and 2 from a semilogarithmic plot (fig. 3.8.) of current against time shows an exponential current growth in the initially slow rising section. This section frequently extended to many electron transit times, and was followed by a hyper-exponential current growth just before maximum and thereafter by approximately exponential decay. Generally, the pulse shape does not depend on the pulse amplitude, which can be seen by comparison of. osc. 1 and 2, the current amplitudes being different by a factor 25.

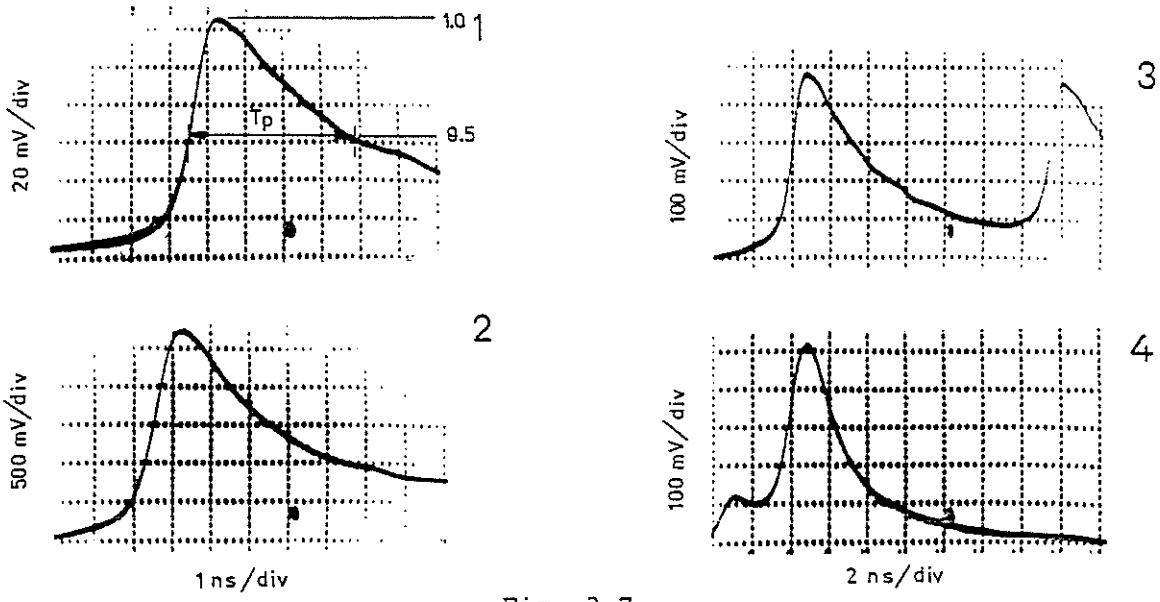

Fig. 3.7.

Rapidly developing partial discharges. Osc. 1,2: typical and osc. 3,4: seldom occurring current waveforms. In the table overleaf are listed the experimental conditions.

Table to fig. 3.7.

osc. no.	cavity depth d	outer discs $d_1=d_2$	k_2	material	air press.	air temp.
-	cm	cm	mA/mV	-	mb	°C
1	0.060	0.20	0.103	polyethylene	982	20
2	0.060	0.20	0.077	epoxy + filler	982	20
3	0.110	0.23	0.012	polypropylene	982	20
4	0.053	0.23	0.125	polypropylene	982	20

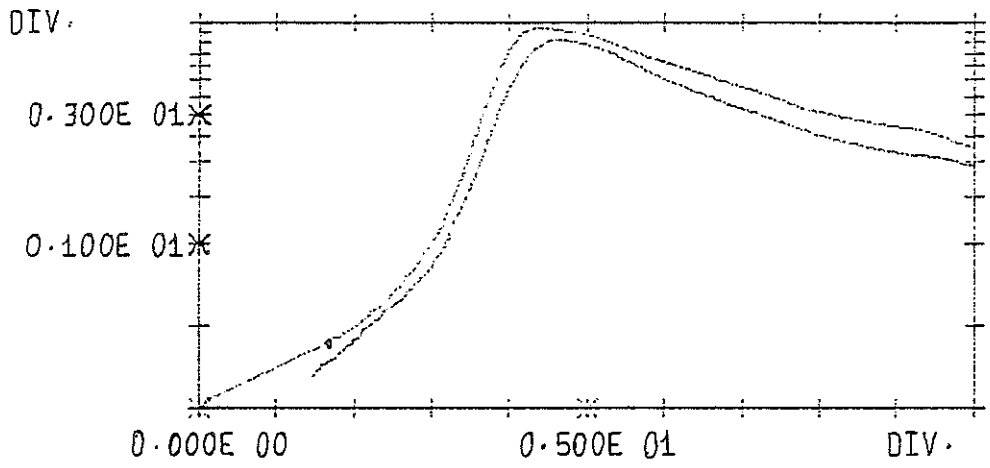

Fig. 3.8.
Oscillograms 1 and 2 from fig. 3.7. digitized and semilogarithmically plotted.

It was found, that the pulse waveforms and durations remained constant when the applied ac test voltage was changed within the range U_{inc} to $3 \cdot U_{inc}$, where U_{inc} is the inception voltage, i.e. the voltage, at which discharges first appear when the voltage is raised. The pulse duration measured as a period T_p of pulse width at half maximum points (osc. 1, fig. 3.7.) tended to increase with increasing cavity depth. T_p obtained from a series af measurements carried out for different materials is plotted against the cavity depth in fig. 3.9. No correlation has been observed between the chemical composition of the test sample material or thicknesses of the outer discs of the test sample, and duration T_p.

The rise times defined as the elapsed times between 0.1 and 0.9 amplitude points were found to be: $1.2 < t_r < 2.6$ ns, for cavity depths 0.02 - 0.2 cm resp. For the smallest cavity depths the measured rise times were influenced by the rise time of the measuring circuit. However, for cavity depths $d > 0.04$ cm the measured rise times were significantly shorter than the calculated electron transit times (see section 3.1.1., fig. 3.5.). The rise times considered are too short to allow any notable contribution to the formation of the fast developing section of the discharge current by either generation processes or by a single avalanche. Therefore, it is resonable to conclude that the fast developing section of the waveform exibiting hyper-exponential current growth corresponds to a space charge accelerated avalanche growth commonly interpreted as streamer formation.

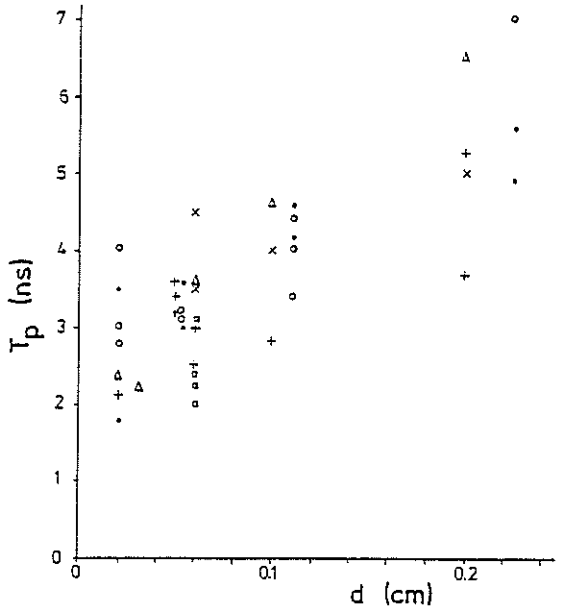

Fig. 3.9.

T_p : the pulse width at half maximum for typical current waveforms shown in fig. 3.1., osc. 1. Δ, x - polyethylene, outer discs 0.02 and 0.2 cm resp., o, • - polypropylene, outer discs 0.227 and 0.55 cm resp., +, □ - epoxy resin, with and without filler resp., outer discs 0.2 cm. Air 982 mb, 20°C.

The decay times measured as the elapsed times between the maximum and half maximum points of the decaying section were: $1 < t_d < 5$ ns for

cavity depths 0.02 - 0.2 cm resp. According to Kärkkäinen (litt. 44), this section of the waveform can be attributed to a secondary surface discharge, which occurs when the transverse field stress "E//" caused by the surface charge due to the primary discharge is sufficiently high.

It was found that the current pulses did not change their characteristic shapes in the pressure range 0.1 to 2 bar for the different test sample materials. In polyethylene test samples the pulse amplitude tended to increase with increasing cavity depth. The most frequent current pulse amplitude (see subsection 3.2.) multiplied by the factor k_2 gives the discharge current i_d (equation 2.2.16.a.). Fig. 3.10. shows a plot of i_d against the cavity depth. The tendency of increasing current with increasing cavity depth as shown was not observed in epoxy resin test samples. In the case of epoxy resins the pulses always achieved amplitudes larger by orders of magnitude, typically in the range 0.1 - 0.5 A for all cavity depths investigated. In this case no correlation was observed between the current amplitude and cavity depth.

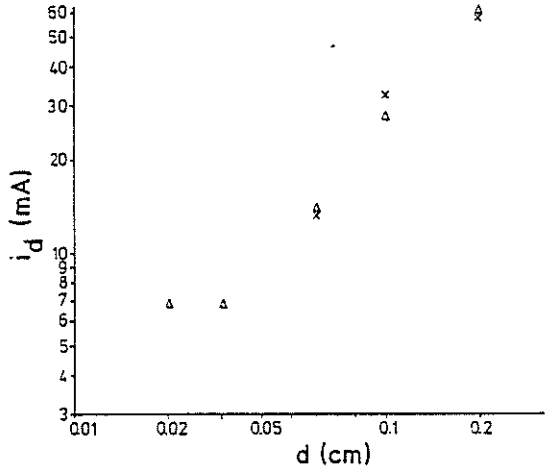

Fig. 3.10.
Current amplitudes for rapidly developing partial discharges. Experimental conditions as for fig. 3.2.

Occasionally during the decaying section an additional rapidly developing discharge occurred (osc. 3, fig. 3.7.) which in some instances preceded the main pulse (osc. 4, fig. 3.7.). The frequency of occurrence of this discharge was low. The elapsed time between the two pulses was random in nature.

The results obtained using the subdivided electrode provided additional information concerning the lateral extension of the discharges. By comparison of the currents induced in the subdivided-electrode current probes a very low probability for the coincidence of signals measured by two different current probes was found. This indicated that the rapidly developing partial discharges did not occur across the whole cavity surface but were restricted to small areas. The repetition rate of discharges in the central part of the cavity was a few per cent greater than at the cavity periphery at the start of the test series. The elapsed time periods between pulses from two electrodes were in the range up to 100 ns. Hence the current pulses shown in osc. 3 and 4 are presumably caused by discharges at two different sides of the cavity.

The measurements of the photon flux emitted from the rapidly developing partial discharges showed that the photon flux exhibited a waveform which was fairly similar to the waveform of the corresponding current pulse. This is illustrated in the oscillograms of fig. 3.11. Initially a process of ionization and excitation progresses rather slowly, recognisable on the oscillograms throughout a time period of at least 10 ns. The duration of this period was reported by Levring (litt. 45) to extend frequently to many electron transit times. This initially slowly developing section does not have an invariable character as it can be seen by comparison of osc. 1 with osc. 2. A faint line on both oscillograms signifies the onset of a rapid acceleration of the ionization and excitation processes consistent with streamer development. After a sharp maximum the photon pulse decay is much faster than that of the electron pulse, thereby clearly indicating that the excitation processes ceases rapidly after the pulse has reached its maximum. From the current pulse waveforms it can be seen that the movement of electrons still exists although the excitation processes have decreased. The ionic component is not visible in the oscillograms; it can be calculated, however, to be in the order 0.01 to 0.03 of the electron current.

The average number of photons emitted per discharge in open test samples, d = 0.1 cm and d = 0.05 cm, were: $n_p = 1.7 \cdot 10^7$ and $n_p = 0.7 \cdot 10^7$ photons resp. The photon flux was integrated for 20 oscillograms and thereafter the mean value of n_p was computed. The standard deviation for n_p was $0.7 \cdot 10^7$ for the 0.1 cm cavity and $0.3 \cdot 10^7$ for the 0.05 cm cavity.

Finally, it should be added that there is strong experimental evidence (litt. 3, 12, 32) that positive and negative Lichtenberg figures are connected with the rapidly developing discharges. This fact is consistent with results of the present investigation. The most important conclusions which emerge from the investigation are summarised below.

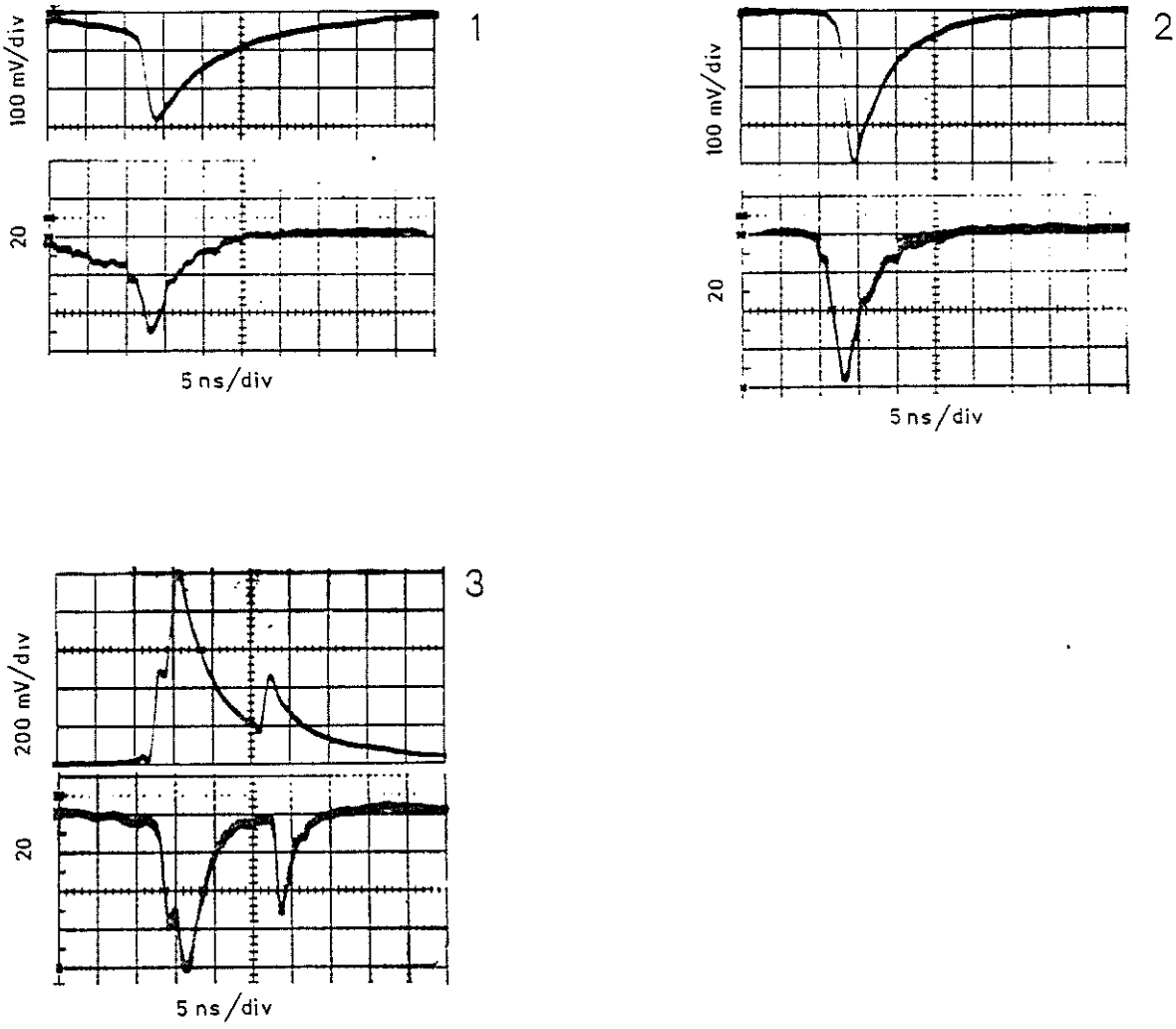

Fig. 3.11.

Comparison of waveforms of current and photon flux emitted from rapidly developing partial discharges in an open test sample, d = 0.1 cm, air, 1010 mb. Upper trace: current, lower trace: light. k_2 = 0.058 mA·mV^{-1}, k_3 = 5.3·10^{16} photons s^{-1}·V^{-1}. Osc. 1,2: typical and osc. 3: seldom occurring waveforms.

The field distribution during the development of the rapidly developing discharge is strongly inhomogeneous. The measurements of the discharge current by means of the subdivided electrode have shown that in this case the discharge is restricted to a small area of the cavity surface.

At the beginning of the rapidly developing partial discharge, the current growth is frequently caused by the avalanche generation. When a field stress, specified by the charge and current distributions becomes sufficiently high a "partial" streamer develops. This streamer onset is still restricted to a small area of the cavity surface. In the last stage, when the streamer impinges and bridges both surfaces, it moves radially outward along the cavity surface producing a charge distribution, which can be detected as Lichtenberg figures.

In subsection 3.3. the above conclusions will be proved in terms of the results of the surface conductivity measurements.

3.2. Repetition Rates and Amplitude Distributions. The Energy of Individual Partial Discharges.

During the tests, the partial discharge repetition rates and the magnitude distribitions were subject to changes. At 50 Hz frequency and ratios $U_{test}/U_{inc} < 2.5$ this change, which was correlated with changes in the surface conductivity, occurred over a period of several minutes or, in some cases, several hours. It was therefore possible to measure repetition rates and distributions without application of automatic recording equipment, using the technique described in subsection 2.3.

It was found, that for a given test sample the repetition rate depended on the amplitude of the applied ac test voltage. This dependence followed a pattern which was characteristic for each distinct discharge type (fig. 3.12.) and could be represented by the empirical relationship:

$$\dot{N}'(u_R) \propto \left(\frac{U_{test}}{U_{inc}}\right) - 1 \qquad (3.2.1.)$$

$\dot{N}'(u_R)$ being the number of current pulses with amplitude greater than u_R, U_{test} being the test voltage, and U_{inc} the inception voltage. The

relationship 3.2.1. was found to apply in the test voltage range $1 < U_{test}/U_{inc} < 2.5$ for tests of up to 5 hours duration. For slowly developing discharges, it was found that the repetition rate was considerably higher than for the rapidly developing type and increased with decreasing thickness d_1 and d_2 of the outer discs of the test sample.

The dependence of the repetition rate on the ratio U_{test}/U_{inc} was analyzed under the following assumptions:

1) the individual partial discharges are extended over the whole cavity, and
2) the duration of an individual partial discharge is short as compared with the time Δt between two succeeding discharges.

Under these conditions the electric field in the cavity during partial discharge repetition is as shown in fig. 3.13.

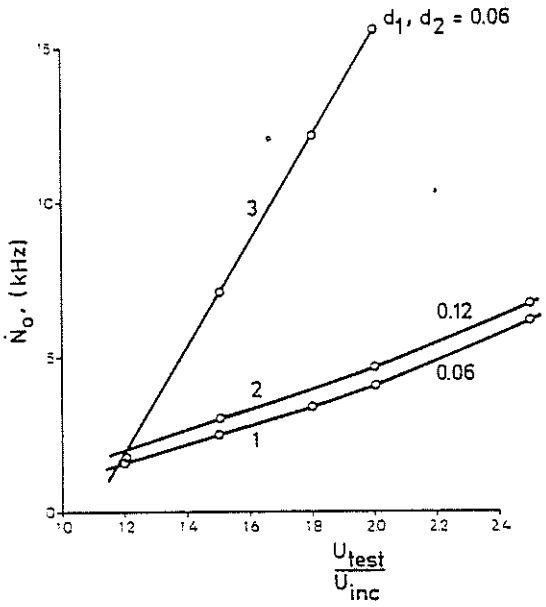

Fig. 3.12.

The pulse repetition rates as a function of the ratio U_{test}/U_{inc}. U_{test}: test voltage, U_{inc}: inception voltage. p = 1010 mb, cavity depth 0.06 cm, cavity diameter 1 cm. Closed test sample, 1 and 2: polypropylene, rapidly developing discharges, 3: polyethylene, slowly developing discharges. The curves were obtained after 1 hour conditioning with $U_{test}/U_{inc} = 1.5$.

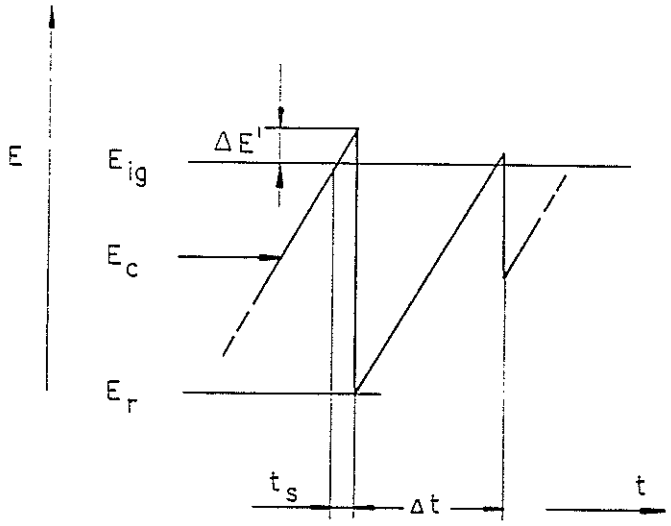

Fig. 3.13.

Illustration of the field stress in the cavity as a function of time for repetitive partial discharges. Δt is assumed to be small in comparison to the period of the applied ac voltage, and the duration of a partial discharge is assumed to be small in comparison to Δt. For the purpose of illustration the E axis has been exaggerated in the above figure.

The intensity of the average field acting in the cavity lies between the breakdown field stress: $E_{ig} + \Delta E'$ and the remanent field stress: E_r; $\Delta E'$ being dependent on the statistical time lags. With reference to Heller's (litt. 46) and Kelen's (litt. 47) results it can be readily shown that the relation between the repetition rate $\dot{N}$ and the ratio U_{test}/U_{inc} for small values of ΔE is given by:

$$\dot{N}_o = \lim \dot{N}'(u_{R\,max}) = 4 \cdot \frac{E_{ig}}{\Delta E} \cdot f \cdot \left(\frac{U_{test}}{U_{inc}} - 1 \right) \qquad (3.2.1.a.$$

$$u_{R\,max} \to 0$$

E_{ig} being the ignition field stress, ΔE being the mean reduction of the field in the cavity by a partial discharge: $\Delta E = E_{ig} - E_r$, and f being the frequency of the applied ac voltage.

The amplitude distribution function $\dot{N}'(u_{R\,max})$ was obtained using the same model under the additional assumption that

3) the discharge amplitude u_{Rmax} is proportional to the field stress

$\Delta E'$ in excess of the ignition field stress acting in the cavity at the onset of the partial discharge

$$u_{R\,max} = C_1 \cdot \Delta E' \qquad (3.2.2.)$$

C_1 being a constant.

$\Delta E'$ is attributed to the statistical time lag t_s between the instant at which the field stress reaches the ignition value and the onset of the partial discharge. From fig. 3.13 it follows that $\Delta E'$ is given by:

$$\Delta E' = \frac{E_{ig} - E_r}{\Delta t - t_s} \cdot t_s = C_2 \cdot t_s \quad \text{for } \Delta t >> t_s \qquad (3.2.3.)$$

where C_2 is the rate of rise of the field stress and is assumed to be equal to the average value, taken for the period in which discharges occur. Equation 3.2.3 upon substitution in equation 3.2.2 gives:

$$u_{R\,max} = C_3 \cdot t_s \qquad (3.2.4.)$$

where $C_3 = C_1 \cdot C_2$.

Hence, the distribution of $u_{R\,max}$ is determinable from the distribution of t_s. The latter type of distributions was measured by Devins (litt. 3) who found that for slowly developing discharges t_s was exponentially distributed. Whence the amplitude distribution is by virtue of equation 3.2.4 given by:

$$\dot{N}'(u_{R\,max}) = \dot{N}_o' \cdot \exp(- u_{R\,max}/C_3 \cdot \tau_s) \qquad (3.2.5.)$$

$\dot{N}'$ being the repetition rate of pulses with a peak value greater than or equal to $u_{R\,max}$ and τ_s is the mean time lag.

Typical amplitude distributions obtained for both discharge types are shown in fig. 3.14. In the case of slowly developing discharges the amplitudes are exponentially distributed in agreement with the theoretical distribution characteristic given by equation 3.2.5. In effect there is experimental evidence (subsec. 3.1) that the assumptions 1) and 2) page 64 are fulfilled for this discharge type and the fulfilment of assumption 3) page 65 was found experimentally to apply for the same discharge type by Devins (litt. 3).

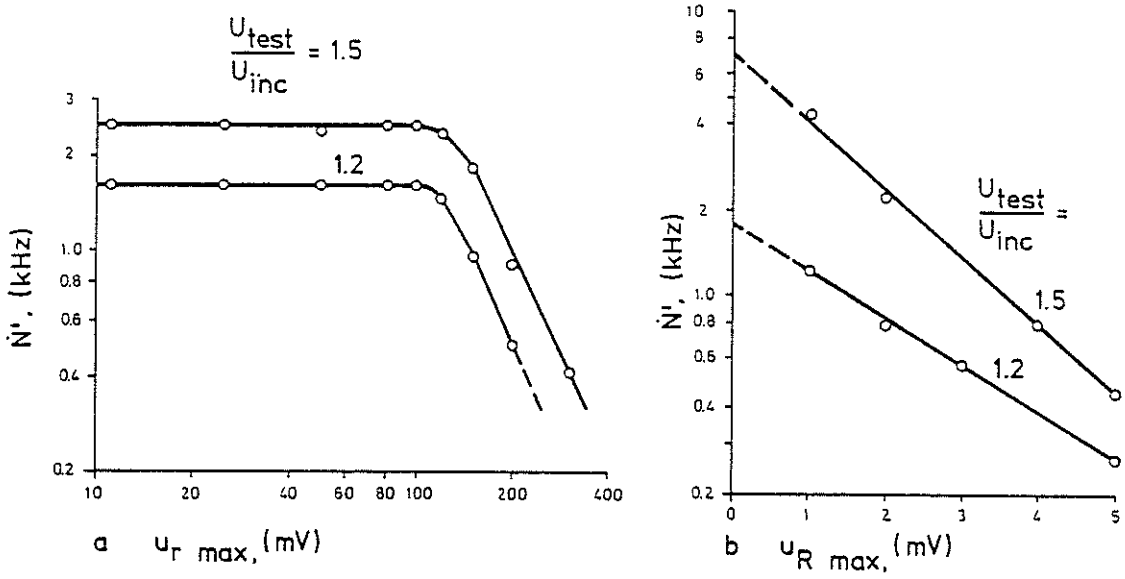

Fig. 3.14.

The repetition rate distribution with the ratio: U_{test}/U_{inc} as parameter. Cavity depth and diameter d = 0.06 cm and D = 0.1 cm resp., d_1, d_2 = 0.06 cm, p = 1010 mb, air. a: rapidly developing discharges, polypropylene; b: slowly developing discharges, polyethylene.

As can be seen from fig. 3.12, curve 3, also the linear dependence of the repetition rate $\dot{N}_o$ on the ratio U_{test}/U_{inc} for the latter discharge type turns out to be in agreement with the theoretical characteristics given by equation 3.2.1.a. Using equation 3.2.1.a the mean value of $\Delta E/E_{ig}$ can be determined from the empirically obtained characteristics and was found to be in the range of 1 - 2 per cent.

The nonlinear repetition rate characteristic shown in fig. 3.12, curves 1 and 2, can be interpreted on the basis of the multiple discharge concept (litt. 12) for the rapidly developing discharges. Provided that n_d is the number of partial discharges necessary to reduce the field stress in the whole cavity from E_{ig} to E_r the repetition rate characteristic is given by:

$$\dot{N}_o = 4 \cdot \frac{E_{ig}}{\Delta E} \cdot n_d \cdot f \cdot (U_{test}/U_{inc} - 1) \qquad (3.2.1.b$$

n_d being an increasing function of the test voltage with the form: $n_d = F(U_{test}/U_{inc} - 1)$. The measured repetition rates for this discharge type lie below the repetition rates of the slowly developing discharges and therefore it can be resonably concluded that the field

reduction caused by the passage of these partial discharges is much higher than for the slowly developing discharges under the assumption that the charge transport is of the same order of magnitude for both discharge types.

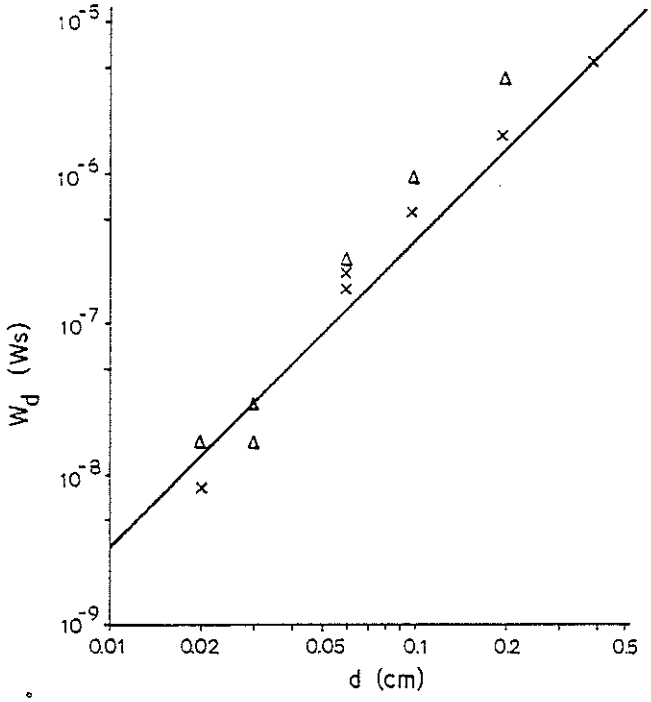

Fig. 3.15.

The energy per discharge for rapidly and slowly developing discharges versus cavity depth; p = 1013 mb.

- rapidly developing discharges. The points (Δ,x) represent the energy of the most frequent discharge pulses occurring in polyethylene. Δ: $d_1 = d_2 = 0.02$ cm; x: $d_1 = d_2 = 0.2$ cm.

- slowly developing discharges. The solid curve represents the energy of slowly developing discharges calculated on the basis of equation 3.2.7.

The Energy of Individual Partial Discharges.

The energy dissipated by an individual rapidly developing partial discharge was calculated from the expression:

$$W_d = \frac{C_{ab}+C_k}{C_k} \cdot \frac{U_{inc}+U_{ext}}{2} \cdot \int_0^{t_1} i_R \, dt$$

$$\simeq \frac{C_{ab}+C_k}{C_k} \cdot U_{inc} \cdot \int_0^{t_1} i_R \cdot dt \qquad (3.2.6.)$$

C_{ab} and C_k being the capacitances between the high voltage electrode and measuring electrode and the high voltage and coupling electrode resp.; U_{inc} and U_{ext} are the inception and extinction voltages resp., and i_R the transient current passing through the measuring shunt R.

The expression is derived by comparison of the potential energy of the network shown in fig. 2.6 before and after the partial discharge. The difference is equal to the sum of energies dissipated in a partial discharge and in the shunt. The latter energy was found to be negligible because of the low shunt resistance. The right hand integral covers the time period t_1 surrounding a discharge.

In polyethylene, the energy dissipated in an individual rapidly developing discharge tended to increase for increasing cavity depth (fig. 3.15). This tendency was not observed in epoxy resins for which the dissipated energy appeared to be independent of the cavity depth. The measured energies were in the range 10^{-6}-10^{-5} Ws and depended solely upon the type of the epoxy resin. It should be remembered that the energy is for this type highly localised, since it is mainly dissipated over the small surface area corresponding to the relevant Lichtenberg figure.

The energy dissipated by an individual slowly developing discharge was approximately calculated under the assumption that the discharge current has a constant equivalent amplitude i_d' and a duration equal to T_p (fig. 3.1-1). Then the dissipated energy is given by:

$$W_d = i_d \cdot T_p \cdot E_{ig} \cdot d \qquad (3.2.7.)$$

W_d calculated with T_p given by equation 3.1.1, p = 1013 mb, and i_d' = 0.1 mA is represented by the solid curve on fig. 3.14.

For the very large slowly developing discharges, the energy can be greater than the energy represented by this curve. However, the repetition rate of such large discharges is low, and therefore the dissipated energy wil usually be less than the energy given by the curve on fig. 3.14. The energy dissipated by an individual slowly developing discharge is evenly distributed over the whole cavity surface.

According to fig. 3.2 the discharge energy strongly decreases with decreasing cavity depth.

3.3. The Conductivity of Surfaces Subjected to Partial Discharges over Extended Test periods. Changes in Surface Topography.

The Conductivity.

During this part of the investigation the major effort was concentrated on the development of suitable measuring methods, test equipment and apparatus to make it possible to perform accelerated examination of test samples subjected to partial discharges over extended test periods. However, it was considered important to study the changes in the partial discharge characteristic as well as changes in the properties of the test sample surfaces when subjected to discharges over test periods of longer duration. The results of these measurements are presented within this subsection although the number of experiments was limited. The test periods were extended up to about 100 hours' duration.

During long term tests with the polyethylene test cells characteristic transformations of the discharge types were observed. When a virgin test sample was examined, series of the slowly developing discharges would occasionally occur during the initial period lasting some few minutes. As the test period progressed, however, mainly rapidly developing discharges were observed. The duration of this period was from less than one minute up to some hours depending upon the ratio U_{test}/U_{inc}, the frequency f, and the dimensions of the test sample. The duration was shortest when the test voltage was highest.

Subsequently, during prolonged tests, the partial discharges change type. The mechanism by which the discharges altered their behaviour was found to be connected with a change in the conductivity of the test sample surface. The change in the partial discharges from the rapidly developing type into the transition type and the slowly developing type was attributed to a rapid increase in the initial value of the surface conductivity to a value of about $10^{-12}\ \Omega^{-1}$ at 50 Hz ac voltage. After this rapid increase the conductivity increased at notably slower rates of about $5 \cdot 10^{-1}\ \Omega^{-1}$/hour for $U_{test}/U_{inc} = 1.7$, d = 0.1 cm, $d_1 = d_2 = 0.03$ cm, polyethylene, and test duration t < 100 hours (litt. 13). When the surface conductivity was sufficiently high (over $10^{-13}\ \Omega^{-1}$) slowly developing and transition discharge types occurred. It was established by additional tests that the rapid rise of the surface conductivity was not due to temperature increases in the cavity. After the termination of the partial discharge

action, the conductivity slowly decreased to its initial value, the decrease being a matter of days or even months.

During the occurrence of the rapidly developing discharges, the charge deposition in the form of Lichtenberg figures creates a strongly inhomogeneous field in the whole cavity. It is supposed that when the surface conductivity is sufficiently high the charge flow over the surface causes a change towards more homogeneous field conditions except in the immediate neighbourhood of the cylindrical wall of the cavity, thereby permitting the above described change in the discharge type.

The period with the slowly developing discharges could be extended over several hundres hours.

In general, the self-extinction of internal discharges is a complex phenomenon depending on the gas generated in the cavity, pressure, temperature rise, and surface conductivity. During the present investigation, the pronounced tendency to self-extinction was observed in polypropylene test samples, $U_{test}/U_{inc} \leq 1.5$, 50 Hz. The self-extinction took place after some hours from the beginning of the test.

The extinction tendency was caused by a very high conductance of the cylindrical wall of the cavity, the total conductance of which was found to be in the range of $10^{-8} - 10^{-11}\ \Omega^{-1}$.

It was anticipated that the increase in the surface conductivity must be reflected in a corresponding increase of the power losses of the test sample. For this reason, additional measurements of power losses were carried out. The power losses were measured by comparison of the power losses in the examined test sample and losses in the "normal" test sample without a cavity by means of an integrating bridge. Descriptions and analysis of the integrating bridge method are for instance given in (litt. 48, 49). The analysis of the bridge method is given by the present author in (litt. 50) together with an analysis of other "classical" partial discharge measuring methods, and hence was not repeated in section 2. The test samples were placed in two similar electrode systems, one of which is shown in fig. 2.3.

It was found that the increase of the surface conductivity was accompanied by a change in the shape of the power loss cyclogram from the form of a parallelogram into the elipse form as well as by the increase in the power losses (fig. 3.16). This indicates a more or less pronounced change of the charge transport mechanism in the cavity from partial discharges to a current across the surface. The mechanisms can

be distinguished by different dependencies of the power losses on the test voltage as shown in fig. 3.16.

The increase in the measured surface conductivity is due to changes in the chemical composition of the test sample surface and/or due to an increase in the mobility and number of charge carriers in the sample material. The mechanism of the increase in conductivity of thin plastic foils subjected to partial discharges has been theoretically and experimentally investigated by Boeck (litt. 28). Boeck has established that partial discharges cause an increase in the conductivity which is associated with the propagation of a negatively charged, conductive zone from the cavity surface into the insulating material. This zone develops due to the electron bombardment of the surface. The development of the conductive zone may well be partly responsible for the increase of power losses observed during the present investigation. It must be stated, however, that the average densities of charges collected on the cavity surface during a period of the ac voltage in Boeck's experiments were several times greater than those collected in the present investigation. This can be interpreted on the basis of equation 4.2.2.a wherein the surface density strongly increases with decreasing thickness of the insulation surrounding the cavity. The foils investigated by Boeck were thin, and consequently the surface charge densities were correspondingly greater, according to equation 4.2.2.a.

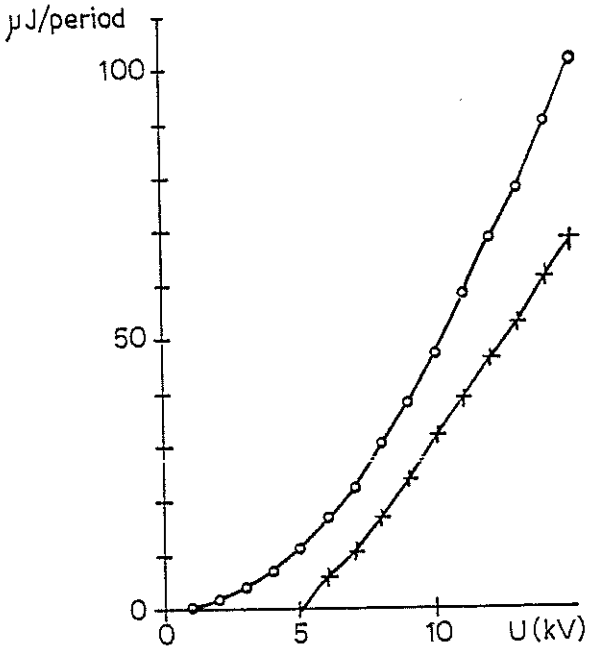

Fig. 3.16.

The power losses versus applied voltage.

+ - the power losses in the beginning of the test.

o - the power losses after 1 hour at $U = 3 \cdot U_{inc}$.

Polyethylene, $d_1 = d_2 = d = 0.3$ cm.

Changes in the Surface Topography.

The stereoscopic examination of the test sample surfaces by means of the scanning electron microscope was restricted to polyethylene test samples. The samples exposed to partial discharges were assembled in the electrode system shown in fig. 2.3. Tests were carried out with 50 Hz as well as 500 Hz voltage applied, the ratio U_{test}/U_{inc} being within the range 1.2 to 1.5, for periods up to 50 hours.

Two quite characteristic types of erosional deterioration were found. On the plane outer disc of a test sample, in the immediate vicinity of the cylindrical wall of the cavity were located numerous separate eroded sites. In appearence these have the shape of rounded craters of $\sim$ 10 - 50 µm diameter and $\sim$ 10 µm in depth. This type of erosion is shown in the micrograph, fig. 3.17. On the remaining part of the surface, the originally protruding features were eroded, resulting in a levelling of the surface. The latter erosion was less pronounced as compared to the erosion along the cylindrical wall.

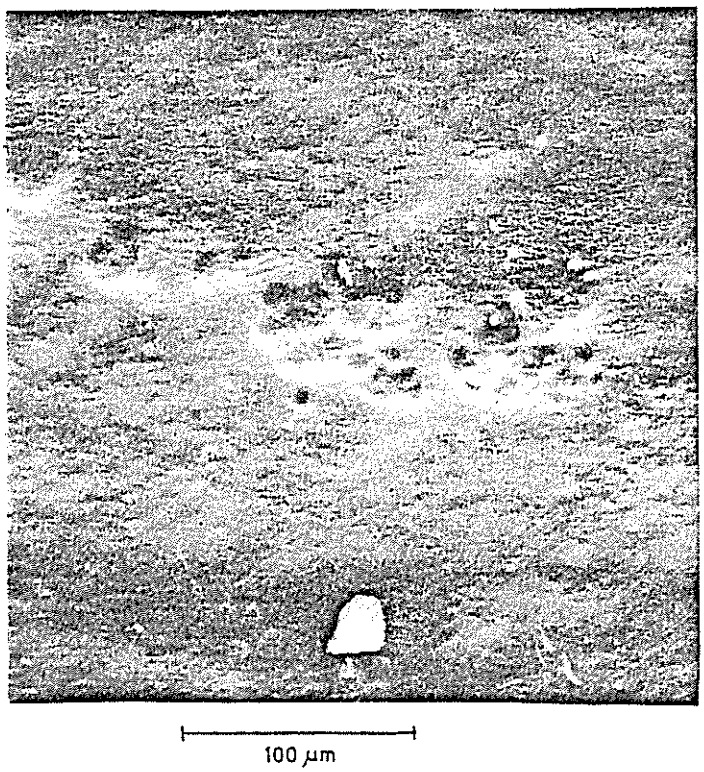

Fig. 3.17.
Micrograph of craters in polyethylene occurring in the vicinity of the cylindrical wall of the cavity.

The discharges resulted in the appearence of deposits on the surface in the form of small "crystals" of rather irregular shapes. Several investigations have detected the appearence of such deposits, which

in the polyethylene test samples occurred solely in oxygen and air and have been identified as oxalic acid. Nørholm (litt. 51) found that similar crystals are formed in epoxy resin foils, and identified them using several different methods also to be oxalic acid.

Both described types of deterioration are erosional processes resulting from the accumulated effects of a great number of succesive discharges. In the beginning of each test the successive discharges were either uniformly distributed on the cavity surface - in the case of rapidly developing discharges - or each individual discharge was extended over the whole cavity surface - in the case of slowly developing discharges - and the levelling erosion due to discharges smoothed out the surface. This type of erosion is therefore believed to be innocuous to the insulation.

When the conductivity of the plane parallel surfaces increases, the field stress in the immediate neighbourhood of the cylindrical wall of the cavity may periodically attain high values as calculated in section 4. Therefore, highly localized rapidly developing discharges are likely to occur along the cylindrical wall forming the craters. After the extinction of the partial discharges, the charge transport across the conductive cylindrical wall may also indicate small undetectable discharges, or alternatively lead to highly localized power dissipation and thereby contribute to further erosion along the cylindrical wall.

There is a strong experimental evidence (litt. 8, 44) that in test samples with cylindrical cavities, exposed to partial discharges during time periods of up to 10^4 hours at low or medium values of the ratio test voltage to inception voltage U_{test}/U_{inc}, the breakdown always develops from the described craters. This holds true for polyethylene and aromatic epoxy resins. Therefore, the mechanism of initiation of these craters is of particular significance for the advance of the breakdown processes. An important conclusion, which can be drawn from the above discussion, is that the primary causes for the growth of craters are the high conductivity of the test sample surface in conjunction with the succession of the rapidly developing partial discharges or the localized power dissipation in other forms.

4. CALCULATIONS OF THE FIELD STRESS DISTRIBUTION IN CYLINDRICAL AND SPHERICAL CAVITIES.

Introduction.

The calculations are carried out for test samples stressed by alternating test voltage. The two possible cases are taken into consideration: A) the applied test voltage is less than the inception voltage, and B) the applied voltage exceeds the inception voltage. The results are given as plots of equipotential and induction lines together with relevant distributions of the field stresses calculated for points in the vicinity of the cavity walls.

The properties and structure of the specific field can by no means be established by a single computation, since they depend upon numerous parameters. They are: the geometry of the cavity and the electrodes, the permittivity and conductivity of the insulation surrounding the cavity, the distributions of electrical charges left on the cavity surface and the instantaneous value of the applied ac voltage. When these parameters are completely specified the equipotential and induction lines in principle can be determined under the assumption of quasi-stationary conditions.

In reality, the considered fields have a transient character: when the internal discharges occur under alternating voltage conditions the densities of charges left on the cavity surface by discharge change with time, and the field, specified by the charge distributions and instantaneous value of the voltage, becomes a function of time. The field intensity also changes with time during the propagation of the individual partial discharge across the cavity. From the above reasons the field in the cavity and its surroundings can only be calculated under simplifying assumptions, which presumably represent the experimental conditions in the best possible way.

Hall and Russek (litt. 52) and Mitra and Salvage (litt. 53) computed field distributions in the cylindrical cavity, the axis of the cavity being oriented orthogonal to the two plane-parallel infinite electrodes. Additionally, they assumed that the conductivity and electrical charges collected on the surface were negligible. They found

that the maximum stress in the cavity occurred along the cavity axis. Maxwell (litt. 54) showed, that the field in an infinite dielectric cylinder, the axis of the cylinder being orthogonal to the applied field, is uniform. The cylinder was introduced into an infinite, originally uniform field; the conductivities were also neglected.

As the measurements (subsec. 3.3) clearly showed that the surface conductivity changes considerably during the tests, the conductance of the surface was taken into account in the present calculations by the introduction of thin conducting surface layers in the model. The calculations were carried out for virgin cavities, which means cavities empty of deposited charges, as well as cavities containing distributed surface charges left by former discharges. Quasi-stationary conditions were assumed. The field distributions were calculated by numerical computations of two-dimensional fields, using a computer program developed by Madsen and Olesen (litt. 55). A cylindrical cavity with the axis oriented orthogonal to the plane-parallel infinite electrodes was assumed, as illustrated in fig. 4.1. The error due to the not realistic assumption of infinite electrodes has been checked by means of additional computations carried out for the finite electrodes used in the investigations, and was found to be negligible. Additionally, the distribution of potentials in a spherical cavity located in a similar electrode configuration has been calculated.

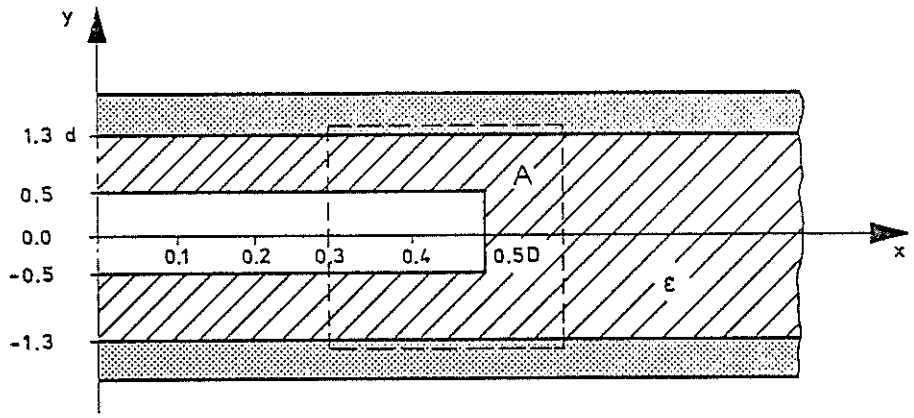

Fig. 4.1.

The test sample presupposed in the calculations made. Cavity diameter D = 1 cm, cavity depth d = 0.1 cm, permittivity ε_r = 2.3. In the next figures the equipotential and induction lines will be shown merely for the area A.

4.1. The Distribution of the Field Stress When the Applied Test Voltage is Less Than the Inception Voltage.

A virgin cavity, i.e. a cavity empty of surface charges left by partial discharges and an isotropic and homogeneous test sample material will be presupposed.

Cylindrical Cavities.

Equipotential and induction lines are plotted on fig. 4.2 merely for the area A which surrounds the cylindrical wall of the cavity (see fig. 4.1). Three cases are considered: 4.2.a - the cavity is introduced into a homogeneous insulation material with permittivity $\varepsilon_r = 2.3$, the surface conductivity is negligible; 4.2.b - two thin conductive and equipotential layers are formed on the surface; 4.2.c - the whole cavity surface is conductive and equipotential. Whereas, in the case 4.2.a, the maximum stress occurs along the cavity axis and the minimum stress across the cylindrical wall, the clearly opposite situation prevails in the case 4.2.b, wherein the sites in the neighbourhood of the cavity edge are the most stressed.

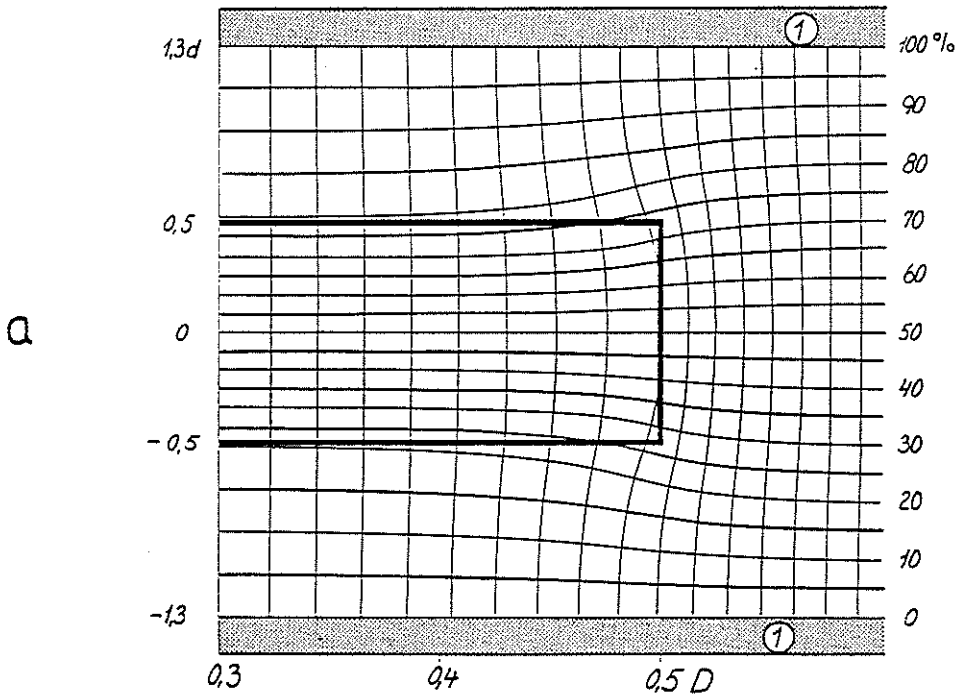

Fig. 4.2.a.

Field in the area A under alternating voltage conditions.
a - the surface and bulk conductivities are negligible.
1 - the electrodes, 2-(overleaf) the conductive layers 0.1 mm in thickness. Cavity depth and diameter 0.1 cm and 1 cm, resp.

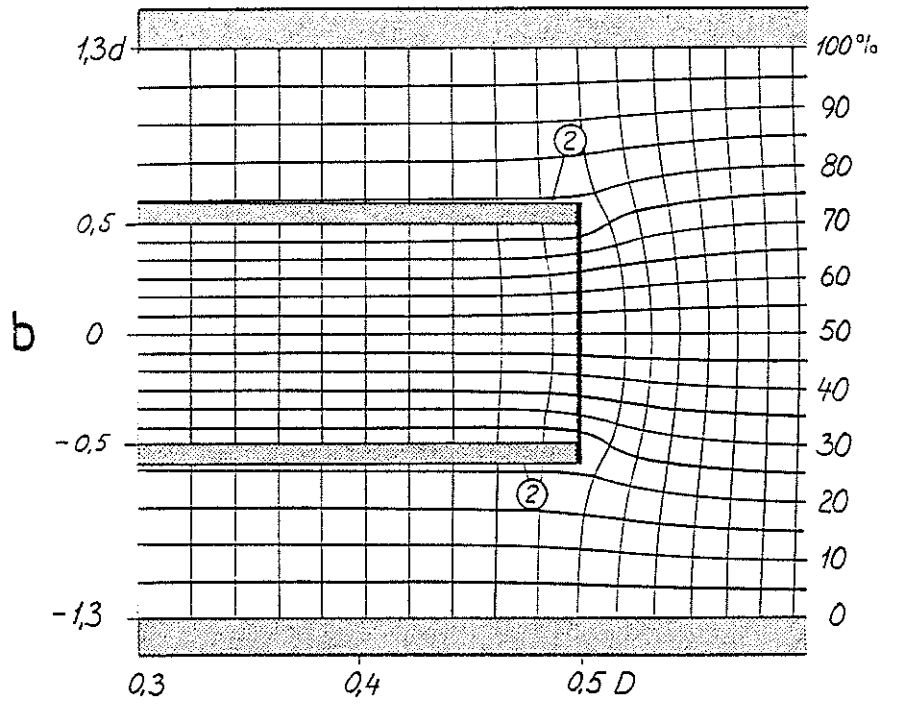

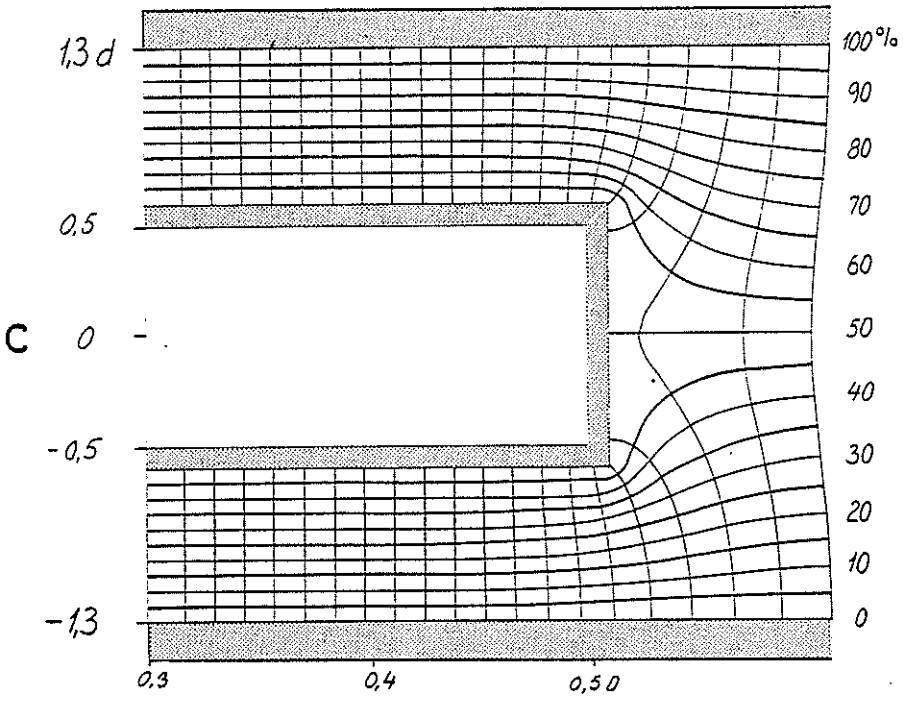

Fig. 4.2. b and c.

Field in the area A under alternating voltage conditions.

b - the upper and lower surfaces are conductive.

c - the whole cavity surface is conductive.

The field stress distributions are calculated along lines given by: x = const. and y = const. The calculated values are normalized by the value E_∞ for the field intensity in a cavity for which the ratio: cavity diameter/cavity depth is great: $D/d \to \infty$. In such a cavity it is permissible to ignore the fringing effects. Thus, the field becomes constant throughout the cavity and is given by:

$$E_\infty = \frac{U}{d+(d_1+d_2)/\varepsilon_1} \qquad \text{for } D/d \to \infty \qquad (4.1.1.)$$

U being the potential across the cavity, d_1 and d_2 being thicknesses of the outer insulation layers placed between electrodes and cavity. For instance, in fig. 4.1, $d_1+d_2 = 0.6\ d$.

The field stress distributions calculated along the lines x = 0.5·D and y = 0.5·d are shown in fig. 4.3. Again, it can be noted that for increasing x the field decreases when the conductivity is negligible, and increases when the conductive layers are present.

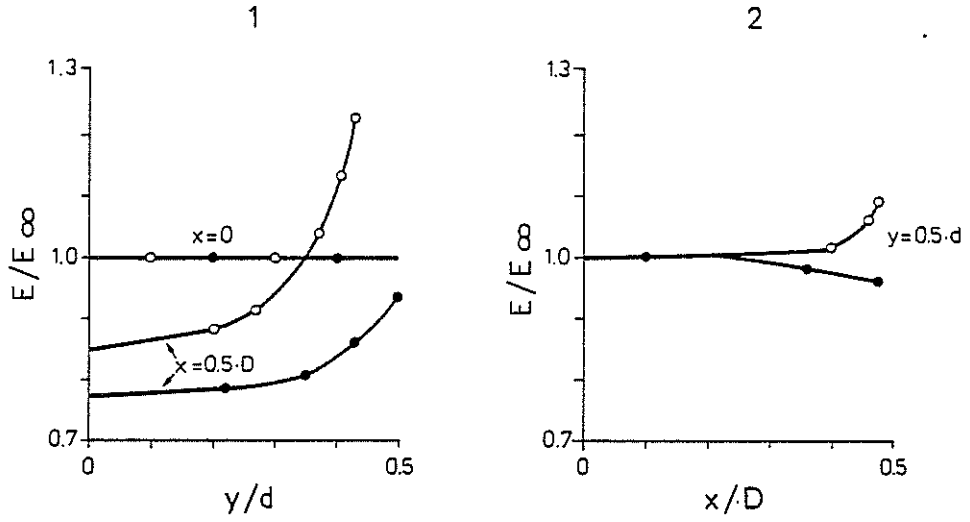

Fig. 4.3.

The distributions of electrical field stress acting in the virgin cylindrical cavity when the field stress is less than the ignition field stress. —•—•— for cavity shown in fig. 4.2.a wherein the conductivity is negligible. —o—o— for cavity shown in fig. 4.2.b wherein thin, conductive layers are present on the top and bottom of the cavity. 1: stress distribution along the cylindrical wall of the cavity, x = 0.5·D. 2: the radially stress distribution along the top of the cavity, y = 0.5·d.

Spherical Cavities.

When an airfilled, spherical cavity is introduced into an infinite, originally uniform field E the field is constant everywhere in the cavity. The field intensity is given by (litt. 22, 54):

$$E_{\infty s} = \frac{3\varepsilon_1}{1+2\varepsilon_1} \cdot E \qquad (4.1.2.)$$

where E is the field applied at great distance from the cavity. The field stress calculated for the cavity, which is shown in fig. 4.4.a, for which the distance between electrodes is $d_3 = 2.6 \cdot D$, is equal to the value given by equation 4.1.2 with an accuracy better than ± 1 %. If conductive layers are formed on the surface the field stress concentrations do occur, as shown in fig. 4.4.b. The field distributions along the line $x = 0.3 \cdot D$ are for both cases shown in fig. 4.5.

Provided that the described mechanism of increasing surface conductivity, which was experimentally established for cylindrical cavities, is in operation also in case of spherical cavities subjected to partial discharges, the following conclusions may be drawn:

1) In the beginning of the test when the surface conductivity is low the partial discharges will set on along the cavity axis parallel with the field stress direction.

2) Subsequently, during prolonged tests when the surface conductivity increases the discharges will set on at the sites where the field concentrations occur (fig. 4.4.b).

3) The inception voltage will decrease progressively during the test.

Weldingh (litt. 56), who closely investigated partial discharges in artificial spherical cavities, found that the inception voltage decreased considerably during tests of longer duration, and that the discharges moved toward the cavity wall as the test progressed. According to Weldingh, the observed changes could be due to the changes of properties of the cavity wall and of the gas enclosed in the cavity. These results seem to support the above drawn conclusions 1), 2), and 3).

It should be emphasized, however, that the models used in the present computations are highly idealised. Under actual experimental

conditions the change in the surface conductivity is believed to be a continuous function of the position. Therefore, the computed distributions give only a qualitative picture of the field in the cavity.

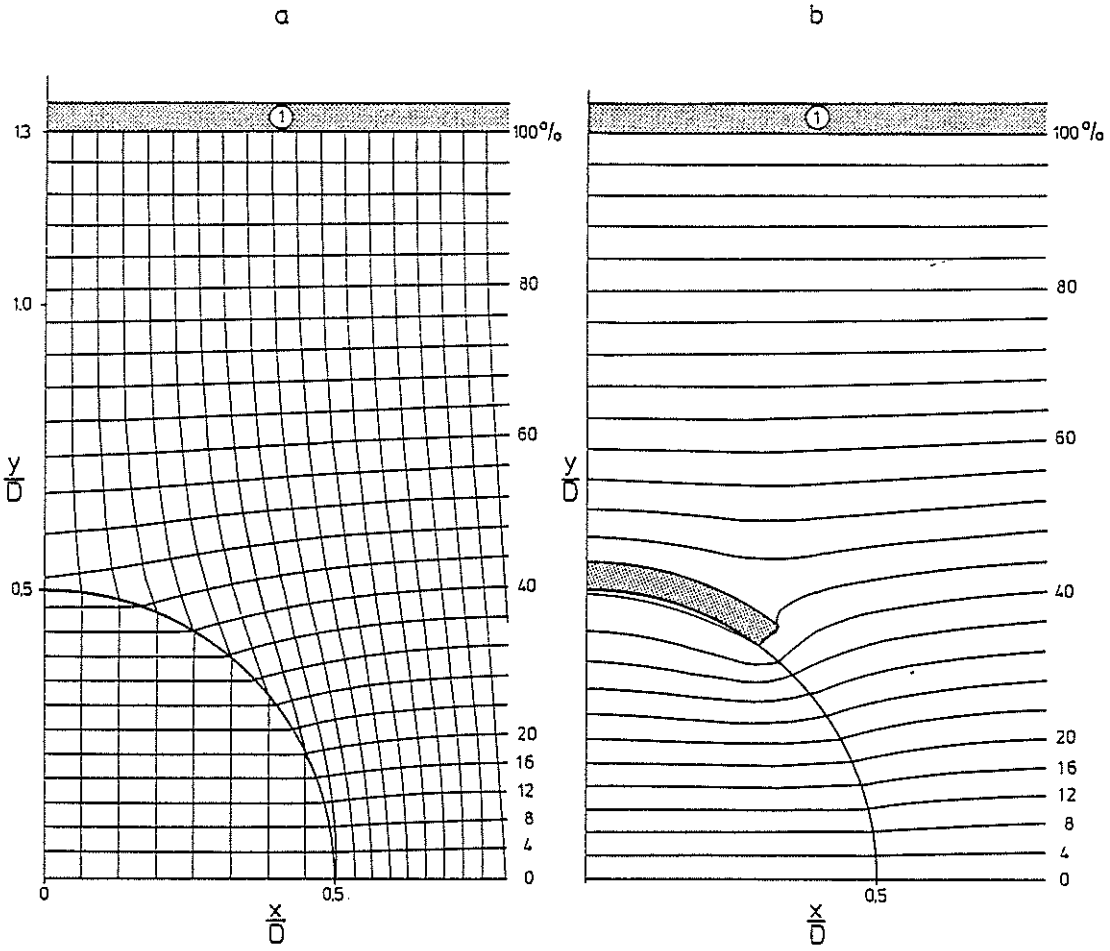

Fig. 4.4.

A spherical cavity with a diameter D introduced into the field between plane-parallel electrodes. a: conductivity negligible. b: there are two conductive lamina in the cavity. They are formed around a common axis which is oriented parallel to the field direction. A quarter of the cavity is shown. The distance between the electrodes is $d_3 = 2.6 \cdot D$.

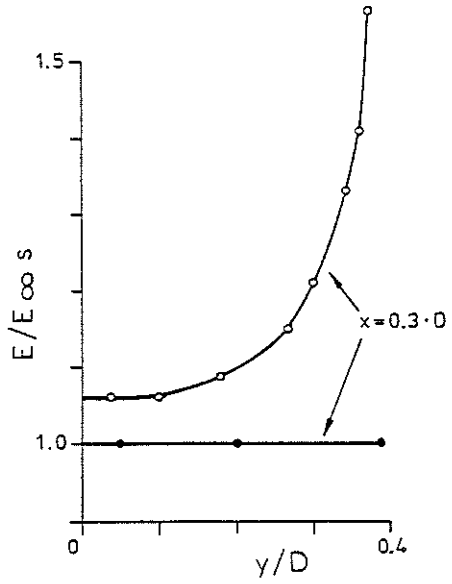

Fig. 4.5.

The field stress distribution for the spherical cavity shown in fig. 4.4 along the line x = 0.3·D. —●—●—●—: surface conductivity negligible, corresponding to fig. 4.4.a. —o—o—o—: two conductive layers are formed in the cavity as shown in fig. 4.4.b.

4.2. Distribution of the Field Stress When the Applied Voltage Exceeds the Inception Voltage.

Plane-parallel Cavity with $D/d \to \infty$.

When the applied voltage exceeds the inception voltage partial discharges occur and leave on the cavity surface a charge which reduces the stress originally acting in the cavity. Let $E(t)$ denote the field stress which would occur in the cavity if there were no partial discharges. For convenience, $E(t)$ will be called the prospective field stress. Suppose that the resultant average field stress E_c acting in the cavity remains constant at a value slightly below or equal to the ignition field stress E_{ig}. Since E_c is the superposition of $E(t)$ and $E_\sigma(t)$ which is the field stress due to the charge left on the cavity surface by discharges, as shown in fig. 4.6.a then:

$$E(t) - E_\sigma(t) \leq E_{ig} \qquad (4.2.1.)$$

Provided that the cavity surface is uniformly charged to a density σ, the field stress component E_σ is given by:

$$E_\sigma = \frac{\sigma}{\varepsilon_0} \cdot \left(1 + \frac{d}{(d_1+d_2)/\varepsilon_1}\right)^{-1} \qquad (4.2.2.)$$

ε_0 being the permittivity of air and ε_1 the relative permittivity of the insulation material. The component E_σ is shown in fig. 4.6.b for the instant when the instantaneous value of the applied voltage and prospective field stress equals zero.

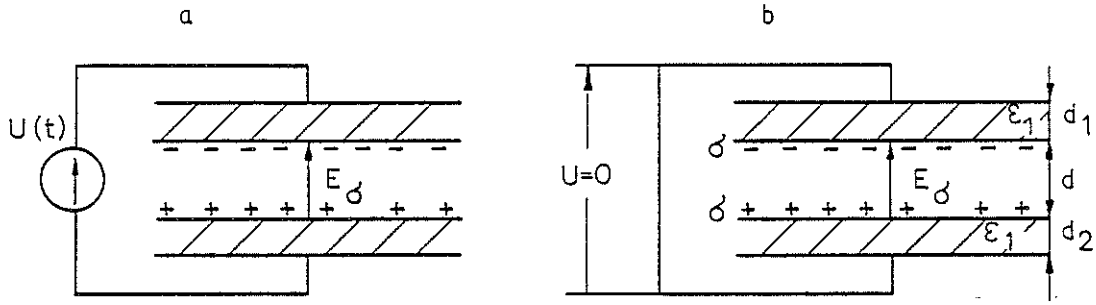

Fig. 4.6.

Schematic representation of the cavity with $D/d \to \infty$.

For the phase intervals of the test voltage, during which the partial discharges occur the inequation 4.2.1 leads by equation 4.2.2 to:

$$\sigma_d(t) \geq \left(\frac{E(t)}{E_{ig}} - 1\right) \cdot E_{ig} \cdot \varepsilon_0 \cdot \left(1 + \frac{d}{(d_1+d_2)/\varepsilon_1}\right) \qquad (4.2.2.a.)$$

The subscript "d" has been added to emphasize the fact that $\sigma_d(t)$ expressed the charge density due to charges left by partial discharges. From the equation 4.2.2 follows that the surface charge density necessary to keep the average value of the field stress acting in the cavity equal to, or slightly below, the constant level E_{ig} increases with increasing applied prospective field stress $E(t)$. Furthermore, the density σ_d depends upon the total thickness d_1+d_2 and permittivity ε_1 of the insulation layers between the cavity and the electrodes. If these layers are very thin the charge density may attain very high magnitudes.

A Cylindrical, Finite Cavity.

As in the latter case it is assumed that the remaning stress acting in the cavity after an individual partial discharge is only slightly smaller than the ignition field stress. Additionally, two thin conductive layers formed on the plane-parallel surfaces are assumed. The calculations are carried out for the ratio $U_{test}/U_{inc} = 2$. It must be recalled that the field E(t) which would occur in the cavity if there were no discharges is for the sake of convenience called the prospective field stress.

In fig. 4.7 the resultant field stress E_c prevailing in the cavity under quasi-stationary conditions is shown as a function of time together with the potential distributions calculated for the times A, B, C, D, and E. In the time period 0A the field intensity in the cavity is constant and equal to E_{ig}. Consequently the surface charge density changes with time according to equation 4.2.2.a. In the period from A to C no discharges occur, the charge density σ_d remains constant, whereas the field stress in the cavity changes from $+ E_{ig}$ to $- E_{ig}$ following the prospective field stress E(t). Equation 4.2.2.a is as a matter of course valid only in the part 0A of the period when the resultant field stress is equal to E_i.

It is seen that in the immediate neighbourhood of the cylindrical cavity wall strong field concentrations occur periodically. Nevertheless, this region of the cavity can be highly stressed as it is for cases A, B, and C, or less stressed as it is for case E. A rather unexpected situation occurs in the case D, when the field is sensibly uniform also in the neighbourhood of the cylindrical wall.

The distributions of the field stress along the cylindrical wall and across the cavity surfaces are given in fig. 4.8. Assessing the curves it can be noted that the frontier separating the domain of the highly stressed part from the remaining parts of the cavity wherein the field is always uniform is very close to the cylindrical wall. This fact has a particular significance for the explanation of the narrow crater ring occurring along the cylindrical wall of the cavity, and adds conviction to the conclusions drawn in the preceeding subsection (subsec. 3.3).

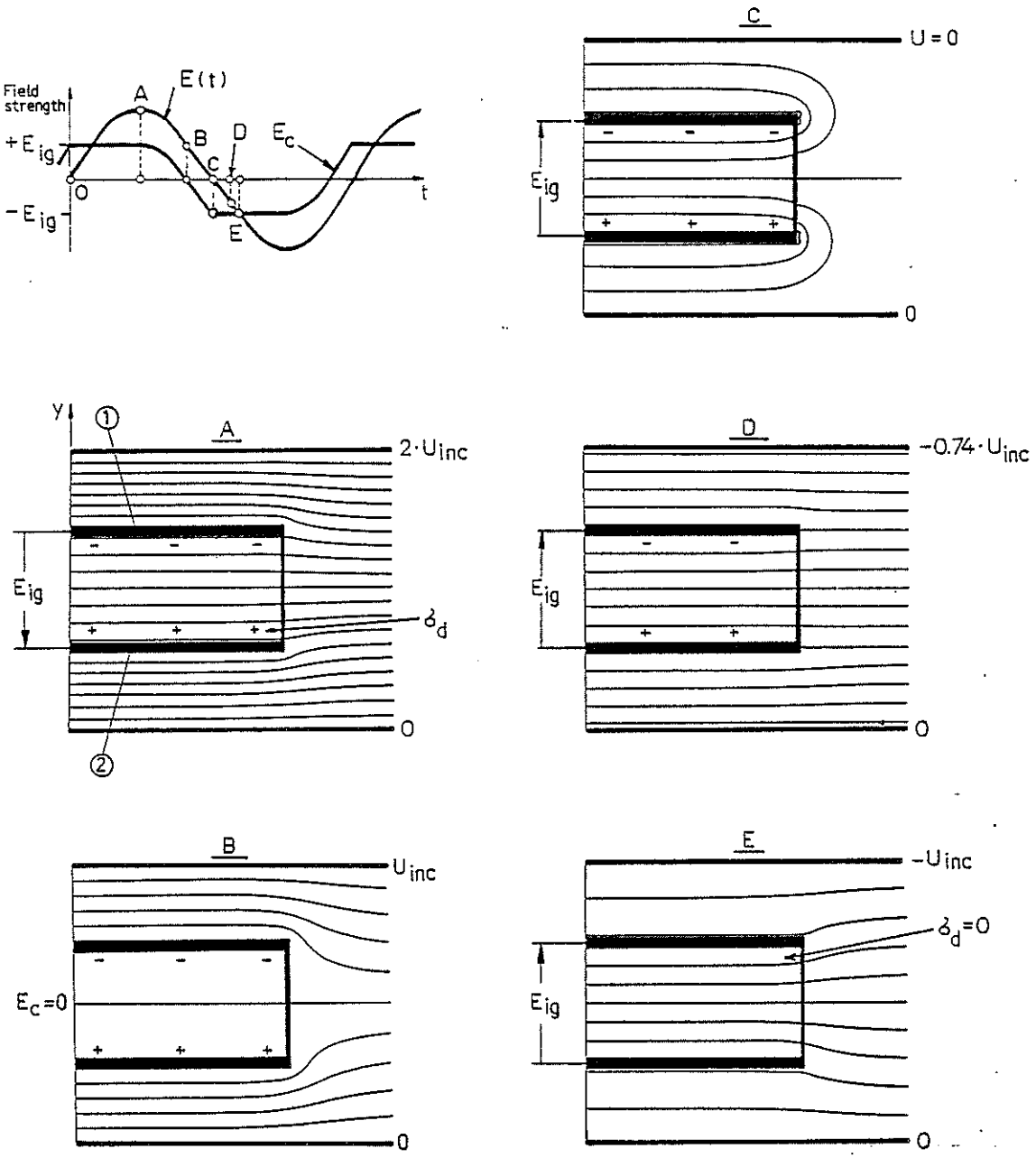

Fig. 4.7.

Field stress in the cavity under alternating voltage conditions. 1,2: the conductive lamina on the cavity surface. E, E_i, E_c: prospective, ignition and resultant field stresses in the cavity resp.; σ_d: charge density caused by the partial discharges. The applied voltage is assumed to be twice the inception voltage.

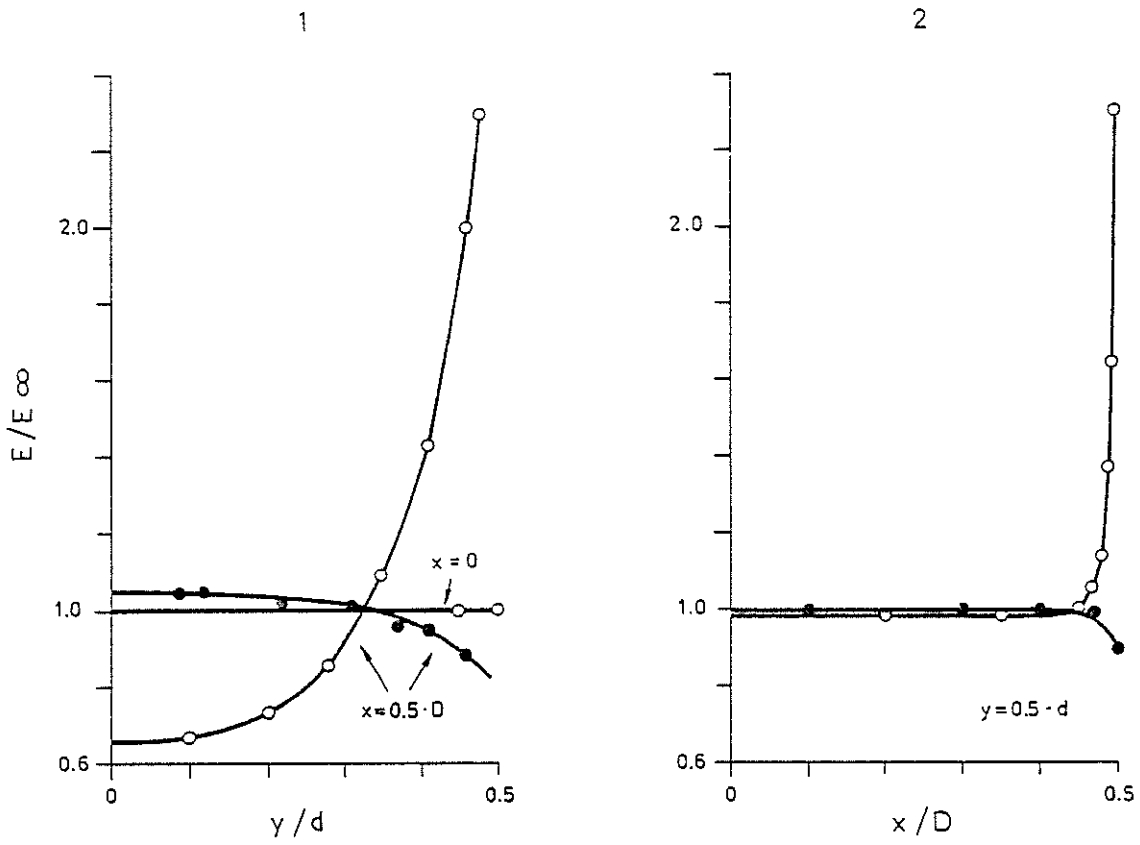

Fig. 4.8.

The field stress distribution when the test voltage exceeds the ignition voltage. —●—●—●— , —○—○—○— : distributions corresponding to fig. 4.7 -A and -C resp. 1: the distributions along the cavity axis x = 0 and the cylindrical wall of the cavity x = 0.5·D. 2: the distributions along the cavity surface y = 0.5·d.

It should be remembered that the calculations were carried out on the assumptions that the surfaces oriented orthogonal to the field direction are conductive, and that the stress in the cavity does not change very much during the passage of an individual partial discharge. It is desirable to discuss the validity and limitations of these assumptions.

It is known that when the conductivity of the surface is low the charges retended on the surface are concentrated in many small areas which can be experimentally detected as Lichtenberg figures. The field stress specified by this charge distribution varies strongly across the surface under such conditions and thus the first necessary

assumption is not fulfilled. As mentioned previously, this is the situation prevailing during the initial period of the test. During the prolonged exposure of the surfaces to partial discharges the surface conductivity increases, facilitating the transition from the rapidly developing discharges into the slowly developing discharges. Apart from the points in the neighbourhood of the cylindrical wall, the field in the cavity is thereafter sensibly uniform and indeed does not decrease very much during the passage of individual partial discharges. Thereby, both assumptions can be fulfilled merely for tests of sufficiently long duration. Since the surface conductivity change in a real cavity as a function of time and position, it must be presumed that the models used in the computations give a rather rough approximation of the real physical conditions.

A question which remains to be answered is in which manner the field stress acting in the cavity is changed during the development of an individual partial discharge. The field is then specified by transient distributions of charges and currents. The distributions will be theoretically established in the next chapter as functions of time and position by means of the transient analysis of the partial discharge currents.

5. OUTLINE OF THE TRANSIENT ANALYSIS OF PARTIAL DISCHARGE CURRENTS.

The aim of this section is to describe the transient growth and decay of the currents of an individual partial discharge. For purposes of mathematical tractability, a cavity with large ratio cavity diameter/ cavity depth is assumed, and hence the fringing effects can be assumed to be negligible. The cavity is introduced into an isotropic and homogeneous dielectric, and the originally applied field is assumed to be orthogonal to the cavity surfaces and to be uniform. In addition, it will be assumed that the electron avalanche generation mechanism is operative.

The following subsection deals with the solution of continuity equations which describe the growth of the partial discharge current in the cavity as a function of time and position. The analytical solutions are obtained by the method of Laplace-transformation for the case of a stationary field acting in the cavity. Since the field stresses are specified by the charge distributions which change with time, the complete solution is obtained taking the field changes into account.

5.1. Continuity Equations.

As previously stated, the volume charge density ρ in the gas filled cavity is a function of both time and position. The continuity equations are differential equations which govern this functional relationship. The continuity expressed in the equations is the continuity of existence, which means that the charges existing in the arbitrary volume V can not leave this volume without crossing a closed surface S bounding the volume V. The equations will be derived in terms of the transport, ionization, and deionization processes.

The charge flowing out across the surface S in unit time is given by the surface integral

$$\oint_S \vec{j} \cdot \vec{n} \cdot ds \qquad (5.1.1.)$$

where $\vec{j}$ is the current density and $\vec{n}$ the unit normal to the surface element ds. The increase of charge in unit time due to the ionization

processes is given by the volume integral

$$\int_V \alpha \cdot \rho \cdot \vec{v} \cdot \vec{d} \cdot dV \qquad (5.1.2.)$$

α being the ionization coefficient, ρ the volume charge density and $\vec{v}$ the drift velocity of the particular species of charge particles in question, and $\vec{d}$ being a unit vector parallel with the field direction. The decrease in charge due to deionization processes is given by the volume integral

$$\int_V \frac{\rho}{\tau_d} \cdot dV \qquad (5.1.3.)$$

where τ_d is a mean life time for the species of charge particles. Because of the continuity, the rate of change of the charge in the region within surface S is given by

$$\int_V \frac{\partial \rho}{\partial t} \cdot dV = - \oint_S j \cdot \vec{n} \cdot ds + \int_V \alpha \cdot \rho \cdot \vec{v} \cdot \vec{d} \cdot dV - \int_V \frac{\rho}{\tau_d} \cdot dV \qquad (5.1.4.)$$

By application of Gauss' divergence theorem, the surface integral is transformed into a volume integral, and hence equation 5.1.4 becomes

$$\int_V \left(\frac{\partial \rho}{\partial t} + \operatorname{div} \vec{j} - \alpha \cdot \rho \cdot \vec{v} \cdot \vec{d} + \frac{\rho}{\tau_d} \right) \cdot dV = 0 \qquad (5.1.5.)$$

Since V is an arbitrary volume and the integrand is assumed to be a continuous function of position it is necessary that the integrand vanish at each ordinary point and the equation in differential form becomes

$$\frac{\partial \rho}{\partial t} + \operatorname{div} \vec{j} - \alpha \cdot \rho \cdot \vec{v} \cdot \vec{d} + \frac{\rho}{\tau_d} = 0 \qquad (5.1.6.)$$

In a partial discharge different types of charge particles will be present, the density of each species of particles being described by the pertinent differential equation. Since the quantities entering equation 5.1.6 are field-dependent the analytical solution of equation 5.1.6 is possible only for the condition of the uniform and stationary field. Unfortunately, the partial discharge fails to satisfy this condition. Nevertheless, the solution is still obtainable for a time period sufficiently short in comparison with the duration of

the partial discharge, so that the field stress can be assumed constant during this period. The complete solution can be obtained by successive computations extended over the whole period of the partial discharge duration.

5.1.1. General solutions for an arbitrary charge density applied in the vicinity of the negative surface.

For a cylindrical cavity introduced into a uniform field, the axis of the cavity being oriented parallel with the field direction, the problem becomes one-dimensional. It is assumed that the x-axis is parallel to the cavity axis, that the zero point of the x-axis is located at the negative surface of the cavity, and that the electron drift velocity is oriented in the positive direction of the x-axis.

Assuming that only the transport and ionization processes are operative, equation 5.1.6 leads immediately to Townsend's differential equations on the form

$$\frac{\partial \rho_-}{\partial t} = - v_- \cdot \frac{\partial \rho_-}{\partial x} + \alpha \cdot \rho_- \cdot v_- \qquad (5.1.7.a.)$$

$$\frac{\partial \rho_+}{\partial t} = v_+ \cdot \frac{\partial \rho_+}{\partial x} + \alpha \cdot \rho_- \cdot v_- \qquad (5.1.7.b.)$$

where ρ_-, ρ_+ and v_-, v_+ are electron and positive ion densities and drift velocities respectively. When the attachment and detachment processes are also taken into account the continuity equations become:

$$\frac{\partial \rho_-}{\partial t} = - v_- \cdot \frac{\partial \rho_-}{\partial x} + (\alpha - \eta) \cdot \rho_- \cdot v_- + \upsilon_n \cdot \rho_n \cdot v_n \qquad (5.1.8.a.$$

$$\frac{\partial \rho_+}{\partial t} = v_+ \cdot \frac{\partial \rho_+}{\partial x} + \alpha \cdot \rho_- \cdot v_- \qquad (5.1.8.b.$$

$$\frac{\partial \rho_n}{\partial t} = - v_n \cdot \frac{\partial \rho_n}{\partial x} + \eta \cdot \rho_- \cdot v_- - \upsilon_n \cdot \rho_n \cdot v_n \qquad (5.1.8.c.$$

where ρ_n and v_n are negative ion density and drift velocity, respectively, and η and υ_n are attachment and detachment coefficients, respectively.

In the following paragraphs the most general solution of equation 5.1.7.a, b as well as the particular solutions in terms of specific initial - boundary conditions will be obtained by application of Laplace transformation.

The functions $\rho_{\pm}(x,t)$ which uniquely determine the solution of the continuity equation 5.1.7.a, b must satisfy both the initial condition

$$\rho_{\pm}(x,0) = 0 \qquad (5.1.9.a.$$

which signifies that there are no charges in the cavity at the time $t = 0$, and the boundary conditions:

$$\rho_{-}(0,t) = \phi(t) \qquad (5.1.9.b$$

$$\rho_{+}(d,t) = 0 \qquad (5.1.9.c$$

General solutions will be given for an arbitrary function $\phi(t)$, whereas the particular solutions will be obtained for definite functions $\phi(t)$ determined by the physical conditions appearing at the boundary.

The Laplace transform of the equation system 5.1.7.a, b gives by virtue of the initial condition 5.1.9.a image equations in the form:

$$s \cdot \rho_{-}(x,s) = -\frac{d\rho_{-}}{dx} \cdot v_{-} + \alpha \rho_{-} \cdot v_{-} \qquad (5.1.10.a$$

$$s \cdot \rho_{+}(x,s) = \frac{d\rho_{+}}{dx} \cdot v_{+} + \alpha \cdot \rho_{-} \cdot v_{-} \qquad (5.1.10.b$$

Equation 5.1.10.a upon separation gives:

$$\frac{d\rho_{-}(x,s)}{\rho_{-}(x,s)} = \left(\alpha - \frac{s}{v_{-}}\right) \cdot dx \qquad (5.1.11.)$$

Integration of equation 5.1.11 leads to:

$$\rho_{-}(x,0) = \rho_{-}(0,s) \cdot \exp\left(-\frac{x}{v_{-}} \cdot s\right) \cdot \exp\left(\alpha \cdot x\right) \qquad (5.1.12)$$

and by application of the translation theorem, inverse transformation leads to the solution

$$\rho_-(x,t) = \rho_- \left(0, t - \frac{x}{v_-}\right) \cdot \exp(\alpha \cdot x) \qquad \text{for } t \geqq \frac{x}{v_-}$$

$$\rho_-(x,t) = 0 \qquad \text{for } t < \frac{x}{v_-} \qquad (5.1.13.)$$

which with $j_-(x,t) = v_- \cdot \rho_-(x,t)$ is equivalent to

$$j_-(x,t) = j_- \left(0, t - \frac{x}{v_-}\right) \cdot \exp(\alpha \cdot x) \qquad (5.1.14.)$$

Physically, equation 5.1.13 means that the electron density at the position x and at the time t is equal to the electron density at the negative surface at the time $(t - x/v_-)$ multiplied by $\exp(\alpha \cdot x)$. In the elementary case of an electron avalanche started by one initial electron appearing in the neighbourhood of the negative cavity surface, the number of electrons at the positive surface x = d calculated from equation 5.1.13 becomes $\exp(\alpha \cdot d)$, a quantity which is well known in electrical engineering applications. As mentioned previously, the charge density at the negative cavity surface (equation 5.1.9.b) is assumed for the general case to be an arbitrary function of time.

The positive ion density $\rho_+(x,t)$ is obtainable by solution of equation 5.1.10.b which with the condition 5.1.9.c and with the equation 5.1.12 after somewhat laborious but elementary calculations leads to the result

$$\rho_+(x,t) = \int_{t-\frac{d}{v}+\frac{x}{v_+}}^{t-\frac{x}{v_-}} v_- \cdot \rho_-(0,\tau) \cdot \alpha \cdot \frac{v}{v_+} \cdot \exp\left(\alpha \cdot v \cdot \left(t + \frac{x}{v_+} - \tau\right)\right) \cdot d\tau \qquad (5.1.15.)$$

where $v = v_+ \cdot v_- / (v_+ + v_-)$. The complete derivation is given by the present author in (litt. 57).

A short explanation of the relation 5.1.15 may be relevant. Suppose that the avalanche is started by a number of initial electrons with the charge density q_0 per unit surface. The charge appears instantaneously in the vicinity of the negative surface so that

$$j_-(0,t) = v_- \cdot \rho_-(0,t) = q_0 \cdot \delta(t) \qquad (5.1.16.)$$

$\delta(t)$ being Dirac's-function. Then the term:

$$\rho_+(x,t)_\delta = q_0 \cdot \alpha \cdot \frac{v}{v_+} \cdot \exp\left[\alpha \cdot v \cdot \left(t + \frac{x}{v_+}\right)\right] \qquad (5.1.17)$$

represents the unit-impulse solution of the equation system 5.1.10. To emphasize this fact the solution has been marked by the subscript "δ". The solution for an arbitrary charge density $\rho_-(0,t)$ can then be determined from the convolution integral given in equation 5.1.15.

5.1.2. Solution for the generation mechanism.

The solutions 5.1.13 and 5.1.15 express the electron and ion densities $\rho_\pm(x,t)$ at any time and point in the cavity as a function of the electron density $\rho_-(0,t)$ in the neighbourhood of the negative surface. From the mathematical standpoint, this density is an arbitrary function of time. Physically, its behaviour is determined by the type of the particular generation mechanism which is operative.

According to Townsend's model the electron density at the negative surface, $\rho_-(0,t)$, is composed of the density due to the external source of ionization, $\rho_0(0,t)$, and the density of the secondary electrons created in the vicinity of the negative surface.* If the probability of the instantaneous production of a secondary electron at the negative surface per ionizing collision is γ, then

$$\rho_-(0,t) = \rho_0(0,t) + \gamma \cdot \int_0^d \alpha \cdot \rho_-(x,t) \cdot dx \qquad (5.1.18.)$$

which by the solution 5.1.13 and with $j_-(x,t) = v_- \cdot \rho_-(x,t)$ leads to

$$j_-(0,t) = j_0(0,t) + \alpha \cdot \gamma \cdot \int_0^d j_-\left(0, t - \frac{x}{v_-}\right) \cdot \exp(\alpha \cdot x) \cdot dx \qquad (5.1.19)$$

*) The secondary emission at the cathode in air and nitrogen is well investigated (Chalmers et al. lit. 63; Chalmers & Tedford lit. 64) in the case where the discharge boundaries are metals. In the case of electrodes coated with insulation material, information concerning the secondary processes is very scarce, see for instance lit. 3, 65, and 66. During the action of partial discharges, the surface conductivity is changed by several orders of magnitude, see page 70. When, however, a Townsend secondary ionization coefficient is assumed the following calculation will apply in any case.

Equation 5.1.19 upon substitutions: $\tau = t - \frac{x}{v_-}$, $T_- = \frac{d}{v_-}$ and

$$j_-(0,t) = f(t) \tag{5.1.20.}$$

is equivalent to

$$f(t) = j_0(0,t) + \alpha \cdot \gamma \cdot v_- \int_{t-T_-}^{t} f(\tau) \cdot \exp(\alpha \cdot v_-(t-\tau)) \cdot d\tau \tag{5.1.21.}$$

With the notations:

$$\begin{aligned} t' &= t/T_-, \ t' \text{ being time in units of } T_-, \\ \lambda &= \gamma \cdot \alpha \cdot d, \\ \alpha \cdot d &= \sigma \end{aligned} \tag{5.1.22.}$$

equation 5.1.21 finally becomes

$$f(t') = j_0(0,t') + \lambda \cdot \int_{t'-1}^{t'} f(\tau') \cdot \exp(\sigma \cdot (t'-\tau')) \cdot d\tau' \tag{5.1.23.}$$

A solution of this integral equation in terms of the initial current density, $j_0(0,t')$, can be achieved in a convenient manner by Laplace transformation. The pertinent image equation is evaluated using the general method of solution of integral equations given for instance by Doetsch (litt. 58) and turns out to be

$$f(s) = j_0(0,s) \cdot \left[1 + \lambda \cdot \frac{1-\exp-(s-\sigma)}{s-\sigma-\lambda \cdot (1-\exp-(s-\sigma))}\right] \tag{5.1.24.}$$

$j_0(0,s)$ being an arbitrary density of the initial current in the neighbourhood of the negative surface.

It is seen that the complete solution is determined by the waveform of the initial current pulse and by the impulse-solution represented by the term in parantheses and obtainable from equation 5.1.24 with

$$j_0(0,s) = q_0 \tag{5.1.25.}$$

or

$$j_0(0,t') = q_0 \cdot \delta(t')$$

q_0 being the density of the initial charge per unit surface.

By application of the expansion theorem to equation 5.1.24 and with 5.1.25 the impulse solution is found to be

$$f(t')_\delta = q_0 \cdot \delta(t') + q_0 \cdot \lambda \cdot \exp(\sigma \cdot t') \sum_{p=1}^{\infty} \left(\frac{s_p}{\lambda \cdot (1-\lambda+s_p)} \cdot \exp(s_p\, t') \right) \qquad (5.1.26.)$$

the s_p's being determined as poles of the function

$$f_1(s) = \frac{1}{\frac{s}{1-\exp(-s)} - \lambda} \qquad (5.1.27.)$$

In accordance with customary convention the impulse solution is again denoted by the subscript "δ".

According to equation 5.1.20 the relation epresses the total current density in the vicinity of the negative surface. The evaluation of the relation 5.1.26 must be effected in terms of the poles of function $f_1(s)$. They are specified as the roots which satisfy the transcedental equation

$$\frac{s}{1-\exp(-s)} = \lambda \qquad (5.1.28.)$$

Provided that $\lambda < 1$, which closely corresponds to the real physical conditions, it is found that $f_1(s)$ has one real pole and an infinite number of complex poles

$$\begin{aligned} &s_1 = a \\ &s_n = a_n \pm jb_n \quad n = 2, 3, 4 \ldots, n, \ldots \\ &0 > a > a_2 > \ldots > a_n > \ldots \end{aligned} \qquad (5.1.29.)$$

Since all poles are located in the left half plane the initial oscillation characterized by the complex poles: s_2, s_3, ... will be progressively attenuated for increasing time. Initially, the current will vary in step with the first generations and thereafter will smooth out and approach an asymptotic curve given by:

$$\lim_{t' \to \infty} j_-(0,t') = \lim_{t' \to \infty} f(t')_\delta = q_0 \cdot \frac{a}{1-\lambda+a} \cdot \exp((\sigma+a) \cdot t') \qquad (5.1.30.)$$

or, turning back to the time t, given by:

$$\lim_{t \to \infty} j_-(0,t) = \lim_{t \to \infty} f(t)_\delta = \frac{q_0}{T_-} \cdot \frac{a}{1-\lambda+a} \cdot \exp((\sigma+a) \cdot t/T_-) \qquad (5.1.31.)$$

Total Electron Current.

The total electron current is defined by equation 2.2.9 which by equations 5.1.14, 5.1.19, 5.1.22, and 5.1.31 leads to

$$\begin{aligned} i_{d-} = \frac{1}{d} \cdot \int_0^d A \cdot j_-(x,t) \cdot dx &= \frac{A}{\alpha \cdot \gamma \cdot d} \cdot (j_-(0,t) - j_0(0,t)) \\ &= \frac{q_0 \cdot A}{T_-} \cdot \frac{1}{\lambda} \cdot \frac{a}{1-\lambda+a} \cdot \exp\left((\sigma+a) \cdot \frac{t}{T_-}\right) \\ &\qquad t \to \infty \end{aligned} \qquad (5.1.32.)$$

The asymptotic behaviour of the current given by equation 5.1.32 is particularly relevant to the present investigation, because this equation substantiates the possibility of the calculation of the partial discharge currents. Thus, a short discussion involving some elementary proof is appropriate.

It must be expected that the present method of approach to the solutions will give essentially the same results for partial breakdown as those predicted on the basis of steady-state analysis of the Townsend regenerative breakdown mechanism. Indeed, if the exponent $\sigma + a > 0$ the current will increase indefinitely, whereas if $\sigma + a < 0$ the current will decrease to zero. The value $\sigma + a = 0$ upon insertion of $s_1 = a = -\sigma$ into equation 5.1.28 gives

$$\gamma \cdot (\exp(\alpha \cdot d) - 1) = 1$$

or neglecting 1 relative to $\exp(\alpha \cdot d)$

$$\gamma \cdot \exp(\alpha \cdot d) = 1 \qquad (5.1.33.)$$

whereby the result is obtained, which is in agreement with the well established Townsend breakdown criterion for a uniform field.

The general solutions 5.1.13 - 5.1.15 are consistent with results given without deriviations and mathematical proofs by Auer and Raether (litt. 59 and 20). The solution 5.1.26 for the generation mechanism is consistent with results obtained by Auer by the method of generating functions and by Laplace-transformation (litt. 59).

As the solution (5.1.24) satisfies the condition of an arbitrary initial current, it is possible to examine the current growth for any particular initial current. Davidson (lit. 67, 68, 69, and 70) has given the exact and approximate solutions for the case of current growth subject to the condition of a constant initial current I_o generated at the cathode by external illumination. It would therefore be desirable to ascertain whether or not the equation 5.1.24 gives results consistent with Davidson' solution. A further discussion is given in appendix 3.

5.2. Calculation of the Partial Discharge Current.

The electrical field in the cavity is specified by the charge density distributions of each species of charge particle produced during the development of the partial discharge. Thus the field change is quantitatively determined in terms of the changes in charge distributions. For a sufficiently short time increment Δt_i, the current and charge distributions can be calculated assuming that the parameters entering into the calculation are constant. At the end of the period Δt_i, new values for the field strength and the field dependent parameters are computed. The end-values for the period Δt_i constitute the initial value for the period Δt_{i+1} in which the calculations are repeated in a similar manner.

In the present subsection the problems will be formulated in the form of a set of equations valid during a time increment Δt_i. The equations will be established in a form which is readily applicable to the numerical computations, so that the laborious work of carrying out the calculations can be done by a computer.

5.2.1. The current and charge distributions.

The time increments are very short in comparison with the duration of a partial discharge and are equal, in most cases, to T_-, which amounts to some few per mille of the discharge duration. For each time increment it is assumed that after the passage through the cavity the electrons are uniformly collected on the positive surface of the cavity, whereas the positive ions, because of their considerably lower drift velocity, are partly accumulated as a space charge in the cavity and partly collected as a charge on the negative surface; both contributions being uniformly distributed in planes oriented orthogonal to the field direction.

The increment of the surface density of the electrons accumulated during a short time increment Δt can be calculated upon integration of the electron current density $j_-(d,t)$ which prevails in the immediate vicinity of the positive surface during this time. With equation 5.1.14 and 5.1.31 this density is given by

$$j_-(d,t) = \frac{q_0}{T_-} \cdot \frac{a}{1-\lambda+a} \cdot \exp\left(\sigma + (\sigma+a) \cdot \left(\frac{t}{T_-} - 1\right)\right) \qquad (5.2.1.)$$

The initial value of the current density $j_-(d,0)$ can be obtained upon inserting $t = 0$ in equation 5.2.1.

The increment of the surface density of the accumulated electrons during the period Δt is given by the integral

$$\Delta\sigma_-(\Delta t) = \int_{t_i}^{t_i+\Delta t} j_-(d,t) \cdot dt \qquad (5.2.2.)$$

and the total charge density can be calculated by

$$\sigma_-(t_i+\Delta t) = \sigma_-(t_i) + \Delta\sigma_-(\Delta t) \qquad (5.2.3.)$$

The number of positive ions produced in the cavity during a period Δt equals the number of electrons created during this period. According to equation 5.1.17, the ions are exponentially distributed in the cavity and will reach the negative surface ("the cathode") with a time delay determined by their drift velocity. It can be shown that the

density of positive ions collected on the negative surface is given by

$$\sigma_+(t_i+\Delta t) = \sum_{t_n} \Delta\sigma_-(t_n) +$$

where $t_n < t_i+\Delta t-T_+$

$$\sum_{t_n} \Delta\sigma_-(t_n) \cdot \exp(\alpha \cdot v \cdot (t_i+\Delta t-t_n - T_+)) \qquad (5.2.4.)$$

where $t_n > t_i+\Delta t-T_+$

T_+ being the transit time of the positive ions.

Those ions, which are not yet collected on the negative surface are distributed within the cavity, and their movement constitutes the ionic current. Since their density at the time $t_i+\Delta t$ is given by $\sigma_-(t_i+\Delta t) - \sigma_+(t_i+\Delta t)$, the ionic current is:

$$i_{d+} = (\sigma_-(t_i+\Delta t) - \sigma_+(t_i+\Delta t)) \cdot A/T_+ \qquad (5.2.5)$$

A being the area of the cavity surface.

Provided that the time increment is chosen sufficiently short, so that the parameters entering equation 5.2.1 can be assumed constant during the periods, the electron current density at any time t during the period $[t_i, t_i+\Delta t]$ can be related to the electron current density in the former period $[t_i-\Delta t, t_i]$ by means of

$$j_-(d,t) = j_-(d,t_i) \cdot \exp\left((\sigma+a) \cdot \frac{t-t_i}{T_-}\right) \cdot \frac{k_j(t_i)}{k_j(t_i-\Delta t)} \quad t_i < t < t_i+\Delta t \qquad (5.2.6.)$$

whence the density at the time $t_i+\Delta t$ is

$$j_-(d,t_i+\Delta t) = j_-(d,t_i) \cdot \exp\left((\sigma+a) \cdot \frac{\Delta t}{T_-}\right) \cdot \frac{k_j(t_i)}{k_j(t_i-\Delta t)} \qquad (5.2.7.)$$

the $k_j(t_i)$, $k_j(t_i-\Delta t)$ being coefficients given by the expression

$$k_j(t_n) = \left[\frac{a \cdot \exp\sigma}{T_- \cdot (1-\lambda+a)}\right]_{t=t_n} \qquad (5.2.8.)$$

Similarly, the total electron current i_{d-} is given by:

$$i_{d-}(t_i+\Delta t) = i_{d-}(t_i) \cdot \exp\left((\sigma+a) \cdot \frac{\Delta t}{T_-}\right) \cdot \frac{k_{id}(t_i)}{k_{id}(t_i-\Delta t)} \qquad (5.2.9.)$$

k_{id} being coefficients given by the expression

$$k_{id} = \left[\frac{a}{T_- \cdot \lambda \cdot (1-\lambda+a)}\right] t = t_n \qquad (5.2.10.)$$

5.2.2. The distribution of the electrical field stress.

From the equations describing the transient currents attention will now be focused on the behaviour of the electrical field. The equation describing the field in the cavity can be obtained either by means of Poisson's equation, or by approximating the discharge by a thin cylinder containing a prescribed charge distribution. According to lit. 71, the first method is valid when the discharge diameter is large (approximately two times the distance between the electrodes). Using Poisson's equation under this assumption and taking into account equations 4.2.2 and 5.1.17, it can be shown that the field stress at the time $t_i + \Delta t$ is given by:

$$E(x,t_i+\Delta t) = E_0 - \left[\frac{\sigma_+}{\varepsilon_0} + \frac{\sigma_- - \sigma_+}{\varepsilon_0} \cdot \exp\left(\alpha \cdot v \cdot (x-d)/v_+\right)\right] \cdot k_d \qquad (5.2.11.)$$

E_0 being the original field intensity acting in the cavity at the time of the onset of the partial discharge, and k_d being the factor associated with the capacitances between the cavity and the electrodes (see equation 4.2.2).

$$k_d = \left(1 + \frac{d}{(d_1+d_2)/\varepsilon_1}\right)^{-1} \qquad (5.2.12.)$$

5.2.3. The parameters entering into the calculations.

The overvoltage, i.e. the voltage in excess of the static breakdown voltage prevailing in the cavity at the onset of the partial discharge, is in the following text denoted by ΔV. The calculations are carried out for a preassumed value of the ΔV alternating corresponding to the preassumed initial value of the exponent $(\sigma + a)$.

The initial values of the parameters σ and a must satisfy the equation 5.1.28. The initial value of the reduced field stress in the cavity E_0/p is calculated as zero for the transcendental function of E/p given by

$$f(E/p) = \frac{\alpha}{p}\left(\frac{E}{p}\right) - \frac{\sigma}{p \cdot d} \qquad (5.2.13.)$$

The first right hand term of the equation specifies the functional dependence of the reduced ionization coefficient α/p upon the reduced field stress E/p. In the present investigation the functional dependence given in (litt. 35) in the form

$$\alpha/p = \exp(\text{pol}\ \{E/p\}) \qquad (5.2.14.)$$

where pol denotes a polynomical function, was employed. The second right hand term of equation 5.2.13 specifies the value of the reduced ionization coefficient α/p corresponding to the initial value of the parameter σ.

The accuracy of equation 5.2.13 was checked by calculating the static ignition field stress for $\sigma_0 = \varphi(d)$, where φ(d) is an empirical function specifying the values of the parameter σ_0 at the breakdown threshold (litt. 60, 61; eq. 5.2.16).

It was found that the values of the breakdown stress calculated in this manner were in agreement with values obtained from the purely empirical equation 3.1.4.a suggested for internal discharges by Bertein (litt. 32) with an agreement better than ± 0.5 % for the E/p range from 39 to 62 $V \cdot cm^{-1} \cdot mbar^{-1}$ (appendix 1). The advantage of the proposed method of calculation of the statical ignition field stress is that it is applicable for any gas type for which the functional dependence α/p = f(E/p) and the reduced ionization coefficient α/p at the threshold are known.

The field dependent drift velocities are calculated from the functional relation $v\pm = F(E/p)$ given in (litt. 35).

A direct calculation of the probability γ of the production of a secondary electron per ionising collision, assuming a given cavity configuration, material, and gas, is not possible at the present time due

to lack of knowledge of the probability of the release of an electron by a photon hitting the cavity surface (litt. 4). Therefore, the probability γ is determined indirectly from Townsend's breakdown criterion. According to (litt. 62) the γ is given by

$$\gamma = (\exp(\alpha \cdot d) - 1)^{-1} \qquad (5.2.15.)$$

where $\alpha \cdot d = \varphi(d)$. On the basis of the data for the ionisation coefficient at the breakdown threshold given by Vibholm (litt. 61), it was found that for the range of the investigated cavity depths: 0.01 cm < d < 0.15 cm, 1013 mb, $\varphi(d)$ is given by

$$\varphi(d) = \int_0^d \alpha(x) \cdot dx = 8.56 + 5.7\{d\} \qquad (5.2.16.)$$

where d is the cavity depth in cm and {d} is the numerical value of the cavity depth.

The value of the probability γ calculated from equation 5.2.15 is held constant during each computation. The validity of this assumption will be discussed in section 5.3.

At each of the subsequent time increments new values of field dependent parameters are calculated to satisfy the field distribution specified by equation 5.2.11. Thus the parameter σ is calculated as

$$\sigma = \int_0^x \alpha(x) \cdot dx \qquad (5.2.17.)$$

where $\alpha(x)$ is the value of the ionization coefficient at a given position x determined by the local value of the field stress E(x) given by equation 5.2.11.

The calculations are carried out for air within the range of the parameter p·d from 2 to 2000 mb·cm. It is assumed that the partial discharge current is built up from one initial electron which instantaneously appears in the immediate vicinity of the negative surface of the cavity.

The calculation of the partial discharge current is terminated after the current has decreased to zero.

5.3. Results of Calculations. Comparison of Measured and Calculated Results.

The shape of the current pulse calculated for a modest overvoltage is shown in fig. 5.1.a. Actually, this is the waveform which is characteristic of the slowly developing partial discharge. The total current is composed of the electron current and the ion current. During the initial phase of the current growth the current density is so small that the space and surface charges does not sensibly influence the field intensity (fig. 5.1.b). Thus, the current increases exponentially as a function of time with $\exp((\sigma + a) \cdot t/T_-)$. Gradually the charges collected at the surfaces become important and decrease the average field stress acting in the cavity. This field reduction causes the current to increase at a slower rate.

After a time period of ≈ 50 generations the current reaches the maximum, at which $(\sigma + a)$ equals zero and hence, by virtue of equation 5.1.33, the probability of the production of one secondary electron per avalanche: $\gamma \cdot \exp \sigma$ has decreased to 1 (fig. 5.1.b). From this instant the electron current decreases with time.

After a total time of 200 - 300 ns, the electron current decreases to a very small value and the ionization processes are definitely terminated.

Since the ions and electrons are created largely in the immediate neighbourhood of the positive cavity surface the ions travel almost the whole cavity before they are collected on the opposite surface. Thus the collection of the positive ions on the opposite surface takes place after a time delay approximately equal to the ion transit time across the cavity: T_+. The collection is visualised as an upturning of the Q_+ curve in fig. 5.1.c.

From fig. 5.1.b it appears that the calculated parameters σ and especially $\gamma \cdot \exp \sigma$ are subject to large relative decreases due to incomparable small decreases of the average field intensity acting in the cavity. This fact is due to the great sensitivity of the ionization coefficient on the field stress.

From fig. 5.1.a it is seen that the area below the electron current curve does not equal the area below the ion current curve. The reason for this inequality is that the average distance the electrons

travel before collection on the surface is shorter by far than that covered by the positive ions. Therefore, the integral of the electron current is smaller than the integral of the ionic current. The integral of the total partial discharge current: $\int i_d \cdot dt$, is approximately equal to the charges of the negatively and the positively charged particles.

The charge: $(k_2 \cdot R \,||\, Z)^{-1} \cdot \int i_d \cdot dt$, induced on the electrodes during the partial discharge is in accordance with common usage called the "apparent charge". This charge is a measure for the charge production in the cavity, if the geometrical and dielectrical relations, i.e. factor k_2, are known.

In order to calculate the number of negative ions the solution given in section 5.2 was modified to include attachment processes. Preliminary calculations showed that the number of negative ions was less than the number of electrons at least by a factor ten. For reasons given in section 3.1 the negative ions do not sensibly affect the waveform of the total current pulse. As the experimental data available at the present time for the reduced attachment coefficient only allowed the estimation of the number of negative ions (litt. 35), accurate calculation of the number of negative ions was not possible during the present study.

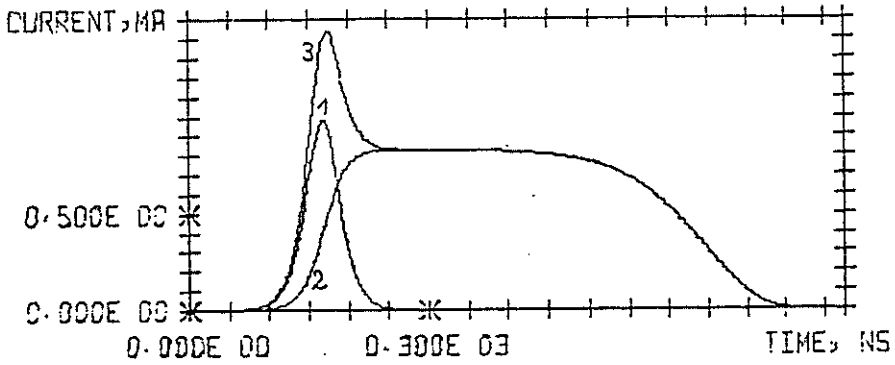

Fig. 5.1.a.

The electron current, ion current, and the total current i_d, curve 1, 2, and 3 resp. Cavity depth and diameter 0.07 and 1 cm resp., p = 1013 mb, air, overvoltage 6.1 per mille.

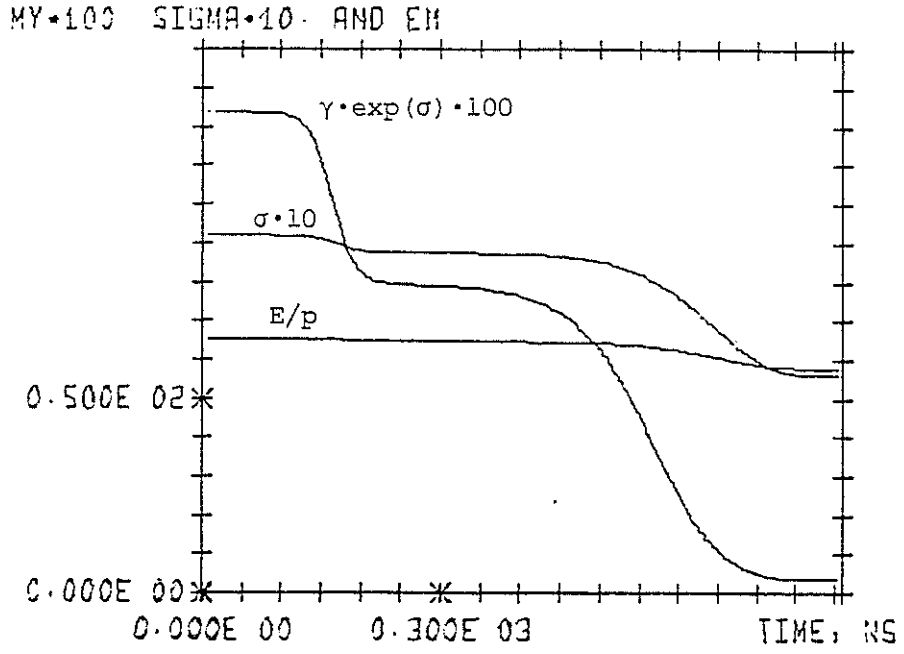

Fig. 5.1.b.

The temporal decrease of the average reduced field stress E/p, V/(cm·torr) and of the field dependent coefficients: $\sigma = \int_0^x \alpha(x) \cdot dx$ and $\gamma \cdot \exp\sigma$ for the partial discharge shown in fig. 5.1.a.

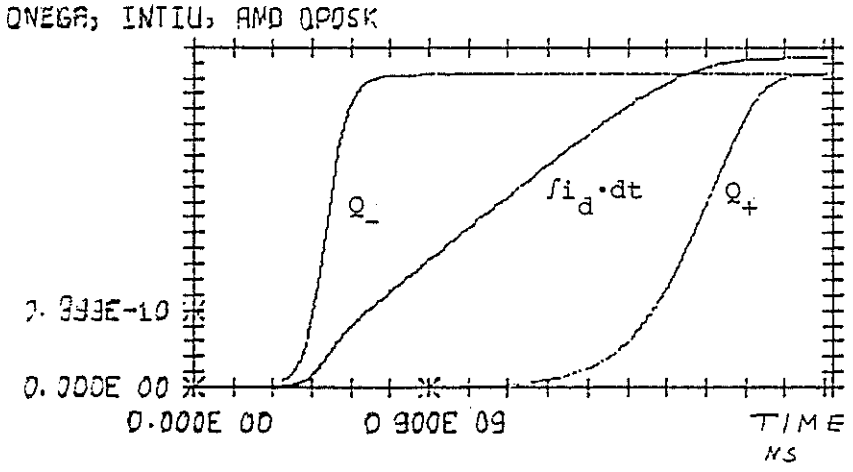

Fig. 5.1.c.

Charges collected on the surfaces of the cavity. Q_-: negative charge. Q_+: positive charge. Curve 3 shows the integral of the partial discharge current: $\int i_d \cdot dt$, all quantities are for the partial discharge shown in fig. 5.1.a.

The method for calculation of the electron and ion currents was developed at a very early stage of the present investigation (litt. 16). The presence of the electron current with the predicted unique characteristics has later been experimentally verified by the measurement of the photon flux. This flux is proportional to the electron current. The measurements of the photon flux always showed the same waveforms as those calculated for the electron current. A comparison of the typical waveform of the photon flux with the calculated electron current is shown in section 3.1, fig. 3.4.

Fig. 5.2. shows the variation of the shape of the partial discharge current pulse with the initial overvoltage applied. A dependence on overvoltage similar to that in fig. 5.2 was reported by Devins (litt. 3, fig. I-5, curves d, c, b). The present calculations were carried out for the same overvoltages, cavity depth and diameter, and pressure as those used in Devins' measurements. The calculated curves exhibit a similar characteristic increase in the pulse amplitude and the sharpness of the current maximum with increasing overvoltage as the waveforms measured by Devins. The calculated current pulse width corresponds closely to the pulse width of the measured waveforms but its magnitude is less than the magnitude measured. This is probably because the effective area of the surface, active during the partial discharge did not cover the whole gab of 25.4 mm in diameter during the measurements of Devins.

A comparison of the observed and calculated values of the partial discharge current is shown in fig. 5.3 for two different pressures. It is seen that the calculations adequately explain the fact that discharges become shorter and smaller with decreasing pressure. For some cavities it was found that the measured amplitude of the partial discharge current was frequently lower than the calculated current by up to a factor two. The cause for this decrease of the measured current amplitudes in relation to the amplitudes expected on the basis of the calculations is probably the variations of the discharge intensity in the directions orthogonal to the applied field. This amplitude reduction differs from one partial discharge to another as shown in fig. 3.3 and appears as a reduction of the average current density in the cavity.

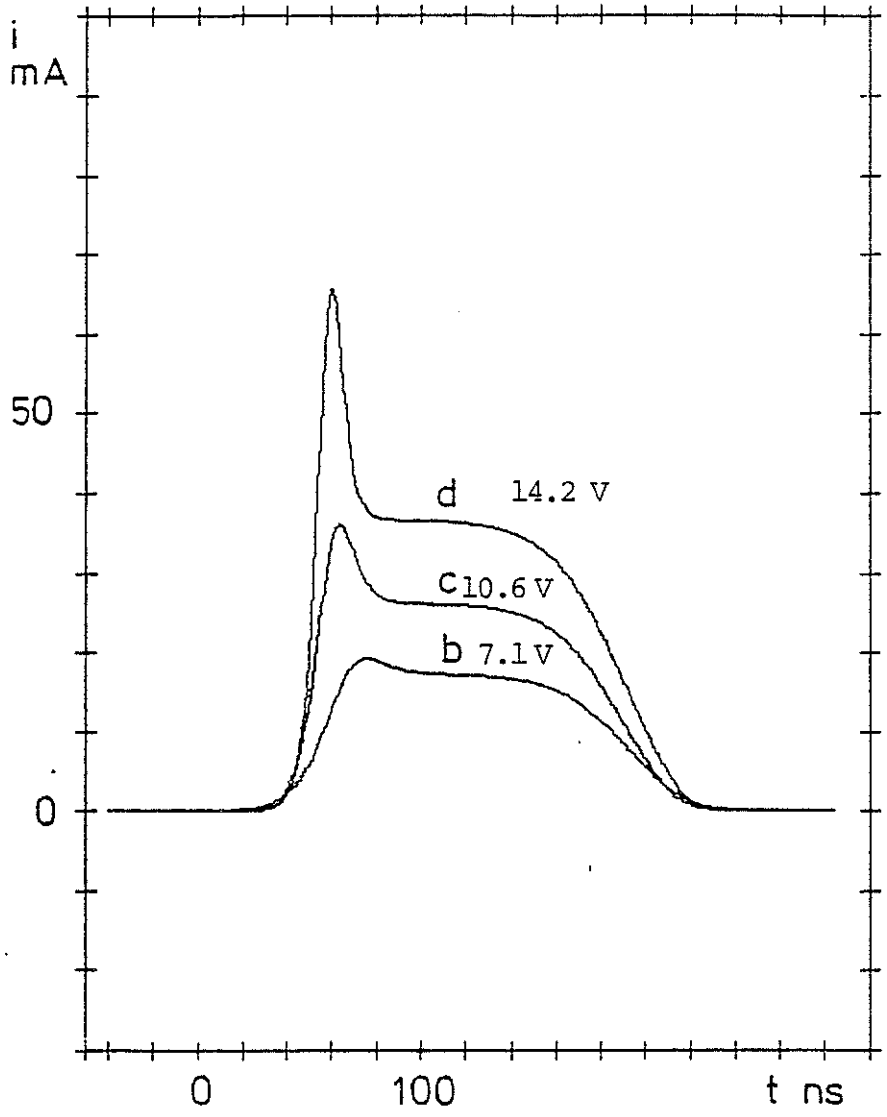

Fig. 5.2.

The partial discharge current with the over-voltage as a parameter. Cavity depth and diameter d = 0.025 cm and 25.4 mm resp., p = 1013 mb, static breakdown voltage 1.67 kV.

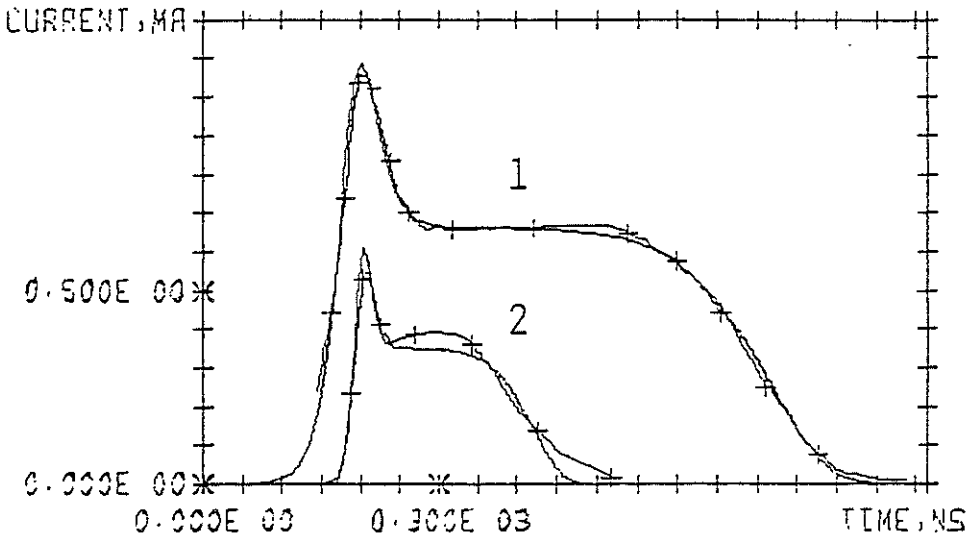

Fig. 5.3.

Comparison of the calculated (——) and measured (+++++) waveforms of the partial discharge current i_d for two different pressures. Cavity depth and diameter d = 0.074 cm and D = 1.0 cm resp.
Curves 1: p = 1013 mb, overvoltage 5 per mille, initial value of the parameter ($\gamma \cdot \exp\sigma$): 1.21.
Curves 2: p = 60 mb, overvoltage 7 per mille, initial value of the parameter ($\gamma \cdot \exp\sigma$): 1.29.

The above comparison indicates that the applied mathematical model in many details satisfactorily explains the properties and behaviour of slowly developing partial discharges under different experimental conditions.

This result will be further examined in the following discussion.

5.4. Discussion of the Simplifying Assumptions.

5.4.1. The constancy of the voltage.

The applied voltage changes during the development of an individual partial discharge, the change ΔU being partly due to 1) - the alternating character of the voltage, and partly due to 2) - the voltage drop on the measuring resistance.

Thus, the considered assumption is a simplification concerning the measuring method but not the mathematical model.

Around the maximum of the rate of change of the applied voltage, the ΔU due to 2) will be negligible in most cases in comparison with ΔU due to 1).

The main effects of the voltage change are:

a) - a change of the discharge amplitude,

b) - a change of the discharge duration.

It is supposed that a) is mainly due to the ΔU and the corresponding change of the parameter σ during the initial period of the partial discharge when the electron current increases. It can be shown that for the majority of discharges the relative change ΔU at 50 Hz is less than $5 \cdot 10^{-4}$ for $\Delta t < 100$ ns.

Thus, it can be resonably concluded that for the overvoltages of about $\Delta V > 5 \cdot 10^{-3}$ the ΔU does not sensibly affect the measured waveform of the majority of the slowly developing partial discharges. On the other hand, for overvoltages $\Delta V < 5 \cdot 10^{-3}$ the discharge magnitudes are very small and it is not possible to observe the effects of ΔU.

The b) is primarily due to the change of the mobility of ions and is of the same order of magnitude as the ΔU. The change b) is considered to be negligible in comparison with the change of the discharge duration due to the field reduction during the development of an individual partial discharge.

5.4.2. The discharge area is equal to the area of the cavity surface.

The discharge current is calculated by multiplying the average curren density by the area A of the cavity (eq. 5.1.32). Apparently, this mathematical asumption represents the physical condition when the discharge

is uniformly distributed over the whole cavity area A. Under real experimental conditions the assumption is not always fulfilled because the discharge intesity can vary across the cavity surface (subsect. 3.1.1). This fact together with the above comparison of the measured and calculated amplitudes indicate that the effective discharged area of the surface can frequently be less than A. For instance, this seems clearly to be the case for the large surfaces as in Devins' (litt. 3) measurements. However, the considered simplification does not influence the waveforms of the calculated currents.

The boundary conditions in the immediate neighbourhood of the cylindrical wall can cause increase as well as decrease of the current density depending on the actual field distribution in this region. The increase of the current in this area can be a probable cause of the occurrence of the "transition type".

5.4.3. The constant probability of the production of the secondary electrons.

The probability γ is assumed to be constant and to satisfy the equation 5.2.15.

The probability of the production of secondary electrons can generally represent secondary emission due to:

a) - incidence of positive ions,
b) - incidence of metastable particles,
c) - photo-ionisation in gas,
d) - photo-electric emission.

Degn (litt. 4) found that the secondary processes a) and b) are not probable because the involved transit times are much longer than the duration of the front of the partial discharge. The measurements of the photon flux emitted from the slowly developing partial discharge (subsec. 3.1.1) supplied a direct experimental proof that a generation mechanism which involves fast secondary processes as for instance c), d), or a still unknown process, is operative. This experimental result supported Degn's assumption about the existence of the generation mechanism.

The mathematical assumption that the probability is constant and satisfies the Townsend breakdown criterion, represents the physical situation when the production of secondary electrons does not depend on the condition at the surface and in the gas. From the physical point

of view, it might of course be expected that the production can be different for the different investigated materials, and additionally that the production will change with time due to the change of surface conductivity and surface charge density.

A quantitative assessment of the influence of the probability-change on the waveform and the amplitude of the partial discharges will be given on the basis of equation 5.1.32. The terms: 1) $(\sigma + a)$ and 2) $\frac{1}{\lambda} \cdot \frac{a}{1-\lambda+a}$ where $\lambda = \gamma \cdot \sigma$ will be considered in the following paragraphs.

The parameter $(\sigma + a)$ governs the rate of the current growth and the waveform of a partial discharge. It can be shown that $(\sigma + a)$ is given by:

$$(\sigma + a) = \Delta\sigma - \ln\left(\frac{-a}{\sigma}\right) \simeq \Delta\sigma \quad \text{for} \quad -a \simeq \sigma \qquad (5.4.1.)$$

where a is given by the equations 5.1.28 and 5.1.29 and $\Delta\sigma$ is the parameter σ in excess of the value of σ_0 at the static breakdown voltage. The $\Delta\sigma$ and thereby the parameter $(\sigma + a)$ depend only on the overvoltage ΔV. Therefore, the waveform of the slowly developing partial discharge will not be influenced by the change of the probability γ.

According to the term 2), the decrease of the probability γ will cause a corresponding increase of the amplitude of a partial discharge at a given overvoltage.

The results of the measurements clearly showed that the waveforms of the slowly developing partial discharges are not sensibly affected by the different types of materials and do not change as a function of time - which is in agreement with the first above conclusion. Also the amplitudes for a given waveform are approximately of the same order for different materials. This indicates that when the slowly developing partial discharges occur, the probability γ does not differ very much for the different considered materials.

From the above discussion it follows that the differences between the measured and calculated amplitudes can be due to the lessening of the effective area of the partial discharge as well as due to the change of the probability γ in relation to the value given by equation 5.2.15. However, the simplifying assumptions do not affect the waveforms of the calculated currents.

6. SUMMARY AND CONCLUSIONS.

The use of polymeric dielectrics in high voltage equipment has undergone a remarkable expansion during the years after World War II because of their attractive electrical and mechanical properties. The replacement of classical insulation materials by polymers allowed a size reduction with maintained ratings. Although the high strength of the polymeric materials would appear to justify much higher average stresses than those previously utilized in the industry, the application of these materials as high voltage insulation was still rather limited because of their low resistance to internal discharges, since the low resistance to the long term deterioration processes substantially limited the operating stress in the polymeric insulation - for instance in cables - to 1 (one) per cent of the short term stress.

Lichtenberg observed in 1777 (litt. 1) that the resin dust settling on a resin surface which has been subjected to a partial discharge formed starlike patterns.

Until the results of investigations conducted by Devins (litt. 3) and Degn (litt. 4) the description of the electrical phenomena related to internal discharges in gas-filled cavities was founded on a capacitive model proposed by Burstyn (litt. 5) and Gemant and Philipoff (litt. 6). An explanation of the current pulses connected with distinct types of partial discharges was not possible, however, because the model did not give a rigorous representation of the physical mechanisms and conditions in the cavity.

Devins, Degn and Neudert (litt. 10) found that at least two distinct types of partial discharges the "rapidly developing" and the "slowly developing" partial discharges occurred in cavities in solid dielectrics.

For the slowly developing partial discharge, both Devins and Degn proposed a generation mechanism which was governed by the changes of the space charge in the cavity. Degn supported this concept by measurements of the rise times and durations of the current pulses and by computations of their fronts and durations based on numerical simulation of physical processes in the partial discharge.

Although there was a general agreement between the measurements and calculations there was a lack of experimental proof of the existence of the generation mechanism in this type of partial discharge.

In order to explain the temporal development of slowly developing partial discharges, a rigorous mathematical model based on analytical solutions of the continuity equations should be established and the calculated waveforms should be compared with the observed waveforms within a wide range of the parameter p·d. Such a solution should furthermore fullfil arbitrarily determined initial conditions in the cavity.

According to Degn, the mechanism of the second type of the partial discharges characterized by very fast increasing current pulses was unexplained. Furthermore, it was not possible to measure the waveforms of the rapidly developing discharges by means of the electrode systems used by the mentioned investigators.

It was not clear, whether or not the deteriorations caused by the two different types are different. Unfortunately the known measuring methods did not provide any direct information, neither on the lateral extension of the distinct types of partial discharges nor on the occurrence of the possible local discharges over the surface. This would help to identify the discharge types which can result in significant changes in the insulation in terms of insulation structure and properties (dangerous discharge types).

Processes other than partial discharges, for instance conduction, could well contribute to the power dissipation in the cavity during the tests of longer duration. Such processes could precipitate the deterioration processes in regions of local high field concentrations.

The changes in the discharge types and the properties of the insulation during the prolonged tests were not clarified.

For the reasons mentioned above, the present work has been undertaken with the particular aim to investigate the different types of individual internal partial discharges occurring in polymeric high voltage insulation under ac voltage conditions, and also to relate this information to observed slow decreases of insulating properties.

6.1. Experimental Methods and Apparatus.

Test specimens made of polymeric materials commonly used as solid insulation in high voltage equipment: polyethylene, polypropylene, and two basic types of epoxy resins were used throughout the investigation.

Test specimens were provided with artificial defects in the form of gas-filled cavities.

For the purpose of the investigation, a special electrode system of high sensitivity was designed which was integrated with the test sample. The electrode system allowed non-oscillatory measurements of extremely fast electrical signals associated with partial discharges. The resulting rise time for this system was ~ 1.6 ns. In addition, facilities were provided for the observance of the fast optical signals of low intensity by means of an externally mounted photomultiplier. The integrated system was assembled in the pressure/vacuum chamber which was suitable for use within the pressure range of 0.1 - 4 bar.

The ac voltage was supplied to the electrodes by a high voltage transformer, which could be operated at 50 Hz as well as at 500 Hz. The measuring equipment together with the high voltage transformer and the control and security circuits were situated in a specially constructed test area.

Three independent methods have been developed and employed in order to investigate the development of individual partial discharges during their extremely short formation times in the range 10^{-9} - 10^{-8} s, and short distances in the range 10^{-2} - 10^{-1} cm. The developed methods are: measurement of the partial discharge current pulses, measurement of the photon flux emitted from a partial discharge, and a method permitting a rough estimation of the extension of the partial discharges in directions oriented orthogonal to the electrical field direction.

The partial discharge current was considered in terms of the densities and drift velocities of the different species of charge particles produced in the cavity due to ionisation and attachment processes. This new method of approach allowed a more detailed representation of the physical conditions in the cavity than did the previously used methods, which adhered to and applied capacitive equivalent circuits of insulation and cavity.

The preliminary test measurements of the partial discharge current obtained by means of the three above mentioned methods were consistent. All three methods allowed the measurement of the waveforms of the transient quantities associated with the development of individual partial discharges, and were particularly applicable for the investigation of processes which lead to breakdown of solid polymeric insulation provided with artificial defects representing defects which would appear during the manufacturing process.

In order to analyse automatically the amplitude distribution of the current pulses and record the repetition rates of partial discharges during accelerated long-term tests, a technique employing a fast analyser, capable of measuring impulses with short rise times was developed for the data acquisition, and computer programs were applied for off line data processing. It is believed that this technique will become particularly suitable for investigations of test samples containing cavities, because it reduces the time and cost of this kind of investigation.

It was expected that during the partial discharge action the test sample would notably change its microscopic parameters in terms of mobilities and densities of charged particles within the insulant, and its structure and composition. Therefore, an experimental technique, employing a three terminal probe by means of which the surface conductivity could be measured, was additionally developed. A scanning electron microscope was used for the examination of the surface topography of the test samples investigated.

6.2. The Experimental Results.

The investigation of partial discharges was concentrated on establishing the general mechanisms governing the development of the partial discharge currents and the interaction with the insulation. From the analysis of the results obtained throughout the investigation in air, nitrogen, and carbon dioxide, two characteristic partial discharge current waveforms were distinguished. These were attributed to two basic and quite distinct partial discharge types, a "rapidly developing" and a "slowly developing" partial discharge, the names referring to the rate of current growth of an individual partial discharge.

6.2.1. The slowly developing partial discharge.

The duration T_p of the total discharge current for the slowly developing discharges was in the range 10^2 to $3 \cdot 10^3$ ns for the cavity depths range 0.02 to 0.3 cm, respectively, and for normal pressure. From the calculations of T_p, taking into account the drift velocities of the positive ions in the cavity, it was expected that the product (duration)$\cdot$(cavity depth) should be a unique function of the parameter $p \cdot d$: $T \cdot p = f(p \cdot d)$. The values of the function, calculated under the assump-

tion that the ignition field stress in the cavity was given by the Paschen curve, were indeed verified experimentally in the p·d range 3 to 300 mb·cm.

The individual slowly developing partial discharges were extended over the major part of the cavity cross section. They occurred at high surface conductivity and a sensibly uniform electrical field acting in the cavity sections which were not located in the immediate neighbourhood of the cylindrical cavity wall. Their repetition rate was a linearly increasing function of the ratio (test voltage)/(inception voltage). The partial discharges with small amplitudes occurred most frequently. It was found that the measured pulse amplitudes were exponentially distributed between the sensitivity limit: ~ 10 μA of the counting device and ~ 1 mA.

The linear character of the repetition rate and the exponential character of the amplitude distribution could be explained theoretically under the assumptions 1) that the individual partial discharges were extended over the whole cavity surface, 2) that the partial discharge magnitude was proportional to the field stress $\Delta E'$ in excess of the ignition field stress acting in the cavity at the onset of the partial discharge, and 3) that the time lags were exponentially distributed. The analysis of the automatically recorded amplitude distributions during long-term tests showed that the knowledge of the exponential character of the distribution of the slowly developing partial discharges has had a practical significance as it has made it possible to identify this partial discharge type directly from records from the analyser, i.e. without direct measurement of the partial discharge waveforms.

The pulse shape of the slowly developing discharges did not alter as the applied voltage increased, and their waveform remained markedly regular for different values of the parameter p·d and the corresponding different ignition voltages appearing across the cavity. In all cases, the pulse shape altered with the pulse amplitude. The total current of this partial discharge type consisted of an ion current and an electron current with unique characteristics. As the measured photon fluxes, which were proportional to the electron current, were characterized by rise times and durations significantly longer than the transit times for the electrons through the cavity, and as the ionic currents were caused by a very high number of ions, it was assumed that the electrons and ions were produced by successive generations.

The existence of individual generations in the initial build up of the current was experimentally stated in the case of carbon dioxide for this particular discharge type.

6.2.2. The rapidly developing partial discharges.

In contradistinction to the slowly developing partial discharges, the rapidly developing partial discharges were restricted to small sections of the cavity surface. Their current and photon flux pulses achieved amplitudes which were much higher than those of slowly developing partial discharges. Their repetition rates lay below those of the slowly developing partial discharges and were a nonlinear function of the ratio test voltage/inception voltage. Thus, it was concluded that the field reduction caused by the passage of these partial discharges was much higher than for the slowly developing discharges.

It was found that the shape of the pulse did not depend on the pulse amplitude. The photon flux emitted from the rapidly developing partial discharges exhibited a waveform which was fairly similar to the waveform of the corresponding current pulse. Initially, the current rose approximately exponentially. This slowly rising section frequently extended to many electron transit times and was followed by a hyper-exponential current growth just before the current and photon flux maximum and thereafter by an approximately exponential decay. The rise times which were mainly determinated by the hyper-exponential current growth were too short to allow a notable contribution to the formation of the fast developing section of the partial discharge current either from generation processes or from a single avalanche. Thus, the fast developing section of the current and photon flux pulses was assumed to correspond to the space charge accelerated avalanche growth commonly interpreted as a streamer formation. The decreasing section of the current pulse was believed to correspond to surface discharges.

6.2.3. The energy of the two types of partial discharges.

It was expected that the two described types of partial discharges will also exist in the natural cavities in different types of electrical insulation. Both types, however, were believed to act in dissimilar manners on the insulation, primarily because of the different energy distributions.

For both discharge types, the energy of the partial discharges was distributed unevenly over the discharge volume. In the slowly developing discharges the maximum energy was dissipated in the immediate vicinity of the momentaneously positive surface of the cavity. The energy of the rapidly developing type was highly localized since it was mainly distributed over a small surface area corresponding to the relevant Lichtenberg figure. Therefore, the rapidly developing discharges were considered to be the most hazardous for electrical insulation. For both types, the dissipated energy was in the range 10^{-9} - 10^{-5} Ws for the cavity range 0.01 - 0.2 cm, p = 1013 mb.

6.2.4. The conductivity of the surfaces subjected to partial discharges over extended test periods.

During the tests, when the ratio test voltage/inception voltage was 1.05 - 1.15 the characteristic transformations of the rapidly developing discharges were observed after time periods ranging from a few minutes to some hours after the beginning of the test.

When the ratio test voltage/inception voltage was higher, 1.5 to 2.5, this transformation occurred almost instantaneously in the beginning of the test. It was found that this transformation occurred simultaneously with a rapid and serious increase in the surface conductivity by several orders of magnitude to a level about 10^{-12} Ω^{-1} which was maintained throughout the tests with durations of up to 100 hours. It was believed that this increase in the surface conductivity produced a change towards more homogeneous field conditions in the cavity region apart from the cylindrical wall, thereby permitting the occurrence of the slowly developing partial discharges in this region.

During the present investigation, the pronounced tendency to self-extinction was observed in polypropylene test samples. The measurements showed that the self-extinction was caused by a very high conductivity in the range of 10^{-11} - 10^{-8} Ω^{-1} on the plane surfaces and the cylindrical wall of the cavity and by an increase of the power losses of the test sample. The increase of power losses was accompanied by a change in the shape of the power loss cyclogram from the form of a parallelogram into the ellipse form.

This indicates a change of the charge transport mechanism in the cavity from the partial discharge to a current across the surface. The

transport mechanisms can be distinguished by different characteristics of the power losses as a function of the test voltage.

6.2.5. The deterioration.

Two characteristic forms of erosional deterioration were found: craters of 10 - 50 μm in diameter and ≈ 10 μm in depth located on the plane surfaces in the vicinity of the cylindrical wall of the cavity, and a levelling erosion of the remaining part of the plane surfaces. Both types of deterioration were purely erosional processes resulting from the accumulated effect of a great number of successive discharges. The levelling type of erosion was believed to be innoxious to the insulation. It was known from previous investigations that in polyethylene and in aromatic epoxy resin breakdown always developed from the described craters. Therefore, it was assumed that the mechanism of the initiation of these craters was of particular significance for the progress of the breakdown process. The primary cause for the growth of the craters was the high conductivity of the test sample surfaces in conjunction with the localized succession of partial discharges.

6.3. Calculation of the Field Stress Distribution in Cylindrical and Spherical Cavities.

The development of craters appearing along the cylindrical cavity wall was explained on the basis of calculations of the electrical field in the cavity.

The field had a transient character - when internal discharges occurred under alternating voltage conditions the densities of charges left on the cavity surface by discharges changed with time, and the field also became a function of time.

The field intensity also changed with time during the propagation of an individual partial discharge across the cavity.

The field was considered in two respects: first, the calculation of the quasi-stationary field appearing between the occurrence of two succeeding partial discharges, and secondly, the calculation of the transient field occurring during the development of an individual partial discharge. The calculations of the quasi-stationary field were

carried out on test samples stressed by alternating voltage. The conductance of the surface was taken into account by introduction of thin conductive surface layers in the model. Two different situations were taken into consideration, when the applied voltage was less than the inception voltage, and when it exceeded the inception voltage. The results were given as a plot of equipotential and induction lines and plots of the field distributions.

At voltages below the inception voltage in the cylindrical cavity with negligible surface conductivity, the maximum field stress occurred along the cavity axis and the minimum field stress across the cylindrical wall, as opposed to the stress distribution in the case of two conductive layers of finite thickness on the plane parallel surfaces, where the sites in the neighbourhood of the cavity edge were the most stressed.

At voltages below the inception voltage in the spherical cavity, the field was homogeneous in the case of no conductive layers. In the case of two conductive layers of finite thickness at the "poles" of the sphere the field concentrations occurred in the previously uniform field.

Thus, at voltages slightly above the inception voltage in both the cylindrical and the spherical cavity with negligible surface conductivity, the partial discharges should occur along the cavity axis which is oriented in parallel with the field direction. Conversely, in cylindrical as well as in spherical cavities with conductive layers discharges should occur at a definite distance from the axis where the field concentrations occurred. In spherical cavities, this distance should increase with increasing conductive areas. Thus, the partial discharges should move away from the cavity axis during the progress of a long-term test, and the inception voltage should progressively decrease.

At voltages considerably above the inception voltage the partial discharges left on the cavity surface a charge which reduced the stress originally acting in the cavity. Therefore, not only the field stress amplitude but also the field distribution itself became a function of time. In the case of low surface conductivity, the charges retained on the surface were concentrated in many small areas known as Lichtenberg figures. This was the situation prevailing during the initial period of the tests. As previously noted, the surface conductivity increased during prolonged exposure of the surface to partial discharges. The

fields calculated for different phase angles show that also in this situation strong field concentrations occurred in the immediate neighbourhood of the cylindrical cavity wall. Nevertheless, it was found that for some phase angles this narrow region could be less stressed than the rest of the cavity cross section.

The surface charge density necessary to keep the average value of the field stress acting in the cavity equal to the ignition field stress, was found to be an increasing function of the applied voltage. The density increased with decreasing thickness of the insulation layers between the cavity and the electrodes; with very thin layers the charge density attained very high magnitudes. The changes of the field stress acting in the cavity during the development of an individual partial discharge were calculated in connection with the transient analysis of the partial discharge currents.

6.4. Calculation of the Temporal Development of the Partial Discharge Currents.

The growth of the partial discharges in time and space was described by continuity equations, the analytic solutions of which were obtained by the method of Laplace transformation for the case of a stationary field acting in the cavity. The general analytic solutions expressed the electron and ion current densities one-dimensionally for any time and position as functions of an arbitrary electron density in the neighbourhood of the negative surface. A particular analytic solution was obtained by considering the generation mechanism, where the mathematical probability of the instantaneous production of a secondary electron at the negative surface per ionizing collision was assumed to be constant. Initially, the current varied concurrently with the first generations and thereafter the oscillations in the current disappeared and the current approached an asymptotic course.

The analytical solutions were applicable only to time periods which were short in comparison with the duration of the partial discharge, so that the field stress could be assumed constant during this period.

The complete solution was obtained by taking the field changes into account. These were quantitatively determined in terms of the

changes in distributions of charge particles produced during the development of the individual partial discharge. The temporal development of the total discharge current and the charge distributions was calculated numerically on the basis of the mathematical model mentioned above.

For each calculation, the initial value of the overvoltage, i.e. the voltage in excess of the static breakdown voltage, at the onset of the partial discharge had to be prechosen, and the calculation was terminated when the calculated current values had decreased to zero. The calculations were carried out for air within the range of the parameter p·d from 2 to $2 \cdot 10^3$ mb·cm.

6.5. Results of the Calculations.

The above method for the calculation of the development of the partial discharge was proposed and developed at a very early stage of the present investigation, and by means of this method it was predicted than an *electron current with unique characteristics should be present.* The presence of this electron current was *two years later experimentally verified* by the measurement of the photon flux, which always showed the same waveforms as those calculated for the electron current.

The calculated total discharge current was composed of the electron current and the ion current and had a waveform which was characteristic of the slowly developing partial discharges. During the initial phase of the current growth the current increased exponentially as a function of time. The electrons which passed through the cavity accumulated as a negative surface charge on the positive surface. The ions drifted to the negative surface to be accumulated there as a positive surface charge. The charges of both polarities decreased the electrical field in the cavity. After a formative period corresponding to 50 - 200 generations, depending on the initial value of the overvoltage, the field decrease had reduced the average number of secondary electrons per avalanche to one. After this instant, the electron current was decreasing and when it became zero, the remaining current was due to the drift of ions towards the negative surface.

The calculated curves exhibited a similar characteristic increase in the pulse magnitude and in the sharpness of the current maximum with increasing overvoltage as the waveforms measured by Devins (litt. 3)

at dc step voltages and up to a few per cent overvoltage. The calculations also adequately explained the fact that the slowly developing partial discharges became shorter and smaller with decreasing pressure. The calculated values of the total decrease of the field stress by the passage of an individual partial discharge were consistent with the values which could be obtained from the repetition rate characteristics. These facts encouraged the conclusion that the applied mathematical model in many details satisfactorily explained the behaviour of the slowly developing partial discharge.

The differences between the measured and the calculated amplitudes were due to the decrease of the effective area of the partial discharge, and to the change in the probability of the production of secondary electrons in relation to the values assumed in the mathematical model. However, the simplifying assumptions did not affect the waveforms of the calculated currents.

It would not be possible to gather the same detailed information especially on the slowly developing discharges solely by the use of traditional capacitive equivalents of a cavity and the discharge phenomena. The considerable number of different measuring methods developed, especially for the present application, take their part of the credit for the results.

The present investigation does not analyse the degree to which the used test cells are representative for the defects occurring in the insulation systems under service conditions. Therefore, further investigation seems to be necessary.

In the future, the rapidly developing and transition types of the partial discharges, which are believed to be most dangerous to the insulation, should of course be further investigated during long term tests, among other things by means of the fast impulse amplitude analyser. The changes in surface conductivity are of major importance for the occurrence of distinct types of partial discharges and for their self-extinction. It will therefore be useful to study the physical and chemical causes of these changes; The high power losses often measured after the self-extinction indicate the possible presence of deterioration mechanisms other than those directly caused by the occurrence of partial discharges.

7. LITERATURE.

1. G.C. Lichtenberg:
"Nova Methodo Naturam ac Motum Fluidi Electrici Investigandi,
Novi commentarii societatis regiae scientarum Gottingensis."
tomus VIII, p. 1968, Göttingen, 1777.

2. P.O. Pedersen:
"On the Lichtenberg Figures."
Det Kgl. Danske Videnskabernes Selskab. Mat.-fys. Meddelelser.
Part 1, 1919; part 2, 1922; part 3, 1929.

3. J.C. Devins, H.L. Greenhaus, D.R. Johnston, F.Y. DuPont, A.L. Lynn, A. Pletenik, H.G. Peiffer:
"Research and Development on Corona-Resistant Materials."
Technical report. Aeronautical System Division, General Electric Research Laboratory, 1962.

4. P. Degn:
"Partial Discharges in Solid Dielectrics."
Ph.D. Thesis. Electric Power Engineering Department, Technical University of Denmark, Lyngby, 1971.

5. W. Burstyn:
"Die Verluste in geschichteten Isolierstoffen."
ETZ 35, 1928.

6. A. Gemant, V. Philipoff:
"Die Funkenstrecke mit Vorkondensator."
Z. für technische Physik 13, 1932.

7. S. Whitehead:
"Dielectric Breakdown of Solids."
Oxford and Clarendon Press, 1951.

8. J.H. Mason:
"The Deterioration and Breakdown of Dielectrics Resulting from Internal Discharges."
Proc. I.E.E., Vol. 98, part I, 1951, 44-51.

9. F.H. Kreuger:
"Discharge Detection in High Voltage Equipment."
A Heywood Book. Temple Press Books LTD, London, 1964.

10. E. Neudert:
"Entladungsvorgänge in Spaltförmigen Einschlüssen von Hochspannungsdielektriken."
Dissertation. Technische Hochschule Ilmenau, 1968.

11. C. Mayoux and M. Goldman:
"Partial Discharges in Solid Dielectrics and Corona Discharge Phenomena."
J. Appl. Phys., vol. 44, 1973.

12. Aa. Pedersen:
"Partielle udladninger i kunstige hulrum."
Nordiskt Symposium om Partielle Urladdninger, Västerås, 1968.

13. B. Luczynski, F. Levring:
"The Spatial and Temporal Development of Distinct Types of Partial Discharges."
Nordiskt Symposium om Elektriska Isoleringer, NORD-IS, 1976.

14. T. Laubst:
"Rapport fra CIGRE-konferencen: Isolationsmaterialer."
Elektroteknikeren, 1972.

15. C.A. Bailey:
"A Study of Internal Discharges in Cable Insulation."
I.E.E.E. Transactions on Electrical Insulation, Vol. EI-2, No. 3, 1967.

16. B. Luczyński:
"Måling af udladningsstrøm og dens virkning på faste isolationer."
Nordiskt Symposium om Isolationsteknik, NORD-IS 74, København, 1974

17. S. Kärkkäinen:
"Physical Mechanisms of Partial Discharges."
Technical Research Centre of Finland, Publication 6, Helsinki, 1974.

18. R. Bartnikas:
"Some Observations on the Character of Corona Discharges in Short Gap Spaces."
I.E.E.E. Transactions on Electrical Insulation, Vol. EI-6, No. 2, 1971.

19. B. Luczyński:
"Levetidsprøver. Prøvecelle."
Internal report. Electric Power Engineering Dapartment, Technical University of Denmark, Lyngby, 1973.

20. H. Raether:
"Electron Avalanches and Breakdown in Gases."
Butterworths, London, 1964.

21. L. Frommhold:
"Das Potential einer Ladung innerhalb paralleller Platen und "Randeffekte" bei Elektronenlawinen."
Zeitschrift für Physik, bd. 145, s. 324 - 340, (1956).

22. J.A. Stratton:
"Electromagnetic Theory."
McGraw - Hill Book Company INc, New York and London, 1941.

23. "Instruction Manual."
Type 1615, Capacitance Bridge, General Radio Comp., 1963.

24. N.M. Bashara:
"The Study of Discharges in Dielectric Voids by Photomultiplier Methods."
AIEE Transactions 115 - 119, 1961.

25. W. Legler:
"Über die UV- Strahlung von Elektronenlawinen in Luft."
Zeitschrift für Physik, Bd. 143, s. 173 - 190, 1955.

26. I. Gallimberti, J.K. Hepworth, R.C. Klewe:
"Spectroscopic Investigation of Impulse Corona Discharges."
J. Phys. D: Appl. Phys., Vol. 7, 1974.

27. F. Levring:
"Amplitudeanalysatoren."
Internal report. High Voltage Laboratory, Electric Power Engineering Department, Technical University of Denmark, Lyngby, 1976.

28. W. Boeck:
"Entstehung und Bedeutung vom Raumladungen in Kunststoff-Folien durch Koronaentladungen."
Dissertation, Fakultät für Machinenwesen der Technischen Hochschule Carola-Wilhelmina zu Braunschweig, 1966.

29. N. Balslev:
"Materiallære."
Akademisk Forlag, 1972.

30. BS 2782 Part 2, method 203 A:
"Surface resistivity."
1970.

31. JEOL (Japan Electron Optics Laboratory Co. LTD.):
"JSM-U3, Scanning Electron Microscope."

32. Hélene Bertein:
"Charges on Insulators Generated by Breakdown of Gas."
J. Phys. D: Appl. Phys., Vol. 6, 1973.

33. Hans Ritz:
"Durchschlagfeldstärke des homogenen Feldes in Luft."
Archiv für Elektrotechnik, XXVI Band, 4 Heft, 219 seite, 1932.

34. W. Toepler:
"Zur Kenntnis der Knickstelle im Verlaufe der Anfangsspannungen beim Funkendurchschlag."
Z. Techn. Physik 13, s. 386, 1932.

35. S. Badaloni, I Gallimberti:
"Basic Data of Air Discharges."
UPee - 72/02, Universita Di Padova, Instituto Di Elletrotecnica E Di Elettronica, June 1972.

36. L. Frommhold:
"Über versögerte Elektronen in Elektronenlawinen, insbesondere in Sauerstoff und Luft, durch Bildung und Zerfall negativer Ionen."
Fortsh. d. Phys. 12, 597, (1964).

37. K.H. Wagner:
"Ionisation, Electron-Attachment, -Detachment and Charge-Transfer in Oxygen and Air."
Z. Physik 241, 258 - 270, 1971.

38. M.S. Bhalla, J.D. Craggs:
"Measurement of Ionisation and Attachment Coefficients in Carbon Dioxide in Uniform Fields."
Proc. Phys. Soc. LXXVI, 3.

39. Hans Schlumbohm:
"Stossionisierungskoeffizient α, mittlere Elektronenenergien und die Beweglichkeit von Elektronen in Gasen."
Zeitschrift für Physik 184, 492 - 505, (1965).

40. L. Frommhold:
"Eine Untersuchung der Elektronenkomponente von Elektronenlawinen im homogenen Feld II."
Z. Physik 160, 554 (1960).

41. H. Schlumbohm:
"Messung der Driftgeschwindigkeiten von Elektronen und Positiven Ionen in Gasen."
Zeitschrift für Physik 182, 317, (1965).

42. H. Schlumbohm:
"Elektronenlawinen in elektronegativen Gasen."
Z. Physik 166, 192 (1962).

43. U. Dibbern:
"Untersuchung der Elektronenkomponente von Einzellawinen mit dem Photomultiplier."
Zeitschrift für Physik 163, 582 - 593, (1961).

44. S. Kärkkäinen:
"Internal Partial Discharges - Pulse Distributions, Physical Mechanisms and Effects on Insulators."
Ph. D. Thesis. Technical Research Centre of Finland, Helsinki, 1976.

45. F. Levring:
"Partielle Udladninger."
Eksamensprojekt, Danmarks tekniske Høsjkole, Stærkstrømsafdelingen, 1975.

46. B. Heller:
"Die Physikalischen Grundlagen der inneren Entladungsvorgänge im festen Dielektrikum."
9 Internationales Kolloquium, Elektrische Isolierstoffe und Hochspannungsteknik, Ilmenau, 1964.

47. A. Kelen:
"Studies on Partial Discharges in Solid Dielectrics - a Contribution to the Discharge Resistance Testing of Insulating Materials."
Acta Polytechnica Scandinavia, Electrical Engineering Series No. 16.

48. T.W. Dakin, P.J. Malinaric:
"A Capacitance Bridge Method for Measuring Integrated Corona-Charge Transfer and Power Loss per Cycle."
AIEE Power App. Systems, 79, p. 648 - 53, 1960.

49. J. Knøster Rasmussen:
"Teoretiske overvejelser vedrørende tabene ved partielle, indre udladninger."
Internal report. High Voltage Laboratory, Electric Power Engineering Department, Technical University of Denmark, 1971.

50. B. Luczyński:
"Måling af partielle udladninger."
Internal report. High Voltage Laboratory, Electric Power Engineering Department, Technical University of Denmark, 1971.

51. Olav Nørholm:
"Nedbrydning af epoxyplast udsat for partielle elektriske udladninger."
Master thesis. Laboratoriet for Elektroteknisk Materiallære, Stærkstrømsafdelingen, Danmarks tekniske Højskole, Lyngby, 1969.

52. H.C. Hall, R.M. Russek:
"Discharge inception and extinction in dielectric voids."
Proc. IEE, vol. 101, part II, 1954.

53. G. Mitra, B. Salvage:
"Electric stress in a circular cylindrical gaseous cavity in a solid dielectric."
Proc. IEE, vol. 113, 1966.

54. J.C. Maxwell:
"A Treatise on Electricity and Magnetism."
1892.

55. J.F. Madsen, Ole Jan Olesen:
"Brugermanual for regnemaskineprogram til beregning af Poissonfelter."
Danmarks tekniske Højskole, Stærkstrømsafdelingen, 1974.

56. H. Weldingh:
"Internal Discharges in Spherical Cavities in Epoxy Resins."
Ph. D. Thesis. Electric Power Engineering Department. Technical University of Denmark, Lyngby, 1977.

57. B. Luczyński:
"Transiente udladningsforløb i homogent felt afgrænset med metalelektroder."
Højspændingslaboratoriet, Stærkstrømsafdelingen, Danmarks tekniske Højskole, 1973.

58. G. Doetsch:
"Guide to the Applications of Laplace Transforms."
D. Van Nostrand, Princeton, N.J., U.S.A., 1961.

59. L.P. Auer:
"Transient Analysis of the Townsend Discharge."
Physical Review, 1958, number 3, page 671.

60. M.O. Jørgensen:
"Elektrische Funkenspannungen mit besonderer Berücksichtigung der Messentladungsstrecke."
Ejnar Munksgaard, Kopenhagen, 1943.

61. S. Vibholm:
"Kuglegabskarakteristikker med specielt henblik på Toeplers knækpunkt."
Ph. D. Thesis. Fysisk Laboratorium II, Technical University of Denmark, Lyngby, 1971.

62. Aa. Pedersen:
"Kompendium i højspændingsteknik."
Sec. 1. High Voltage Laboratory, Electric Power Engineering Department, Technical University of Denmark, 1972.

63. I.D. Chalmers, H. Duffy, and D.J. Tedford:
"The Mechanism of Spark Breakdown in Nitrogen, Oxygen, and Sulphur Hexafluoride."
Proc. Royal Society of London, A, 329, 171 (1972).

64. I.D. Chalmers and D.J. Tedford:
"Formative Time Lags in Nitrogen and Dry Air."
J. Phys. D: Appl. Phys., 8, 943 (1975).

65. F. Hai, M.J. Bernstein:
"Photoemission from Polymers."
The Aerospace Corporation, El Segundo, California 90045.

66. H.G. Kranz:
"Physikalische Vorgänge bei der Zündung von Teilentladungen in polymeren Isolierstoffen."
ETZ-A, 98, 1977.

67. P.M. Davidson:
Appendix to a paper by J. Dutton, S.C. Haydon & F. Llewellyn Jones:
"The Growth of Ionization Currents in a Uniform Field E (> E_s)."
British Journal of Applied Physics, 4, 170 (1953).

68. P.M. Davidson:
"Growth of Current Between Parallel Plates."
Phys. Rev., 99, 1072, 1955.

69. P.M. Davidson:
"Temporal Growth of Current Between Parallel Plates."
Phys. Rev., 103, 1897, 1956.

70. P.M. Davidson:
"Growth of Current Between Parallel Plates."
Phys. Rev., 106, 1, 1957.

71. A.J. Davies, C.J. Evans, and F. Llewellyn Jones:
"Electrical Breakdown of Gases: The Spatio-Temporal Growth of Ionization in Fields Distorted by Space Charge."
Proc. Royal Society of London, A, 281, 164, 1964.

APPENDIX 1.

Statical Breakdown Field Stress in Homogeneous Field for Air, 1013 mb, 20 °C.

d	I	II	III
cm	V · (cm · mb)$^{-1}$		
0.02	71.4	70.2	72.2
0.03	61.8	61.8	62.7
0.04	56.5	56.8	57.1
0.05	53.0	53.3	53.4
0.06	50.6	50.8	50.6
0.07	48.6	48.8	48.7
0.08	47.0	47.2	47.0
0.09	45.8	45.9	45.7
0.10	44.6	44.8	44.6
0.15	40.7	41.0	

I - calculated from equation 5.2.13.

II - calculated from equation 3.1.4.a.

III - tabulated values (litt. 61).

APPENDIX 2.

Programs for Computations of the Temporal Development of the Slowly Developing Partial Discharge.

The programs are written in FORTRAN - and have been compiled and tested on an 1800 IBM computer. The comments on the programs are written in Danish.

Contents.

A.2.1. Listing of the subroutines and the main program BLF-25. The program computes the temporal development of the partial discharge currents, charges, and several associated quantities. The output of this program consists of the printed tables. The computed waveforms can be displayed on a screen and/or plotted.

A.2.2. Listing of the main program BLU-25. The program computes the same quantities as the program BLF-25, but the output of this program is punched on cards and/or printed.

A.2.3. Compilation of the subroutines.

A.2.4. Compilation of the main program BLF-25, and an example of calculations.

APPENDIX 3.

Discussion of Equation 5.1.24 for the Case of a Constant Initial Current.

Davidson (lit. 67, 68, 69, and 70) has given the exact and approximate solutions of the continuity equations for the case involving two secondary processes at the cathode. The solution fulfils the condition of an arbitrary initial charge distribution in the gap and of a constant initial current I_o.

In the absence of the initial charge distribution the boundary conditions are:

$$I(o, t) = I_o + \gamma_i \cdot I_+(o, t) + \delta \cdot \int_o^d \alpha \cdot I_-(x, t) \cdot dx \qquad \text{(A3.1}$$

and

$$I_+(d, t) = 0 \qquad \text{(A3.2}$$

where $I_-(x, t)$ and $I_+(x, t)$ are the electron and positive ion currents, I_o is the current generated at the cathode by the constant, external illumination, while γ_i and δ are the Townsend secondary ionization coefficients representing the electron emission from the cathode due to the incidence of positive ions and electrons, respectively.

The approximate solution is obtained by omitting the oscillatory terms and approaches the exact solution when t is of the order of several electron transit times. This solution is given by:

$$I_-(o, t) = A - B \exp \Lambda \cdot t \qquad \text{(A3.3}$$

where Λ is specified as the real root of the equation:

$$1 - (\alpha \cdot \gamma_i/\phi) \cdot [\exp(\phi \cdot d) - 1] - (\delta/\psi) \cdot [\exp(\psi \cdot d) - 1] = 0 \qquad \text{(A3.4}$$

and

$$\phi = \alpha - \Lambda/v \qquad \psi = \alpha - \Lambda/v_- \qquad 1/v = 1/v_- + 1/v_+$$

The constant A, according to lit. 71, is:

$$A = \frac{I_o}{1 - (\gamma_i + \delta/\alpha) \cdot (\exp(\alpha \cdot d) - 1)} \qquad \text{(A3.5}$$

The image equation (5.1.24) in the present work expresses the solution of continuity equations (5.1.7) subject to the initial condition (5.1.9a) and boundary conditions (5.1.9b) and (5.1.9c), i.e. for the case of arbitrary initial current density.

Hence, the exact solution for the case of the constant, initial current density $j_o(o, t) = j_o$ may be obtained directly from the equation (5.1.24) by substituting $j_o(o, s) = j_o/s$:

$$f(s) = \frac{j_o}{s} \cdot \left(1 + \lambda \cdot \frac{1 - \exp -(s - \sigma)}{s - \sigma - \lambda \cdot (1 - \exp -(s - \sigma))}\right)$$
$$= \frac{j_o}{s} \cdot \frac{s - \sigma}{s - \sigma - \lambda \cdot (1 - \exp -(s - \sigma))} \qquad \text{(A3.6)}$$

The inverse transformation of (A3.6) yields then the solution:

$$f(t') = j_o\left(\frac{1}{1 - \gamma(\exp(\alpha \cdot d) - 1)} + \sum_{1}^{\infty} \frac{s_p \cdot \exp[(s_p + \sigma) \cdot t']}{(1 + s_p - \lambda) \cdot (s_p + \sigma)}\right) \qquad \text{(A3.7)}$$

where the s_p's are roots of the equation (5.1.28) and $t' = t/T_-$.

The approximate solution obtained by omitting the oscillatory terms is:

$$\lim_{t' \to \infty} f(t') = \frac{j_o}{1 - \gamma(\exp(\alpha \cdot d) - 1)} + \frac{j_o \cdot a \cdot \exp[(a + \sigma) \cdot t']}{(1 + a - \lambda) \cdot (a + \sigma)} \qquad \text{(A3.8)}$$

The above expression is seen to agree with the equation (A3.3) under the assumption that the growth constant is given by the relation:

$$(a + \sigma)/T_- = \Lambda \qquad \text{(A3.9)}$$

This assumption is verified by obtaining the expression for Λ which may be deduced by substituting $a = \Lambda \cdot T_- - \sigma$ in the equation (5.1.28):

$$\frac{\Lambda \cdot T_- - \sigma}{1 - \exp(\sigma - \Lambda \cdot T_-)} = \lambda$$

which after rearrangements becomes:

$$1 - \frac{\gamma \cdot \alpha}{\alpha - \frac{\Lambda}{v_-}} \cdot \left(\exp\left(\alpha - \frac{\Lambda}{v_-}\right) \cdot d - 1\right) = 0 \qquad \text{(A3.10)}$$

The above expression is seen to agree with the equation (A3.4) for $\gamma_i = 0$. Hence the equation (5.1.24) gives for the considered case of constant initial current the results which are consistent with Davidson's solutions.